

EFFECTS OF BODY SIZE, MORPHOLOGICAL MODULARITY, AND FLIGHT BEHAVIOR ON THE
EVOLUTION OF AVIAN WING SHAPE

Jonathan Andrew Rader

A dissertation submitted to the faculty at the University of North Carolina at Chapel Hill in
partial fulfillment of the requirements for the degree of Doctor of Philosophy in the
Department of Biology.

Chapel Hill
2021

Approved by:

Tyson L. Hedrick

William M. Kier

Kenneth J. Lohmann

Martha M. Muñoz

Sheila N. Patek

© 2021
Jonathan Andrew Rader
ALL RIGHTS RESERVE

ABSTRACT

Jonathan A. Rader: Effects of body size, morphological modularity, and flight behavior on the evolution of avian wing shape
(Under the guidance of Tyson L. Hedrick)

The evolution of wing morphology among birds and its functional consequences remains an open question despite much attention. Here I provide a new look at how bird wings scale with body size, what constrains wing dimensions, how flight style and the structure of the wing impact the evolution of wing shape, and how birds can tune their flight to environmental challenges in the absence of morphological adaptation. I used a first-principles approach to develop testable hypotheses regarding the evolution of wing size and shape among birds. I 3-dimensionally (3D) scanned wings from 178 species of birds to measure wing shape and measured the lengths and diameters of the wing bones and lengths of the handwing feathers. I found that the wing is organized into two discrete morphological modules, the handwing and the armwing, separated by the wrist joint. Despite this modularity, the evolutionary tempo and morphological disparity follow a continuous gradient predicted by a model of aerodynamic force production along the length of flapping wings. Most wing shape traits scaled either isometrically with respect to mass, or with negative allometry, such that large bird species have disproportionately small wings, but that camber increases with size and can compensate for relatively reduced wing area. The thickness of the armwing is decoupled from the skeleton and correlates with aerodynamic traits rather than a load bearing model, but handwing thickness is

tied to load bearing. I found that gliding birds had greater wing aspect ratio and camber than non-gliders, morphological differences that combined to yield greater coefficient of lift and reduced sinking speed in simulations of gliding birds. The simulations identified two discrete combinations of wing aspect ratio and camber in gliders, corresponding to adaptations to minimize cost per unit time and cost per unit distance. Finally, I found that turkey vultures adjust their airspeed to compensate for low air density at high elevations. My dissertation brought modern techniques and a new dataset together to answer important questions about the drivers and constraints of wing evolution in birds and provides insight into how biomechanics and form-function relationships shape the evolution of morphology.

To Mrs. Creger, who saw my budding interest in science and encouraged me to pursue it, and
to the teachers everywhere who inspire and support curious minds.

ACKNOWLEDGEMENTS

Science does not happen in a vacuum, and I certainly would not have been able to complete this dissertation without the network of support that I have been fortunate to have.

I am eternally grateful to my advisor, Dr. Tyson Hedrick for giving me the opportunity to conduct my dissertation work under his guidance, and for giving me the latitude to pursue my interests and develop my own research program. Also, his dedication to his craft is inspiring, and his deep understanding of flight and the underlying physics proved instrumental in shaping my approach to understanding the evolution of bird wings. I thank him for his patience, which I am certain to have tested repeatedly, and for always pushing me to improve.

I also thank the members of my graduate committee. Specifically, I thank Dr. Kenneth Lohmann for helping me to find my scientific identity and for welcoming me when I inadvertently crashed his lab's writing seminar. Dr. William Kier's enthusiasm for biomechanics and physiology are a perpetual source of inspiration for me. Moreover, though, Dr. Kier is an incredibly kind and supportive person, and I can't imagine my time at UNC without him.

Chapter 4 of this dissertation precipitated directly from a conversation with Martha Muñoz at the 2017 meeting of the Society for Integrative and Comparative Biology in New Orleans, LA, and my subsequent discussions with Dr. Muñoz and Sheila Patek enriched every part of my work.

This dissertation would not have been possible without the North Carolina Museum of Natural Sciences and the staff of the Ornithology collection there. I thank Brian O'Shea and John Gerwin, for access to specimens and assistance throughout the wing scanning operation. Brian went above and beyond to loan me a storage case to keep wings on the UNC campus, and was eternally patient with the lengthy loans of wings for scanning.

I worked with a phenomenal group of undergraduate lab assistants: Eli Bradley, Alaowei Amanah, Lucy Herrero, Alva Rönn, Colton Sanders, Sarah Yaghoubi, Russel Lo, Elliot Cho, Sophia Chizhikova, Zhitong Yu, and Raghuvara Padma. Without their tireless assistance scanning wings, processing wings, and measuring skeletons and feathers, I would not have been able to pull the data together for this dissertation. I wish them all the best for their very bright futures.

My time at UNC would not have been the same without Pranav Khandelwal. He has been a wonderful companion, colleague, sounding board, and, at times, counselor. And he is a life-long friend. I have also been fortunate to have a wonderful group of friends surrounding me throughout my graduate career, but I especially want to mention Braden Godwin, Antonio Serrato-Capuchina, Joseph Leistman, Jake Peters, Jon Philips and Juliet Homme, Lauren Corcoran, and my current and former lab mates Laura Mendez, Sonja Friman, Jeremy Greeter, Aaron Corcoran, and Dennis Evangelista. Finally, a heartfelt thank you to my friend and colleague Lindsay Waldrop for years of advice, and a fascinating (and ongoing) collaboration.

I especially thank Brenna Hansen, my partner in all things, for allowing me to drag us to North Carolina, listening to me prattle on endlessly about bird wings, pushing me out the door for bike rides (and sanity), and putting food in front of me at regular intervals while I was

writing. My parents and brother have been eternally supportive through everything, including my exploration of “all of the -ologies”.

I would also like to thank Kenlyn Merritt in the UNC Biology Department for keeping me on track with degree requirements and being so patient when I (frequently) dropped the ball. I thank the Society of Integrative and Comparative Biology for hosting the symposium Melding Modeling and Morphology, from which the work presented in my third chapter emerged. I further thank the Company of Biologists, the National Science Foundation, Sigma Xi, and NextEngine, Inc. for providing financial and material support for my work. To those who I’ve forgotten, thank you, and my humble apologies.

TABLE OF CONTENTS

LIST OF TABLES	xv
LIST OF FIGURES	xvi
LIST OF SYMBOLS AND ABBREVIATIONS	xviii
CHAPTER 1: INTRODUCTION	1
1.1 Background.....	1
1.1.1 The diversity of birds.....	2
1.1.2 Form-function relationships in birds	3
1.2 Tools and techniques	5
1.2.1 Museum collections	5
1.2.2 3-Dimensional scanning as a tool to study shape	6
1.2.3 A first-principles approach	7
1.3 Concluding remarks	8
REFERENCES.....	9
1.4 Figures	14
CHAPTER 2: ALLOMETRY, ISOMETRY, AND A PARADOX: BODY SIZE AFFECTS THE EVOLUTION OF AVIAN WING SHAPE	18
2.1 Introduction.....	18
2.1.1 A matter of size: scaling of wing morphology	18
2.1.2 Wings are 3-dimensional structures	21
2.1.3 Camber: maintaining lift with less wing area?	21
2.1.4 Wing thickness: maximize stiffness or minimize drag?	22

2.1.5	Wing cross-sectional area: minimize cost of flapping or facilitate maneuvering?	22
2.1.6	Summary and predictions	23
2.2	Methods	24
2.2.1	Wing scanning, scan processing, and shape analysis	24
2.2.2	Measurements of the wing skeleton.....	26
2.2.3	Measurements of primary flight feathers	26
2.2.4	Phylogenetic Analyses.....	27
2.2.5	Describing scaling relationships	27
2.2.6	Evolutionary dynamics of wing shape	27
2.2.7	Hypothesis testing: What predicts wing thickness?	28
2.3	Results	29
2.3.1	Datasets	29
2.3.2	On the utility of spread wings	29
2.3.3	External wing morphology	29
2.3.4	Skeletal measurements.....	30
2.3.5	The primary flight feathers	31
2.3.6	Evolutionary dynamics	31
2.3.6.1	Mode.....	31
2.3.6.2	Tempo	32
2.3.7	Hypothesis testing: What predicts wing thickness?	32
2.4	Discussion	33
2.4.1	A paradox remains: negative allometry of wing size.....	33
2.4.1.1	Why do big birds have (proportionally) small wings?.....	33

2.4.1.2	Building bigger wings: scaling of the wing skeleton and feathers	35
2.4.1.3	Beyond simple measurements: posture affects wing geometry	37
2.4.1.4	Resolving the paradox?	38
2.4.2	A mosaic of evolutionary dynamics.....	39
2.4.3	Aerodynamics drive external wing shape while load shapes the skeleton	40
2.4.4	Concluding remarks	41
REFERENCES.....		43
2.5	Figures	48
2.6	Tables	55
CHAPTER 3: FUNCTIONAL MORPHOLOGY OF GLIDING FLIGHT. MORPHOLOGY FOLLOWS PREDICTIONS OF GLIDING PERFORMANCE		
		59
3.1	Introduction.....	59
3.2	Methods	63
3.2.1	Wing scanning and 3D wing morphology	63
3.2.2	Measuring wing geometry	64
3.2.3	Modeling effects of wing geometry on gliding flight.....	65
3.2.4	Analysis and hypothesis testing	66
3.2.4.1	Hypothesis 1: Wing morphology differs between gliders and non-gliders	67
3.2.4.2	Hypothesis 2: Two gliding strategies lead to disparate gliding morphotypes.....	68
3.3	Results	69
3.3.1	Morphometric summary	69
3.3.2	Hypothesis 1:	70

3.3.3	Hypothesis 2:	71
3.4	Discussion	72
3.4.1	Performance landscapes predict differences in gliding performance	72
3.4.2	Equivocal support for two gliding strategies	74
3.4.3	On performance landscapes	75
3.4.4	Considering the third dimension	76
	REFERENCES	77
3.5	Figures	82
3.6	Tables	87
CHAPTER 4: MORPHOLOGICAL MODULARITY AND EVOLUTION OF 3-DIMENSIONAL SHAPE IN BIRD WINGS		89
4.1	Introduction	89
4.1.1	Form begets function in bird wings	90
4.1.2	Are birds wings modular?	91
4.1.3	Are evolutionary dynamics in the wing modular?	92
4.2	Methods	93
4.2.1	Wing scanning and measurement	93
4.2.2	Phylogenetics	95
4.2.3	Morphological modularity analysis	95
4.2.3.1	Modularity	95
4.2.3.2	Disparity	96
4.2.4	Evolutionary modularity analysis	97
4.2.4.1	Evolutionary tempo and mode	97
4.3	Results	97

4.3.1	Dataset.....	97
4.3.2	Morphological modularity	98
4.3.3	Morphological disparity	98
4.3.4	Evolutionary tempo and phylogenetic signal	99
4.4	Discussion	99
4.4.1	Bird wings are modular structures	100
4.4.2	Trait evolution follows a gradient rather than modules.....	102
4.4.3	Additional considerations	104
4.4.4	Concluding remarks	105
	REFERENCES.....	107
4.5	Figures	112
4.6	Tables	116
CHAPTER 5: BEHAVIORAL COMPENSATION FOR LOW AIR DENSITY IN TURKEY		
	VULTURES (<i>CATHARTES AURA</i>).....	117
4.7	Introduction.....	117
4.8	Methods	120
4.8.1	Vulture recordings	120
4.8.2	Air density and airspeed	122
4.8.3	Air density and flapping behavior	124
4.9	Results	125
4.9.1	Vulture tracks, air density, and flight speeds	125
4.9.2	Flapping analysis	126
4.10	Discussion	127
4.10.1	Summary of results	127
4.10.2	Increased airspeed compensates for decreased air density.....	128

4.10.3	Concluding remarks	129
REFERENCES.....		131
4.11	Figures	134
4.12	Tables	138
CHAPTER 6: CONCLUSIONS.....		139
5.1	Body size and evolving wings	140
5.1.1	Resolving a paradox	140
5.1.2	Constraints and tradeoffs affect wing size	141
5.1.3	Important questions remain	142
5.2	Gliding specialists have diverged in wing shape	142
5.2.1	Gliding versus non-gliding morphology.....	143
5.2.2	Two strategies for gliding.....	144
5.2.3	Beyond the hypotheses: Performance landscapes and 3D wings	145
5.3	Wing anatomy and modular evolution.....	145
5.3.1	Looking for modules in the wing.....	146
5.3.2	Testing evolutionary dynamics of the wing modules	147
5.4	Flying in thin air	147
5.4.1	Vultures flew faster at high elevation	148
5.5	What does it all mean?	149
5.5.1	The challenge of deep time.....	149
5.5.2	A new dataset and analytical techniques.....	150
5.5.3	Evolution in three dimensions	151
5.5.4	Looking forward	152
REFERENCES.....		154

LIST OF TABLES

Table 2.1 Scaling relationships and phylogenetic signal.....	55
Table 2.2 A comparison of the effects of phylogenetic assumptions on scaling models.	56
Table 2.3 Evolutionary dynamics of wing shape traits.	57
Table 2.4 Hypothesis testing results.....	58
Table 3.1 Phylogenetic signal.....	87
Table 3.2 Model outputs.....	88
Table 4.1 Evolutionary dynamics.....	116
Table 5.1 Model selection results.	138

LIST OF FIGURES

Figure 1.1 Birds are diverse in their body size and their wing morphology.....	14
Figure 1.2 The NextEngine 3D Scanner Ultra HD, with integrated turntable.	15
Figure 1.3 Spread wings	16
Figure 1.4 The upper surface of the scan	17
Figure 2.1 Workflow for extracting data from 3D scanned bird wings.....	48
Figure 2.2 The species included in the scanned wing dataset.....	49
Figure 2.3 Phylogenetic distribution of shape traits.....	50
Figure 2.4 The species included in the skeleton (A.) and feather (B.) datasets	51
Figure 2.5 Phylogenetic distributions of the skeletal and feather datasets.....	52
Figure 2.6 Scaling relationships of wing shape traits.....	53
Figure 2.7 Size-related effects.....	54
Figure 3.1 Morphological configurations and relevant metrics.....	82
Figure 3.2 (Preceding page) Phylogenetic distribution of flight behavior and gliding strategy ...	84
Figure 3.3 Phylogenetic distribution of shape traits.....	85
Figure 3.4 Gliding flight performance landscapes	86
Figure 4.1 Bird wings are complex biological structures	112
Figure 4.2 a.) Slice-wise profiles of wing shape.....	113
Figure 4.3 The covariance ratio test.....	114
Figure 4.4 Morphological disparity (dashed line) and evolutionary rate.....	115
Figure 5.1 Overhead view of the Laramie, WY recording site	134
Figure 5.2 Median airspeed decreased with increasing air density.....	135

Figure 5.3 Proportion of detected flapping events	136
Figure 5.4 Flapping behavior as a function of wind speed	137

LIST OF SYMBOLS AND ABBREVIATIONS

2D	Two-dimensional
3D	Three-dimensional
AR	Wing aspect ratio
AW	Armwing
C	Chord
\bar{C}	Mean wing chord
\bar{C}_{ND}	Mean wing chord, non-dimensionalized relative to body mass
C_D	Coefficient of drag
C_L	Coefficient of lift
C_L/C_D	Lift to drag ratio
CR	Covariance ratio
F_L	Lift force
HW	Handwing
K	Blomberg's K
M_b	Body mass
Q	Camber
\bar{Q}	Mean wing camber
r	Wing length
r_{ND}	Wing length, non-dimensionalized relative to body mass
Re	Reynolds number

S_f	Frontal area of the wing
S_p	Wing area
\bar{t}	Mean wing thickness
V	Velocity
$V_{z,min}$	Minimum sinking speed
XST	Cross-sectional thickness
XSA	Cross-sectional area
δ	Pagel's delta
λ	Pagel's lambda
ρ	Air density
σ^2	Evolutionary rate parameter
W_V	Wing volume

CHAPTER 1: INTRODUCTION

1.1 Background

My dissertation explores the evolution of wing shape and flight behavior in birds. Broadly, this dissertation is divided into four aims. 1) I describe how the size of birds' wings scales with their body size, and how physical tradeoffs and the biological materials that compose the wing (specifically bone and feather keratin) limit wing size, and indeed, potentially also the maximum body size of flying birds. 2) I quantify and discuss how adaptation to gliding as a primary flight style has shaped bird wings across a variety of species. 3) I show that the wing surface is subdivided into discrete regions related to the hand and arm portions of the wing skeleton. Further, I test whether these regions have evolved as discrete units, or if the evolution of wing shape follows the distribution of flight-related forces along the wing. 4) I explore one way in which a ubiquitous bird species, the turkey vulture (*Cathartes aura*), copes with a fundamental environmental challenge that they experience across their range: that air density, and therefore the lift that the wings produce at a given flight speed, decreases with altitude. I used novel methodologies, 3-dimensional scanning, to acquire shape data from museum-preserved wings, and 3-dimensional videography to track flying birds, and show that both have applicability to a broad range of studies focused on the movement and associated morphology of animals.

In this introductory chapter, I will discuss why the diversity of birds and rich history of studying wing shape and aerodynamics make this an ideal system to generate and test hypotheses about morphological evolution. I will also discuss the strengths and potential pitfalls of working with 3D shape data and varying approaches to its analysis. Finally, I will make a case for why I think it is timely to revisit some previously described patterns of avian wing shape variation in light of new methods and data.

1.1.1 The diversity of birds

Birds are the most speciose lineage of terrestrial vertebrates (del Hoyo et al. 1992; Sibley et al. 2009; Jetz et al. 2012; Barrowclough et al. 2016), with traditional estimates of ~10,000 species (e.g., Jetz et al. 2012). A recent estimate suggests that the number of bird species may be much higher, around 18,000 species (Barrowclough et al. 2016). Birds inhabit every continent and range from sea level to the highest mountains (del Hoyo et al. 1992; Sibley et al. 2009). Avian ecology is also extremely diverse (Sibley et al. 2009; e.g. Jetz et al. 2012; Stiller and Zhang 2019; Machac 2020; and many more). For example, some birds conduct the longest known migrations (Egevang et al. 2010; Fijn et al. 2013), regularly traverse the Himalayas (Bishop et al. 2015), and dive into the ocean and swim to catch their prey (Lovvorn et al. 2001; Lovvorn and Liggins 2002). Others make their living in forests, gleaning insects from foliage (Airola and Barrett 1985; Sibley et al. 2009), perching at forest boundaries and catching prey on the wing (Verbeek 1975; Norberg 1986), foraging on the forest floor (Sibley et al. 2009), and in many other ways (e.g. Landmann and Winding 1993; Hedenstrom 1995; Sabat et al. 2003; Irestedt et al. 2006; Felice, Tobias, et al. 2019, and others). Their ecological diversity

accompanies an impressive diversity of shape, size, and behavior among birds (Grant 1999; e.g. Claramunt 2010; Derryberry et al. 2011, 2018; Claramunt et al. 2012; Sheard et al. 2020, and many others) that has long held naturalists' fascination (e.g. Audubon and Audubon 1875; Lack 1953; Barrow 2000; Camerini 2015).

1.1.2 Form-function relationships in birds

To exploit a wide array of different resources, birds have diverged in several aspects of their morphology and there is a rich history of study of these form-function relationships. In the classic example of Darwin's finches, birds within a recently-diverged lineage were shown to have adapted to be able to open and consume a variety of different seed types (Grant 1968, 2006; Boag and Grant 1981). Bill shape and size are related to diet across a range of bird taxa (Stiles 1995; Nebel et al. 2005; Temeles et al. 2009; Leisler and Winkler 2015). However, bill size and shape also impose tradeoffs that impact the evolution of other aspects of bird biology such as song (Podos 2001; Derryberry et al. 2018; Demery et al. 2021). Further, diet is not always predictive of bill morphology, and is more attributable to evolutionary relatedness among taxa (Cataudela and Palacio 2021), which is especially true deep within the avian phylogeny (Cooney et al. 2017). Bill morphology appears to have experienced an early, rapid divergence into disparate morphologies among the primary bird lineages, followed by a reduction in evolutionary rate and a transition to a pattern of fine-tuning of shape within each lineage (Cooney et al. 2017). Similar observations of early diversification of morphology, followed by decelerating evolution have been made regarding other aspects of avian morphology, including wing shape and body size (Phillips et al. 2020).

Wings have an obvious and important function for most birds: flight. A long history of aerodynamic work has demonstrated that the shape of wing affects its aerodynamics (e.g. Milne-Thomson 1966; Nachtigall 1975, 1979), and many attempts have been made to describe how avian wing shape varies among lineages of birds (e.g. Rayner 1988; Lockwood et al. 1998, and others), with flight behavior (Lockwood et al. 1998; Leisler and Winkler 2003; Swaddle and Lockwood 2003), and other aspects of bird biology (Swaddle and Lockwood 1998; Stoddard et al. 2017; Sheard et al. 2020). Outwardly, birds appear to have an impressive diversity of wing shape (Fig. 1), however, despite the breadth of work that has aimed to understand the linkage between form and function in bird wings, much of the picture remains unclear.

Attempts to link wing shape to ecology in birds have produced conflicting and sometimes perplexing results (Taylor and Thomas 2014). Many studies have been hampered by composite datasets (Greenewalt 1975; Rayner 1988; Taylor and Thomas 2014), or by the confounding effects of phylogenetic relatedness among bird taxa (Greenewalt 1975; Rayner 1988). Indeed, wing shape is frequently better predicted by taxonomic group than by function or ecological factors (Taylor and Thomas 2014; Baliga et al. 2019a). Furthermore, tradeoffs in wing shape come from the inertia of flapping wings (van den Berg and Rayner 1995) – aerodynamic theory suggests that longer wings are advantageous for efficient lift production (Milne-Thomson 1966), however longer wings require more energy to flap. Habitat can also impose selective pressure on wing shape both among taxa, and among individuals within a single species (Landmann and Winding 1993; Vanhooydonck et al. 2009). Despite being aerodynamically advantageous, long wings may be unwieldy in tight spaces. For example, Himalayan chats that live in tight, closed habitats like forests and scrub have shorter, rounder

wings than birds living in more open habitats, while species that live at the edges of open spaces and hunt in open airspace tend to have longer, more pointed wings (Landmann and Winding 1993). Similarly, populations of *Geospiza fortis* (the medium ground finch, one of Darwin's finches; Grant 1999) fluctuate between dominance of individuals with more rounded wings during wet years when vegetation on the islands flourishes and those with longer, more pointed wings during drier, less lush years (Vanhooydonck et al. 2009). Wings may also be constrained by their evolutionary history as limbs (Oyston et al. 2015) or by the materials that comprise them (Nudds 2007; Nudds et al. 2011; Wang et al. 2012).

1.2 Tools and techniques

1.2.1 Museum collections

Vertebrate collections in natural history museums provide an unparalleled repository of natural history data that has been accumulated over the last couple of centuries. Collections are both vast in their taxonomic breadth, and in the number of samples available for many taxa. Furthermore, because specimens were collected at various times in history, they can provide opportunity for time series comparisons that would not otherwise be possible. Collection and preservation style priorities have fluctuated through time, however. For example, preservation of spread bird wings such as those that I used for my dissertation work was not started until the mid 1980's, and did not gain much momentum until the late 1990's. That said, several museums, including the North Carolina Museum of Natural Sciences, prioritized the development of spread wing collections, and now have a substantial and growing number of accessioned specimens available for study. These collections provide a valuable opportunity to

conduct broad studies of the evolution of form and function, and I hope that my dissertation will provide a roadmap for future collections-based research.

1.2.2 3-Dimensional scanning as a tool to study shape

I used a NextEngine 3D Scanner Ultra HD (Nextengine, inc., Santa Monica, CA; Fig. 2) to collect 3D data from preserved wings (Fig. 3). This scanner is a self-contained unit that uses laser triangulation to record shape and surface detail of objects with a working range of 0.1 to 0.6 m, a maximum resolution of 0.1 mm, and a maximum accuracy of 0.125 mm. The NextEngine software provides a convenient user interface for collection of 3D shape data, and data can be saved in multiple file formats (OBJ, PLY, STL, VRML, XYZ). I worked with OBJ files, as these were easily imported into Matlab for further processing.

Despite the ease with which the scanner is operated, scanning bird wings was not without its pitfalls. The optical properties of feather differ between the upper and lower surfaces of the feather, which had the effect of slightly altering the resolved distance between the scanner and the wing, such that the lower surface would intersect through the upper surface when the scanner was set to automatically conduct full 360-degree scans. To resolve this difficulty, I scanned the wings in two parts, the upper surface and the lower surface, and then used the 3D modeling software Meshlab (Cignoni et al. 2008) to reassemble the two halves (Fig. 4). Additionally, some colors of plumage proved to be problematic. Blue coloration in birds is not the result of pigmentation, but rather by scattering of non-blue wavelengths of light by the feather keratin (Hill et al. 2006; Stoddard and Prum 2011). This has the somewhat obvious, but (at least for this project) unfortunate effect of rendering blue colored birds difficult

to scan. Darker blues, presumably with more melanin content in the keratin, scanned well, however I was utterly unable to scan wings from the eastern bluebird (*Sialia sialis*).

1.2.3 A first-principles approach

We live in a world of big data, which provides exciting new possibilities for the study of comparative and evolutionary biomechanics (Muñoz and Price 2019). There are nevertheless also novel challenges such as the curation and analysis of big data sets, which can be computationally demanding. Complex multivariate data can also be statistically unwieldy (Walker 2010), with large amounts of autocorrelated data. In these cases, many researchers have turned to dimensional-reduction techniques like principal component analysis (PCA) to study evolutionary diversification of morphology among taxa (Jolliffe and Cadima 2016). PCA is a powerful tool for exploring very large data sets because it reduces the dimensionality of a morphological data set. Changes in morphology, as captured by principal components axes, can be mapped onto phylogenies and then correlated with observations of ecology or behavior. From those analyses, we can infer the pressures that have driven adaptive evolution in morphology (e.g. Lockwood et al. 2002; McCoy et al. 2006). This approach is inherently correlational, however, and lacks a fundamental mechanistic explanation of the functional consequences of specific changes in morphology. Furthermore, the relationship between principal-component axes and specific morphological features is frequently murky and subjective, so the results of PCA and similar *post hoc* dimensional-reduction techniques can be difficult to evaluate as functional hypotheses.

Modeling and first-principles approaches, because they are rooted in the underlying physics of the system, can provide the explanatory power that correlational approaches lack. The power of these approaches is that they provide a simplified view of otherwise complex form–function systems, stripping away traits that are irrelevant to the performance outputs of interest. In doing so, strategies of *a priori* dimensional reduction foster development of testable hypotheses by highlighting traits with strong relationships to functional output (high mechanical sensitivity, for examples see Anderson and Patek 2015; Muñoz et al. 2017; Waldrop et al. 2020a).

1.3 Concluding remarks

This dissertation is a novel attempt to quantify 3D wing shape among birds using a first-principles approach to identify axes of variation that are known to be relevant to flight performance. In the following chapters, I present my work pursuing four questions related to form and function of bird wings: 1) How does wing morphology scale with body size, and what factors constrain wing evolution? 2) Does flight behavior affect the evolution of wing shape? 3) Wings are complex structures; does that complexity affect wing evolution? 4) How do birds cope with environmental challenges in the absence of morphological adaptation? I made use of the invaluable resource found in museum collections, used cutting-edge tools to collect 3-dimensional shape data, and developed novel methods to analyze shape traits.

REFERENCES

- Airola DA, Barrett RH. 1985. Foraging and Habitat Relationships of Insect-Gleaning Birds in a Sierra Nevada Mixed-Conifer Forest. *The Condor* 87:205–16.
- Anderson PSL, Patek SN. 2015. Mechanical sensitivity reveals evolutionary dynamics of mechanical systems. *Proc R Soc B Biol Sci* 282:20143088.
- Audubon JJ, Audubon LGB. 1875. *The Life of John James Audubon, the Naturalist* G. P. Putman's sons.
- Baliga VB, Szabo I, Altshuler DL. 2019. Range of motion in the avian wing is strongly associated with flight behavior and body mass. *Sci Adv* 5:eaaw6670.
- Barrow M. 2000. *A Passion for Birds: American Ornithology After Audubon* Princeton University Press.
- Barrowclough GF, Cracraft J, Klicka J, Zink RM. 2016. How Many Kinds of Birds Are There and Why Does It Matter? *PLOS ONE* 11:e0166307.
- Berg C, Rayner J. 1995. The moment of inertia of bird wings and the inertial power requirement for flapping flight. *J Exp Biol* 198:1655–64.
- Bishop CM, Spivey RJ, Hawkes LA, Batbayar N, Chua B, Frappell PB, Milsom WK, Natsagdorj T, Newman SH, Scott GR, Takekawa JY, Wikelski M, Butler PJ. 2015. The roller coaster flight strategy of bar-headed geese conserves energy during Himalayan migrations. *Science* 347:250–54.
- Boag PT, Grant PR. 1981. Intense Natural Selection in a Population of Darwin's Finches (Geospizinae) in the Galápagos. *Science* 214:82–85.
- Camerini JR. 2015. Wallace in the Field. *Osiris*.
- Cataudela JF, Palacio FX. 2021. Habitat and phylogeny, but not morphology, are linked to fruit consumption in the most ecologically diverse bird family, the Furnariidae. *Emu - Austral Ornithol* 0:1–8.
- Cignoni P, Callieri M, Corsini M, Dellepiane M, Ganovelli F, Ranzuglia G. 2008. MeshLab: an Open-Source Mesh Processing Tool. 8.
- Claramunt S. 2010. Discovering Exceptional Diversifications at Continental Scales: The Case of the Endemic Families of Neotropical Suboscine Passerines. *Evolution* 64:2004–19.
- Claramunt S, Derryberry EP, Brumfield RT, Remsen JV. 2012. Ecological Opportunity and Diversification in a Continental Radiation of Birds: Climbing Adaptations and Cladogenesis in the Furnariidae. *Am Nat* 179:649–66.

- Cooney CR, Bright JA, Capp EJR, Chira AM, Hughes EC, Moody CJA, Nouri LO, Varley ZK, Thomas GH. 2017. Mega-evolutionary dynamics of the adaptive radiation of birds. *Nature* 542:344–47.
- del Hoyo J, Elliott Andrew, Sargatal Jordi, Cabot José. 1992. *Handbook of the birds of the world* Barcelona: Lynx Edicions.
- Demery A-JC, Burns KJ, Mason NA. 2021. Bill size, bill shape, and body size constrain bird song evolution on a macroevolutionary scale. *Ornithology* 138.
- Derryberry EP, Claramunt S, Derryberry G, Chesser RT, Cracraft J, Aleixo A, Pérez-Emán J, Remsen, Jr. JV, Brumfield RT. 2011. Lineage diversification and morphological evolution in a large-scale continental radiation: The neotropical ovenbirds and woodcreepers (aves: Furnariidae). *Evolution* 65:2973–86.
- Derryberry EP, Seddon N, Derryberry GE, Claramunt S, Seeholzer GF, Brumfield RT, Tobias JA. 2018. Ecological drivers of song evolution in birds: Disentangling the effects of habitat and morphology. *Ecol Evol* 8:1890–1905.
- Egevang C, Stenhouse IJ, Phillips RA, Petersen A, Fox JW, Silk JRD. 2010. Tracking of Arctic terns *Sterna paradisaea* reveals longest animal migration. *Proc Natl Acad Sci* 107:2078–81.
- Felice RN, Tobias JA, Pigot AL, Goswami A. 2019. Dietary niche and the evolution of cranial morphology in birds. *Proc R Soc B Biol Sci* 286:20182677.
- Fijn RC, Hiemstra D, Phillips RA, Winden J van der. 2013. Arctic Terns *Sterna paradisaea* from the Netherlands Migrate Record Distances Across Three Oceans to Wilkes Land, East Antarctica. *Ardea* 101:3–12.
- Grant PR. 1968. Bill Size, Body Size, and the Ecological Adaptations of Bird Species to Competitive Situations on Islands. *Syst Biol* 17:319–33.
- Grant PR. 1999. *Ecology and evolution of Darwin's finches* Princeton, N.J.: Princeton University Press.
- Grant PR. 2006. Evolution of Character Displacement in Darwin's Finches. *Science* 313:224–26.
- Greenewalt CH. 1975. The Flight of Birds: The Significant Dimensions, Their Departure from the Requirements for Dimensional Similarity, and the Effect on Flight Aerodynamics of That Departure. *Trans Am Philos Soc* 65:1–67.
- Hedenstrom A. 1995. Song Flight Performance in the Skylark *Alauda arvensis*. *J Avian Biol* 26:337.
- Hill GE, Hill GE, McGraw KJ, McGraw KJ. 2006. *Bird Coloration, Volume 1: Mechanisms and Measurements* Harvard University Press.

- Irestedt M, Fjeldså J, Ericson PGP. 2006. Evolution of the ovenbird-woodcreeper assemblage (Aves: Furnariidae) - major shifts in nest architecture and adaptive radiation. *J Avian Biol* 37:260–72.
- Jetz W, Thomas GH, Joy JB, Hartmann K, Mooers AO. 2012. The global diversity of birds in space and time. *Nature* 491:444–48.
- Jolliffe IT, Cadima J. 2016. Principal component analysis: a review and recent developments. *Philos Trans R Soc Math Phys Eng Sci* 374:20150202.
- Lack D. 1953. Darwin's Finches. *Sci Am* 188:66–73.
- Landmann A, Winding N. 1993. Niche segregation in high-altitude Himalayan chats (Aves, Turdidae): does morphology match ecology? *Oecologia* 95:506–19.
- Leisler B, Winkler H. 2003. Morphological Consequences of Migration in Passerines. In: Berthold P, Gwinner E, Sonnenschein E, editors. *Avian Migration* Springer Berlin Heidelberg. p. 175–86.
- Leisler B, Winkler H. 2015. Evolution of island warblers: beyond bills and masses. *J Avian Biol* n/a-n/a.
- Lockwood CA, Lynch JM, Kimbel WH. 2002. Quantifying temporal bone morphology of great apes and humans: an approach using geometric morphometrics. *J Anat* 201:447–64.
- Lockwood R, Swaddle JP, Rayner JMV. 1998. Avian wingtip shape reconsidered: Wingtip shape indices and morphological adaptations to migration. *J Avian Biol* 29:273–92.
- Lovvorn J, Liggins GA, Borstad MH, Calisal SM, Mikkelsen J. 2001. Hydrodynamic drag of diving birds: effects of body size, body shape and feathers at steady speeds. *J Exp Biol* 204:1547–57.
- Lovvorn JR, Liggins GA. 2002. Interactions of body shape, body size and stroke-acceleration patterns in costs of underwater swimming by birds. *Funct Ecol* 16:106–12.
- Machac A. 2020. The Dynamics of Bird Diversity in the New World. *Syst Biol* 69:1180–99.
- McCoy MW, Bolker BM, Osenberg CW, Miner BG, Vonesh JR. 2006. Size correction: comparing morphological traits among populations and environments. *Oecologia* 148:547–54.
- Milne-Thomson LM. 1966. *Theoretical Aerodynamics* New York, NY: MacMillan and Company.
- Muñoz MM, Anderson PSL, Patek SN. 2017. Mechanical sensitivity and the dynamics of evolutionary rate shifts in biomechanical systems. *Proc R Soc B Biol Sci* 284:20162325.

- Muñoz MM, Price SA. 2019. The Future is Bright for Evolutionary Morphology and Biomechanics in the Era of Big Data. *Integr Comp Biol* 59:599–603.
- Nachtigall W. 1975. BIRD WINGS AND GLIDING FLIGHT INTRODUCTION TO THE AERODYNAMIC ASPECTS OF THE WING. *J Fuer Ornithol* 116:1–38.
- Nachtigall W. 1979. THE PIGEONS WING DURING GLIDING FLIGHT GEOMETRICAL CHARACTERISTICS OF WING PROFILES AND GENERATION OF AERODYNAMIC FORCE COMPONENTS. *J Fuer Ornithol* 120:30–40.
- Nebel, Jackson, Elner. 2005. Functional association of bill morphology and foraging behaviour in calidrid sandpipers. *Anim Biol* 55:235–43.
- Norberg UM. 1986. Evolutionary Convergence in Foraging Niche and Flight Morphology in Insectivorous Aerial-Hawking Birds and Bats. *Ornis Scand Scand J Ornithol* 17:253–60.
- Nudds RL. 2007. Wing-bone length allometry in birds. *J Avian Biol* 38:515–19.
- Nudds RL, Kaiser GW, Dyke GJ. 2011. Scaling of Avian Primary Feather Length. *PLoS ONE* 6:e15665.
- Oyston JW, Hughes M, Wagner PJ, Gerber S, Wills MA. 2015. What limits the morphological disparity of clades? *Interface Focus* 5:20150042.
- Phillips AG, Töpfer T, Böhning-Gaese K, Fritz SA. 2020. Rates of ecomorphological trait evolution in passerine bird clades are independent of age. *Biol J Linn Soc* 129:543–57.
- Podos J. 2001. Correlated evolution of morphology and vocal signal structure in Darwin's finches. *Nature* 409:185–88.
- Rayner JMV. 1988. Form and Function in Avian Flight. In: Johnston RF, editor. *Current Ornithology*. Current Ornithology Boston, MA: Springer US. p. 1–66.
- Sabat P, Farina JM, Soto-Gamboa M. 2003. Terrestrial birds living on marine environments: Does dietary composition of *Cinclodes nigrofumosus* (Passeriformes: Furnariidae) predict their osmotic load? *Rev Chil Hist Nat* 76:335–43.
- Sheard C, Neate-Clegg MHC, Alioravainen N, Jones SEI, Vincent C, MacGregor HEA, Bregman TP, Claramunt S, Tobias JA. 2020. Ecological drivers of global gradients in avian dispersal inferred from wing morphology. *Nat Commun* 11:2463.
- Sibley D, Elphick C, Dunning JB. 2009. *The Sibley Guide to Bird Life & Behavior* Alfred A. Knopf.
- Stiles FG. 1995. Behavioral, Ecological and Morphological Correlates of Foraging for Arthropods by the Hummingbirds of a Tropical Wet Forest. *The Condor* 97:853–78.

- Stiller J, Zhang G. 2019. Comparative Phylogenomics, a Stepping Stone for Bird Biodiversity Studies. *Diversity* 11:115.
- Stoddard MC, Prum RO. 2011. How colorful are birds? Evolution of the avian plumage color gamut. *Behav Ecol* 22:1042–52.
- Stoddard MC, Yong EH, Akkaynak D, Sheard C, Tobias JA, Mahadevan L. 2017. Avian egg shape: Form, function, and evolution. *Science* 356:1249–54.
- Swaddle JP, Lockwood R. 1998. Morphological adaptations to predation risk in passerines. *J Avian Biol* 29:172–76.
- Swaddle JP, Lockwood R. 2003. Wingtip shape and flight performance in the European Starling *Sturnus vulgaris*. *Ibis* 145:457–64.
- Taylor G, Thomas A. 2014. *Evolutionary Biomechanics* Oxford University Press.
- Temeles EJ, Koulouris CR, Sander SE, Kress WJ. 2009. Effect of flower shape and size on foraging performance and trade-offs in a tropical hummingbird. *Ecology* 90:1147–61.
- Vanhooydonck B, Herrel A, Gabela A, Podos J. 2009. Wing shape variation in the medium ground finch (*Geospiza fortis*): an ecomorphological approach. *Biol J Linn Soc* 98:129–38.
- Verbeek NAM. 1975. Comparative Feeding Behavior of Three Coexisting Tyrannid Flycatchers. *Wilson Bull* 87:231–40.
- Waldrop LD, He Y, Hedrick TL, Rader JA. 2020. Functional Morphology of Gliding Flight I: Modeling Reveals Distinct Performance Landscapes Based on Soaring Strategies. *Integr Comp Biol* 60:1283–96.
- Walker JA. 2010. An Integrative Model of Evolutionary Covariance: A Symposium on Body Shape in Fishes. *Integr Comp Biol* 50:1051–56.
- Wang X, Nudds RL, Palmer C, Dyke GJ. 2012. Size scaling and stiffness of avian primary feathers: implications for the flight of Mesozoic birds. *J Evol Biol* 25:547–55.

1.4 Figures

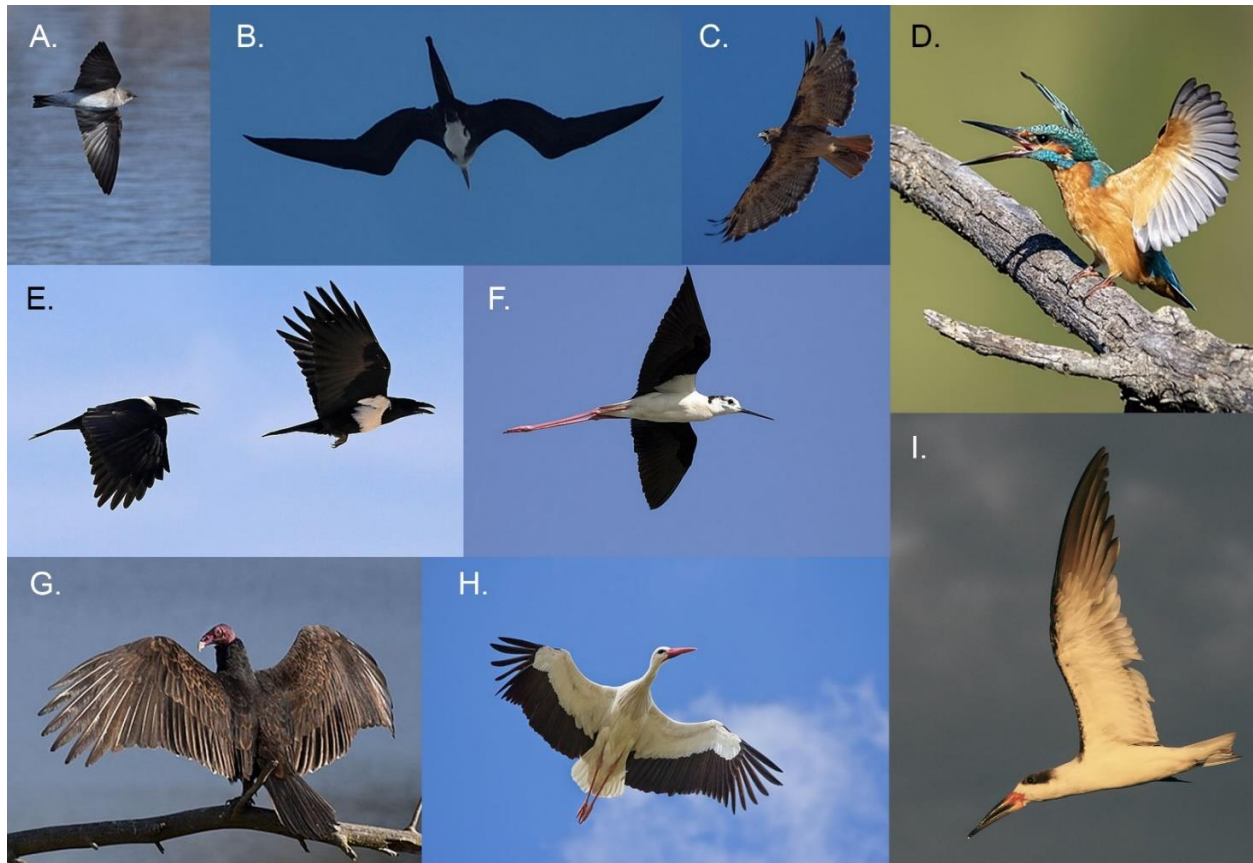


Figure 1.1 Birds are diverse in their body size and their wing morphology, as exemplified by a small sample of bird species: A. tree swallow (*Tachycineta bicolor*), B. magnificent frigatebird (*Fregata magnificens*), C. red-tailed hawk (*Buteo jamaicensis*), D. common kingfisher (*Alcedo atthis*), E. pied crow (*Corvus albus*), F. black-necked stilt (*Himantopus mexicanus*), G. turkey vulture (*Cathartes aura*), H. white stork (*Ciconia Ciconia*), I. black skimmer (*Rynchops niger*). Image credits: panes A. – H. creative commons license from Wikimedia Commons. Pane I.: Jonathan Rader.



Figure 1.2 The NextEngine 3D Scanner Ultra HD, with integrated turntable. Image credit: NextEngine, inc.

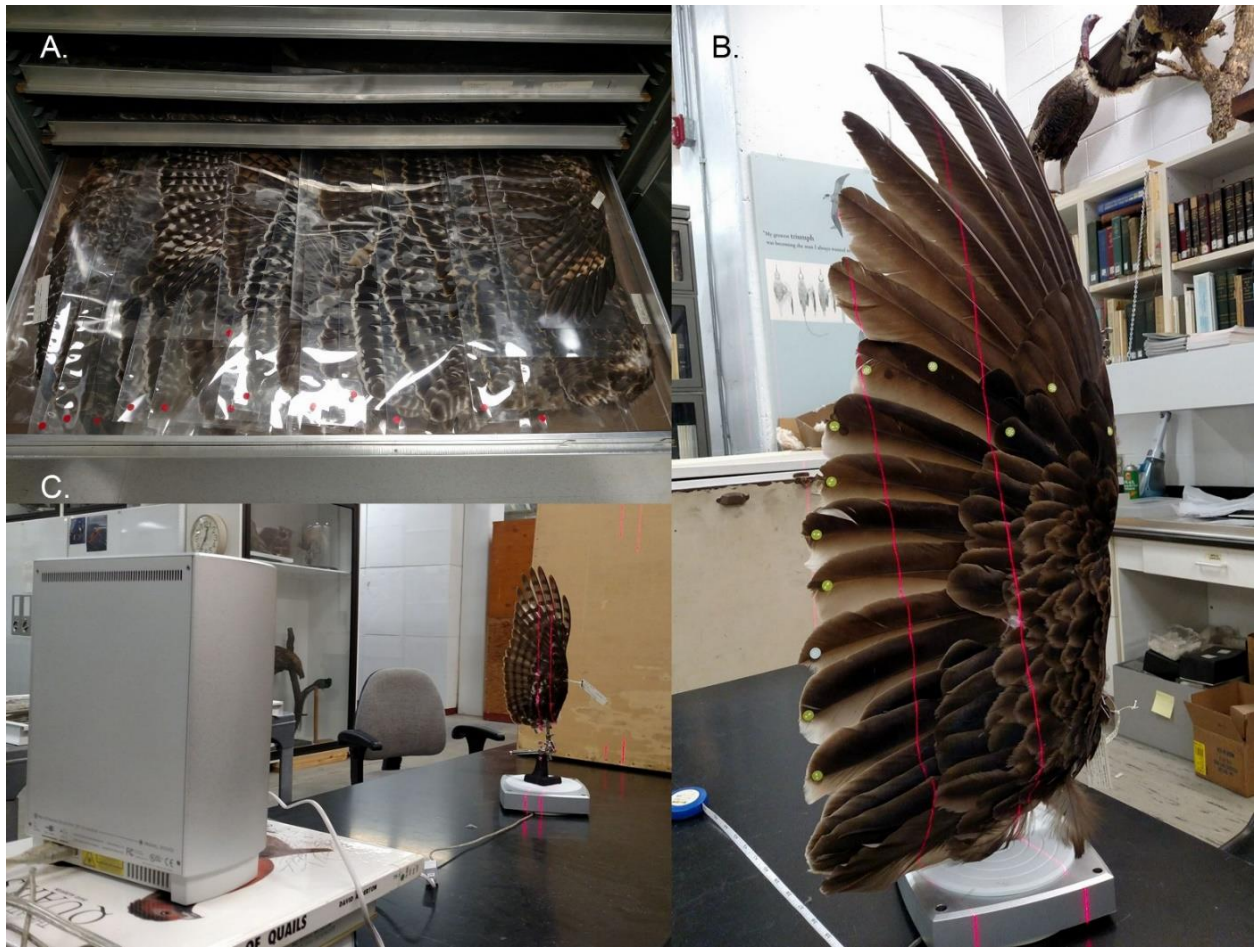


Figure 1.3 Spread wings were loaned from the collections at the North Carolina Museum of Natural Sciences in Raleigh, NC. (A.). I used a Nextengine 3D Scanner Ultra HD laser scanner to collect 3D data from preserved wings (B.). The wings were mounted to a vertical stand on an automated turntable (C.) to permit the scanner to automatically rotate the wings and collect data from multiple angles.

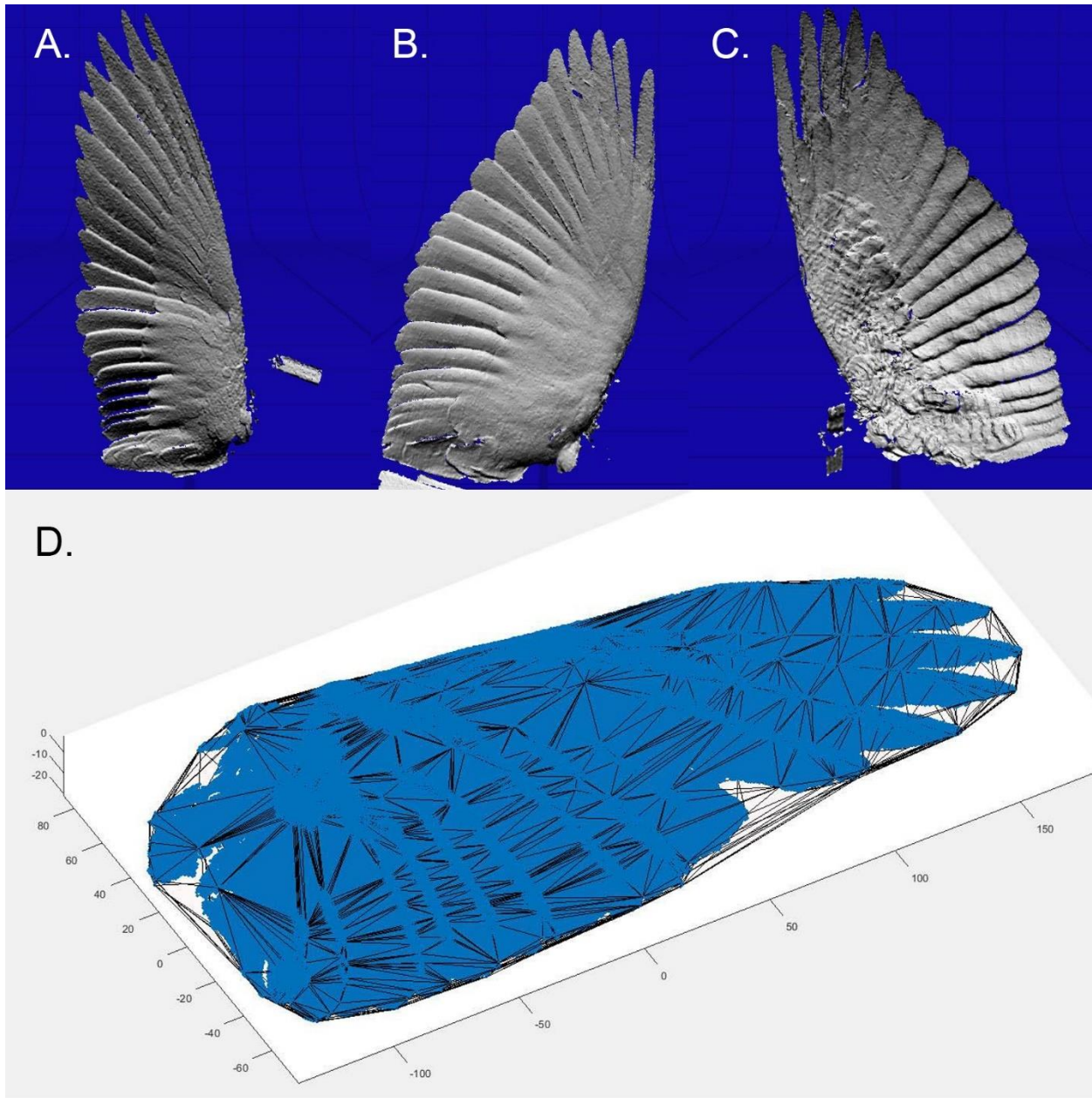


Figure 1.4 The upper surface of the scan output for a peregrine falcon (*Falco peregrinus*) wing (A.), the upper (B.) and lower (C.) surfaces of a Cooper's hawk (*Accipiter cooperi*) wing. Scans not only captured overall shape, but also preserved surface detail, as demonstrated by panels A – C. Hulls that conformed to the surface of the scanned wings (as seen in D.) were fitted to each wing to measure wing volume.

CHAPTER 2: ALLOMETRY, ISOMETRY, AND A PARADOX: BODY SIZE AFFECTS THE EVOLUTION OF AVIAN WING SHAPE

2.1 Introduction

2.1.1 *A matter of size: scaling of wing morphology*

Body size influences numerous aspects of avian biology (Lindstedt and Calder 1976; Case et al. 1983; e.g., Brooke et al. 1999; Lovvorn and Liggins 2002; Speakman 2005, and many more; Brumm 2009; Olson et al. 2009), and its effects on locomotion are especially pronounced (Fedak et al. 1982; Heglund, Cavagna, et al. 1982; Heglund, Fedak, et al. 1982; Taylor et al. 1982; Tobalske and Dial 2000; Lovvorn et al. 2001; Lovvorn and Liggins 2002). Body size scaling poses a challenge to fliers because of the different dimensionality of wing area (S , proportional to length²) and body mass (M_b , which is proportional to volume, i.e., length³). If we consider two hypothetical geometrically-similar birds that differ only in their body size, the larger bird will have proportionally smaller wings following an isometric scaling relationship of:

$$S = M_b^{0.67}$$

In this scenario, the larger bird will also display greater wing loading – the proportion of mass supported by each unit of wing area (Warham 1977; Vogel 1981). The amount of lift force that is produced to offset body weight in flight is proportional to wing area:

$$F_L = \frac{1}{2} \rho C_L S V^2$$

where S is wing planform area (Vogel 1981), in addition to air density (ρ) and flight speed (V). Lift is also affected by aspects of wing geometry such as camber (Shyy et al. 1999; Brown 2001; Null and Shkarayev 2005; Gamble et al. 2017), which modulates the coefficient of lift (C_L in the above equation). Because the isometric scaling of wing area may physically limit the ability to fly, one might predict that wing area would scale with positive allometry, such that larger birds have disproportionately large wings corresponding with their increased mass, maintaining functional similarity (Greenewalt 1975; Rayner 1988). Paradoxically, however, prior studies of wing scaling have found that wing area scales with negative allometry (e.g., $M_b^{0.53}$ for songbirds, $M_b^{0.56}$ in shorebirds, $M_b^{0.57}$ in ducks, Greenewalt 1975; and $M_b^{0.58}$ in procellariiform seabirds, Warham 1977). Large birds can also offset the deleterious effect of their relatively small wing areas by flying faster, as lift forces are a function of V^2 . Indeed, Alerstam et al. (2007) have shown that average flight speed increases with body size. That said, cruising speed is only part of flight, and large birds are still likely to encounter difficulties imposed by their reduced wing area during slow-speed landing and takeoff.

Many studies of wing allometry in birds have focused on one or a handful of taxonomic groups. The various life histories, flight and foraging modes, and migratory strategies among bird taxa impart unique constellations of selective pressures upon locomotor morphology. For example, soaring birds have proportionally longer wings than non-soarers (Taylor and Thomas 2014), and wing chord is greater in birds that soar over land when compared to seabirds (Taylor and Thomas 2014). Migratory birds have been shown to have adaptations that reduce distal

wing mass and enhance energetic efficiency, such as more pointed wingtips both among taxa (Mönkkönen 1995; Lockwood et al. 1998; Rader et al. 2015) and within individual species (Mulvihill and Chandler 1990; Copete et al. 1999; Arizaga et al. 2006; Baldwin et al. 2010, but see Grilli et al. 2017). Risk of predation from aerial-hunting raptors is also associated with pointed wingtips (Swaddle and Lockwood 1998). It is also reasonable to suspect that the diversity of ecology and flight requirements among taxa influences within-lineage scaling of wing area, limiting the generalizability of taxon-specific scaling studies.

Rayner (1988) leveraged data from multiple sources to do a taxonomically-broad assessment of wing scaling, finding the predicted positive allometry in both wing length ($M_b^{0.39}$) and wing area ($M_b^{0.72}$). However this work was done before the advent of modern phylogenetic techniques, and phylogenetic covariance among taxa can bias estimates of slope in sometimes unpredictable ways (Felsenstein 1985). Taylor and Thomas (2014) conducted a phylogenetically-aware reappraisal of wing scaling using the dataset from Rayner (1988), and found a scaling relationship ($M_b^{0.668}$) which was indistinguishable from isometry. These authors also pointed out, however, that the dataset was a composite from sources using disparate methods of measurement, and potentially varying degrees of precision. Nevertheless, the isometric scaling of wing area with respect to body mass found by Taylor and Thomas (2014) is the best existing picture of how wing size scales with body size among birds. Their result suggests that larger birds are indeed at a disadvantage relative to small birds, and begs the question whether other shape traits scale differently and could potentially offset consequences of reduced wing area on aerodynamic force production.

2.1.2 *Wings are 3-dimensional structures*

Wings are not just 2-dimensional (2D), planform structures, but also have important 3-dimensional (3D) shape attributes including, but not limited to, the linear thickness of the wing cross section (XST), the cross-sectional area of the wing (XSA), the upward curvature of the wing surface (camber, Q), and the distribution of these attributes along the span of the wing. These traits have important implications for the aerodynamics, moment of inertia, and structure of the wing, and are likely to experience body size-related selective pressures.

2.1.3 *Camber: maintaining lift with less wing area?*

All else being equal, the lift produced by a wing is proportional to its area and thus positive allometry of wing area is required to maintain the ratio of lift produced relative to body mass. However, all else need not be equal, and other aspects of airfoil shape can also compensate for reduced wing area by increasing the wing's coefficient of lift (Withers 1981). Camber, the upward curvature of the wing surface, is one such attribute, and the best candidate for adaptation among birds. There has never been a comprehensive study of camber among birds, and little is known about the effects of wing camber for fliers in the size range of most birds (but see Waldrop et al. 2020a). However, empirical studies of wing aerodynamics of micro air vehicles and model airplanes suggest that wing camber should increase with the size of the aircraft to maintain optimal performance (Schmitz 1967; Brown 2001; Null and Shkarayev 2005). I therefore predicted a positive relationship between body mass and camber.

2.1.4 *Wing thickness: maximize stiffness or minimize drag?*

Wings must have appropriate shape for producing the aerodynamic forces necessary for flight (Rayner 1988), but they must also be stiff enough to support the load imposed upon them by the birds' body weight and the forces generated by flapping and maneuvering (van den Berg and Rayner 1995). The long bones of the wing (the humerus and radius/ulna) are the load-bearing members within the armwing. These bones can be considered as cantilever beams supporting body weight. The ability of a beam to resist bending under load is proportional to its length and the second moment of its cross-sectional area, so a model of bending load should predict the thickness of the wing skeletal elements. The minimum bound of total wing thickness is set by the thickness of the skeleton, and should therefore be similarly predictable by modeling bending load. Additional wing thickness is likely to be related to the aerodynamic function of the wing. Thicker wings present more frontal area to the air, increasing profile drag (Vogel 1981), and wing thickness is likely linked to wing camber and thus lift production (Shyy et al. 1999; Brown 2001). Because wing thickness also affects aerodynamic properties, how the thickness of the wing skeleton influences the shape of the overall wing is less clear, and creates a scenario of competing pressures.

2.1.5 *Wing cross-sectional area: minimize cost of flapping or facilitate maneuvering?*

Because the wing has thickness, it also has volume and by extension, mass. Further, the thickness of the wing is not uniformly distributed along the length of the wing, meaning that neither is its mass. The distribution of mass along the wing has implications for its moment of inertia, and therefore on the cost of accelerating the wing during flapping flight (van den Berg

and Rayner 1995; Hedrick et al. 2004). Flapping fliers can also use their wing inertia to initiate maneuvers (Lin et al. 2012; Bergou et al. 2015). Detailed discussion of the distribution of wing volume will follow in Chapter 5 of this thesis. To my knowledge, there has never been a systematic study of how wing volume scales with respect to body size in birds, which is what I will address here. Wing volume shares dimensionality with body mass (i.e., length³), so the expectation for isometric scaling with respect to body mass is M_b^1 , scaling of wing volume is expected to be tied to scaling of wing area. If wing area scales allometrically, wing volume is likely to follow, though this relationship may be disrupted by opposing scaling of wing thickness.

2.1.6 *Summary and predictions*

Herein, I present a new dataset of wing shape and size featuring 178 species from a broad range of avian lineages. I used phylogenetically-informed analyses to describe the scaling of 2-dimensional wing shape traits: wing length, chord and planform area in bird wings across this broad taxonomic sample of birds. I also measured and tested scaling of 3-dimensional attributes: wing cross-sectional thickness, camber and wing volume. Given the lengthy history of such studies, I predicted results similar to prior work with scaling relationships estimated by phylogenetic regression falling somewhere between the isometric expectation and the allometry described by Rayner (1988).

I also explored the apparent mismatch between wing size and body size scaling in two ways. 1) I investigated how the flight feathers and the bones of the wing scale with respect to body mass, in an effort to identify what components of the wing exert constraint on the

evolution of wing size. And 2) I tested whether wing camber, a 3D property of the wing, can provide partial compensation for reduced wing area in large birds. To this end, I predicted that wing camber would increase with body size, as greater wing camber increases the coefficient of lift and enhances area-specific lift production.

Finally, I tested a hypothetical tradeoff between the aerodynamics of the wing and its structural rigidity to determine if the thickness of the wing is evolutionarily coupled with the underlying skeleton and structural support requirements, or separately shaped by aerodynamic performance. I predicted that the skeleton thickness would be related to load bearing. I had competing predictions that the overall thickness of the wing would be minimally bounded by skeletal thickness, but that additional wing thickness beyond that of the wing bones would be best predicted by other shape attributes of the wing, suggesting aerodynamic functionality is the leading selective pressure on the surface geometry of the wing.

2.2 Methods

2.2.1 Wing scanning, scan processing, and shape analysis

Spread wings representing a diverse sample of bird species were loaned from the North Carolina Museum of Natural Sciences (NCMNS, Raleigh, NC), and I collected shape data from them using a NextEngine 3D Scanner Ultra HD laser scanner (NextEngine, Inc., Santa Monica, CA; see Fig. 1). Because the optical properties of feathers differ between the upper and lower surfaces of the wing, each wing was scanned in two parts and then reassembled using Meshlab 3D editing software (Cignoni et al. 2008). I analyzed 2D and 3D shape variables from the wing scans. When there were sufficient samples from the collection, I randomly selected and

scanned 16 individuals per species, attempting to maintain a balanced sex ratio. The scanned wings were stripped down to their vertices, and the shape of the resulting point clouds were analyzed using custom programs in MATLAB (The MathWorks, Natick, MA, USA); statistical analyses were conducted in R (R Development Core Team 2013). From each wing, I measured wing length (W_L), mean chord (W_C), planform area (S_p), frontal area (S_f), and wing volume (W_V). I calculated wing aspect ratio as:

$$AR = \frac{4W_L^2}{S}$$

Body mass (M_b) was obtained from the museum tag data associated with the wing specimens. Species for which mass data were not recorded on tags were supplemented with mean mass values from the CRC Handbook of Avian Masses (Dunning Jr. 2007).

The proximal portion of the wings were subject to variable preservational artifacts, owing to their removal from the birds' bodies during specimen preparation. Therefore, the proximal 1/3rd of the arm wing was excluded from analyses. The remainder of the wings were subdivided into chord-wise slices along their length, with the width of the slices scaled to 1/25th of the distance between the wingtip and the wrist joint. This standardized the number of slices representing the hand portion of the wing, facilitating direct comparison across samples and taxa. The number of slices representing the arm portion of the wing varied phylogenetically, as wing proportions differ among species and higher order taxonomy. From each of these slices I measured wing chord (W_C), maximum section thickness (XST , the maximum distance between the upper and lower wing surfaces), and cross-sectional area (XSA). The volume of each slice

was estimated by multiplying the cross-sectional area by the width of the slice. Analyses of the slice-wise measures will be discussed at length in Chapter 5.

2.2.2 Measurements of the wing skeleton

Bird skeletons were sourced from the collection at the NCMNS in Raleigh, NC. Each specimen was photographed against a black cloth using a Canon EOS 6D digital SLR camera (Canon, Inc.) mounted on a tripod. Two photographs were taken of each specimen, and the results averaged. A ruler was placed in the photo frame for calibration. A custom MATLAB graphical interface was created to facilitate digitizing and measuring the length along the longest axis of the humerus, radius, and ulna, as well as their diameters at mid-shaft. Body mass for each specimen was recorded from the museum tags, and when not available, supplemented from the CRC Handbook of Avian Masses (Dunning Jr. 2007).

2.2.3 Measurements of primary flight feathers

The lengths and rachis diameters were measured using digital calipers with a precision of ± 0.05 mm from the twelve distal-most flight feathers in a broad taxonomic sample of preserved wings from the NCMNS (see Fig. 2). Because the number of primary feathers varies from 9 to 11 among clades, this series represents the whole primary series, and a variable number of distal secondaries.

2.2.4 *Phylogenetic Analyses*

Phylogenetic trees were pruned from the Jetz et al. supertree (Jetz et al. 2012), acquired from birdtree.org (Rubolini et al. 2015). I calculated phylogenetic signal (both Pagel's λ and Blomberg's K) for all of the wing shape, skeleton, and feather traits using the '*phylosig*' function in the '*phytools*' package (Revell 2012) in the R statistical computing environment (R Development Core Team 2013).

2.2.5 *Describing scaling relationships*

Scaling relationships between the variables were explored using both Phylogenetic Generalized Least Squares (PGLS) regression, and non-phylogenetic generalized linear models (GLM). The use of both model types allowed us to assess whether my results were robust to varying assumptions of phylogenetic relatedness. PGLS models were conducted on \log_{10} -transformed variables using '*pgls*' function in the '*caper*' package in R, using a maximum-likelihood method to estimate the optimal value of Pagel's lambda (λ). Wald Chi-squared tests were used to determine if scaling factors diverged significantly from the assumption of isometry. I also, separately, conducted PGLS regressions optimizing Pagel's delta (δ) and kappa (κ) to assess the robustness of the outcomes to transformations of branch lengths, and thus to varying assumptions of evolutionary dynamics.

2.2.6 *Evolutionary dynamics of wing shape*

I used the '*fitcontinuous*' function in the *phytools* R package (Revell 2012) to model evolutionary dynamics of each measured wing shape trait. I fit four models of evolution

(Brownian motion, Ornstein-Uhlenbeck, early-burst, and white-noise) to each shape trait.

Akaike's Information Criterion, corrected for small sample size (AICc) was used to choose the best-fit model. I extracted the evolutionary rate parameter (σ^2) from the best-fit model. The magnitude of σ^2 scales with the magnitude of the modeled trait, so to facilitate comparison of evolutionary rate among shape traits with different magnitudes, I rescaled each shape trait to a 0 – 1 scale and recalculated σ^2 using *'fitcontinuous'* with the previously determined evolutionary model.

2.2.7 Hypothesis testing: What predicts wing thickness?

I assembled a suite of phylogenetically-aware multiple regression models that considered wing thickness in the handwing and the armwing as functions of a prediction of load derived from beam theory and the 2nd moment of area of a cylinder (since the wing bones are roughly cylindrical in shape):

$$\text{Wing thickness} \propto (\text{Mass} \cdot \text{Wing Length})^{1/4}.$$

Note that this model does not assume any particular internal geometry for the wing bones, but does assume all taxa have a similar internal bone geometry. I further tested wing thickness against other models that considered thickness as a function of W_C and W_L , as well as their interactions. I also tested a model of wing thickness as an allometric function of body mass. I assessed the relative predictive power of these models using AICc. These tests were iterated to predict humerus diameter and the combined diameters of the radius and ulna as the response variables.

2.3 Results

2.3.1 Datasets

I scanned 1096 wings of 178 species of birds (see Fig. 1) in 15 major lineages (Fig. 2), including owls and hawks, seabirds, ducks, doves, shorebirds, and numerous lineages of songbirds. The feather and skeletal datasets include 180 and 217 individuals from 87 and 64 species, respectively (see Fig. 3). The diversity of sampled lineages is similar among the datasets, though there is imperfect overlap in species and little overlap of individuals resulting from the preservation priorities of the museum.

2.3.2 *On the utility of spread wings*

I focused on my measurements of wing camber to test the quality and usability of data acquired from scanning preserved spread wings because it is a dimensionless quantity, meaning that preservation-induced variance is not expected to change as a function of its magnitude. Also, if preservation or storage methods alter wing shape, camber is likely to be the most sensitive, obliterating signal at the level of taxonomic groups. Estimated phylogenetic signal was high ($\lambda > 0.8$) for camber in the handwing and the armwing across multiple tests, which I interpret to mean that preservational artifacts are relatively minor and do not impact the interpretability of my analyses of wing shape.

2.3.3 *External wing morphology*

There was a 300-fold range of median body size among the species in my sample, ranging from 6.75 to 2,060 g. There was high phylogenetic signal in body size ($\lambda = 0.89$). Overall

wing dimensions (W_L , S_P , and W_V) scaled with negative allometry ($M_b^{0.29}$, $M_b^{0.59}$, and $M_b^{0.91}$, respectively; see Table 1) in phylogenetically-informed analyses, contrasting with the results of non-phylogenetic regression ($M_b^{0.37}$, $M_b^{0.66}$, and $M_b^{1.08}$, respectively; Table 2). Wing chord also showed negative allometry in both the handwing and the armwing ($M_b^{0.28}$ and $M_b^{0.27}$) in both phylogenetic and non-phylogenetic models. Cross-sectional thickness of the wing showed slightly negative allometry in the armwing ($M_b^{0.30}$) and positive allometry in the handwing ($M_b^{0.38}$). Phylogenetic signal was high in all allometric relationships ($\lambda > 0.73$; Table 1). There is no theoretical scaling expectation for wing camber, but camber showed a positive relationship with body size. Interestingly, the camber scaling factor was greater in the handwing ($M_b^{0.019}$, $\lambda = 0.85$) than in the armwing ($M_b^{0.009}$, $\lambda = 0.80$).

2.3.4 *Skeletal measurements*

Species median body mass in the skeletal dataset ranged from 8.8 to 3,727 g, and phylogenetic signal was high ($\lambda = 1.0$). Humerus, radius and ulna lengths scaled with positive allometry ($M_b^{0.40}$, $M_b^{0.39}$, and $M_b^{0.39}$, respectively; see Table 1) in phylogenetic models. Non-phylogenetic models of the long bone lengths show similar positive allometry, but with slightly greater estimated scaling factors ($M_b^{0.43}$, $M_b^{0.41}$, and $M_b^{0.40}$, respectively; see Table 2). Both phylogenetic and non-phylogenetic models also show slightly positive allometry in the diameters of the humerus and radius (PGLS: $M_b^{0.36}$, $M_b^{0.36}$, respectively), but isometric scaling in the ulna ($M_b^{0.33}$). Phylogenetic signal was high in most skeletal traits ($\lambda > 0.85$), but somewhat moderate for ulna diameter ($\lambda = 0.65$). The radius and ulna form a unit that shares load-bearing,

so I also tested scaling of their combined diameters and found that the composite diameters scale isometrically ($M_b^{0.34}$).

2.3.5 *The primary flight feathers*

The range of species median body masses in the feather dataset was greater than in the scan or skeletal dataset, from 3.1 to 5,118 g, and phylogenetic signal of body mass was high ($\lambda = 0.82$). Average length of the primary feathers and of the distal secondary scaled isometrically with respect to mass ($M_b^{0.34}$, $M_b^{0.35}$, respectively) in both phylogenetic and non-phylogenetic models. Phylogenetic signal was high in models of feather length scaling ($\lambda = 0.99$). However, mean rachis diameter showed strong positive allometry ($M_b^{0.41}$), and phylogenetic signal was moderate ($\lambda = 0.69$).

2.3.6 *Evolutionary dynamics*

2.3.6.1 *Mode*

The AICc preferred model of evolution (evolutionary mode) differed among wing shape traits. Phylogenetic covariance was important in all traits, and white noise was not the preferred model in any case. Brownian motion (BM) was the preferred model (all AICc weights > 0.5, see Table 3) for wing chord (in both the handwing and the armwing), diameters of the wing bones, and primary and secondary feather lengths. An early burst (EB) model was preferred (all AICc weights > 0.45) for wing area, wing volume, XST_{HW} as well as humerus length. The early burst model was also favored for the length of the radius (AICc weight = 0.47), but perplexingly not for ulna length (AICc weigh = 0.37 vs. 0.48 for a BM model). Evolutionary mode of wing length,

camber (in both the handwing and armwing) and XST_{AW} is best described by an Ornstein-Uhlenbeck (OU) model (all AICc weights > 0.4).

2.3.6.2 Tempo

Evolutionary rate (σ^2) estimates vary with the magnitude of the trait, rendering comparison among traits that differ in size futile. To facilitate comparison of σ^2 among traits, I normalized each trait to a 0 to 1 range, and estimated σ^2 using the best-fit evolutionary model from the non-normalized data. There was five-fold variation in normalized σ^2 (Table 3).

Evolutionary rate was generally higher in traits that showed OU and EB modes than in traits best modeled by BM (see Table 3).

2.3.7 Hypothesis testing: What predicts wing thickness?

I used a model selection framework to test among several models predicting the average thickness of the wing, as well as thickness in the handwing and the armwing, and the diameters of the long bones of the wing. A model including W_C , W_L , and their interaction were the best predictors of average wing thickness (AICc weight = 0.89, see Table 4). Thickness of the armwing was best predicted by W_C and W_L , but without the interaction term (AICc weight = 0.60), however the model including the interaction also received some support (AICc weight = 0.40). The model of bending load fared poorly in both cases (AICc weight = 0.00), as did M_b (AICc weight = 0.00). In contrast, handwing thickness and the diameters of the skeletal elements are best predicted by bending load (all AICc weights > 0.80), with aspects of 2D wing shape garnering less support (all AICc weights < 0.10).

2.4 Discussion

2.4.1 *A paradox remains: negative allometry of wing size*

2.4.1.1 Why do big birds have (proportionally) small wings?

Prior estimates of the scaling relationship between wing area and body size have ranged from strongly negative allometry, approximately $M_b^{0.55}$ (Greenewalt 1975; Warham 1977) to strongly positive, $M_b^{0.72}$ (Rayner 1988) with non-phylogenetic methods. The studies that found negative allometry were restricted in their phylogenetic scope, potentially limiting their generalizability. Rayner (1988) pooled data from those individual lineages and added additional data, however the results of his analysis were potentially biased by the underlying phylogenetically-imposed covariance structure of the data (Felsenstein 1985; Taylor and Thomas 2014). A reanalysis of the same data that accounted for phylogenetic covariance found a scaling factor of $M_b^{0.668}$, statistically identical to the expectation from isometry (Taylor and Thomas 2014). As noted by Taylor and Thomas (2014), the dataset used for these analyses was compiled at different times and by different researchers, and may therefore be subject to unquantifiable error impacting the scaling factor estimated across bird lineages, despite the authors' best efforts to avoid such difficulties. Here, I have collected and analyzed a new dataset of bird wing size and shape. The new dataset has a broad taxonomic sample, and data were collected in a consistent and robust manner, thus bypassing potential pitfalls inherent to the prior composite dataset.

I found significant negative allometry of wing area with respect to body size (PGLS, $M_b^{0.59}$, Table 1) that most closely resembles the lineage-specific relationships found by

Greenewalt (1975) and Warham (1977). Phylogenetic signal in the model was high ($\lambda = 0.92$) suggesting that the phylogeny contributes considerably to the result. However, I also tested the scaling relationship without phylogenetic correction, finding a scaling factor of $M_b^{0.66}$ – the isometric expectation. Additionally, I found negative allometry in the basic components of wing area: wing length ($M_b^{0.29}$, see Table 1) and chord measured in both the handwing and the armwing ($M_b^{0.28}$ and $M_b^{0.27}$ respectively, Table 1). Taken together, my results reaffirm the paradox: larger birds have disproportionately small wings, contrasting with *a priori* predictions of positive allometry that would maintain aerodynamic lift production in proportion to body mass (Greenewalt 1975). I posit that these results imply constraint on the evolution of wing size in birds, which I will explore in the following paragraphs.

Bird wings are complex structures composed of multiple tissue types, each with their own material properties and structural and evolutionary tradeoffs that shape the overall wing (Pennycuik 1967, 1989; Norberg 1990; Habib and Ruff 2008). I assembled datasets of skeletal and feather dimensions, in addition to the dataset of external wing morphology from 3D scanned wings. Scaling and size-related effects of skeletal and feather morphology have both been explored in prior work (Worcester 1996; Nudds 2007; Nudds et al. 2011; Wang et al. 2012; Sullivan et al. 2019), however, to my knowledge these traits have not previously been considered in tandem in a phylogenetic context. Concurrent analysis of outer wing morphology, paired with scaling of the wing skeleton and feathers may shed light on the factors that limit wing scaling in birds.

2.4.1.2 Building bigger wings: scaling of the wing skeleton and feathers

I found that the length of the long bones in the wing scaled with significant positive allometry ($M_b^{0.40}$ in the humerus and $M_b^{0.39}$ in the radius and ulna), which largely agrees with prior results (Nudds 2007). So, larger birds have proportionally longer wing skeletons, while at the same time, the overall length of their wings, on average, are shorter, meaning that the proportion of wing length comprised by the skeleton increases with body size. The long bones of the wing are the weight-bearing components of the wing during flight and are subject to their own dimensional mismatch constraint. If the wing is modeled as a cantilever beam, fixed to the body and supporting its weight through lift generated along its length, beam theory suggests that the diameter of the beam (in this case the wing skeleton, which is bearing the load) should be proportional to both the load and to the length of the beam (Vogel 2013; Sullivan et al. 2019), which in this case is overall wing length, as aerodynamic forces are distributed across the surface of the wing, not its skeleton. Longer wings thus necessitate thicker wing bones, though negative allometry of wing length may help manage this effect. Compounding this, the load that they support is proportional to a volume (i.e., length³), meaning that larger birds (with longer wings) also must support a disproportionately great load, necessitating even greater skeletal thickness, and implying that the diameters of the bones should show positive allometry to maintain similar structural rigidity across body sizes. Defying this prediction, the diameters of the humerus and radius in my sample scaled with weakly positive allometry ($M_b^{0.36}$ for both), while the diameter of the ulna and the combined diameters of the radius and ulna scaled isometrically ($M_b^{0.33}$). Even though the skeleton displays positive length allometry, the degree to which wing length can scale via skeletal hypertrophy may be

limited by structural constraint. Further, skeletal allometry may be limited by the tensile strength of bone (Sullivan et al. 2019).

The primary flight feathers are components of overall wing length (and especially of the handwing) in the distal portion of their series, while the proximal ones converge with the length of the secondary feathers and form a component of wing chord. Combined, they define the area of the handwing. The length of the secondary flight feathers is correlated with wing chord (Lockwood et al. 1998). The number of secondary feathers in the wing is related to the length of the wing (especially the armwing), and varies among taxa (Sibley et al. 2009). Much attention has been paid to the relative lengths of the primary feathers, wingtip geometry, and its correlates in other aspects of bird biology (Mulvihill and Chandler 1990; e.g., Lockwood et al. 1998; Stoddard et al. 2017, and many more; Sheard et al. 2019, 2020; Pigot et al. 2020).

Despite the documented diversity in wingtip shape, there has been less focus on how the evolutionary lability of feather dimensions may constrain overall proportions of the wing. Mean primary feather length scaled isometrically ($M_b^{0.34}$) in my sample and in prior work (Worcester 1996; Wang et al. 2012; $M_b^{0.30}$, Sullivan et al. 2019). The length of the distal secondary feathers in my sample also scaled isometrically with respect to body mass ($M_b^{0.35}$), contrasting with negative allometry of wing chord in both the handwing and the armwing. Worcester (1996) also tested feather flexibility, and showed that despite maintaining geometric similarity, feather stiffness decreased significantly as body size increased. That the structural strength of the feathers decreases as their size increases may impose an upper limit on their size, and by extension, on the planform area of the handwing.

The nature of the feathers, as a biological tissue may play a role in size-related scaling not just of the feathers themselves, but also of the wing surface. Feather keratin is a metabolically inert tissue, meaning that feathers experience substantial degradation over time, and do not get repaired. Therefore, they must be periodically molted and regrown, affecting numerous aspects of avian biology (Miller 1941; Tucker 1991a; Murphy 1996; Chandler et al. 2010). Moreover, producing new feathers has been shown to be costly (Murphy 1996; Guillemette et al. 2007), potentially imposing energetic constraints on the size of feathers. Finally, feather replacement during molt takes disproportionately longer in large birds (Rohwer et al. 2009), potentially further limiting the overall scaling of wings with respect to body size.

2.4.1.3 Beyond simple measurements: posture affects wing geometry

Positive length allometry within the wing skeleton and isometry of the primary feather lengths would still imply positive allometry of the overall wing, however this view neglects the contribution of wing posture. Wing length is also affected by the neutral posture of the shoulder, elbow, and wrist joints when the wing is extended. It is possible that the amount of joint flexion in the neutral extended position of the wing also varies with body size and flight style or phylogeny. Neutral joint angle may be a primary determinant of wing aspect ratio, especially at large body sizes. If the lengths of the wing bones and feathers are held constant, wings with neutral joint positions that are more extended (joint angles approaching 180°) will have greater overall lengths than if the neutral joint angles are more flexed (smaller joint angles). Wing chord should exhibit an opposing trend, with more flexed joints producing a shorter but broader wing. Albatrosses ($M_b \approx 8$ kg, $AR \approx 15$; Shaffer et al. 2001) may exemplify the extended joint angle format, while vultures et al. ($M_b \approx 2$ kg, $AR \approx 6$; present dataset) might

have more flexed neutral joint angles. Furthermore, because neutral joint angle is unlikely to be impacted by size-related constraints caused by material properties or dimensional mismatch, and given its effect on overall wing geometry, it may be especially evolutionary labile. Indeed, range of motion of the wing joints varies with flight style and among taxonomic groups, though less predictably with body size (Baliga et al. 2019b). However, Baliga et al. (2019b) did not assess whether neutral joint position varied with body size, so this remains an avenue for future pursuit.

Unfortunately, it is impossible to ascertain the relative proportions of skeleton and feather lengths in my sample, owing to the imperfect overlap of species and the fact that the skeletal, feather, and overall wing measurements were taken from different individuals. Additionally, I was unable to assess joint positions within the wings via surface scanning. Future work would benefit from methodology (for example, micro-CT scanning of spread wings) that permits concurrent measurement of these traits in addition to joint and skeletal geometry within the spread wings.

2.4.1.4 Resolving the paradox?

Despite the negative allometry of wing area, and the associated increase of wing loading, there are other traits that can offset the impacts on aerodynamic force production (Vogel 1981; Withers 1981; Pennycuick 1989; Norberg 1990). My results show that camber increases with body size in both the handwing and the armwing ($M_b^{0.019}$ and $M_b^{0.009}$, respectively), as does mean wing camber (see Fig. 7). Wing camber is correlated with maximum coefficient of lift (Withers 1981; C_L , Waldrop et al. 2020a). Values of C_L estimated for each of

the species in my scanned wing sample via fluid dynamics simulations (see Waldrop et al. 2020a for details on simulation methods) increased with wing camber, and with body size. The increase in C_L with body size indicates that size-related increases in wing camber can, at least in part, compensate for the relative loss of available wing area due to negative allometry by enhancing lift production. Furthermore, flight speed has also been shown to increase with body size and wing loading (Alerstam et al. 2007), providing a further mechanism of compensation for reduced wing area at cruising speeds, but still leaving necessary low-speed events such as takeoff and landing problematic for larger species.

2.4.2 *A mosaic of evolutionary dynamics*

Much like the assemblage of anatomical components in wing, evolutionary dynamics within the wing are a complex mosaic of varying tempos and modes, and unsurprisingly, body size seems to be a central feature in the broader picture of wing evolution. Body mass has high phylogenetic signal in all analyses, and is non-randomly distributed on the phylogeny (see Fig. 3). Other traits that have strong size-related effects are likely to show correlated evolution with body size. How this would be expected to manifest in shifting evolutionary modes is unclear, but the effect is rather apparent in the normalized evolutionary rates. Body size has one of the highest normalized evolutionary rates in my sample. Wing bone lengths and wing camber, which I have shown to be heavily influenced by body size, particularly those that also show allometric scaling relationships, have similarly high normalized σ^2 . Traits whose variance can be explained mostly by tree topology, i.e., those that follow a BM model of evolution, rather than

being drawn toward evolutionary optima (i.e., OU evolution) also seemed to have the lowest normalized σ^2 . Intriguingly, these traits also tended to follow isometric scaling patterns.

2.4.3 *Aerodynamics drive external wing shape while load shapes the skeleton*

Body size scaling imposes multiple and potentially competing tradeoffs for both the overall wing and its underlying skeletal support structure. A fundamental tradeoff is that thicker bones (and therefore thicker wings) are more resistant to bending, but also present greater frontal area to the air during flight and increase drag. Wing thickness may also be linked to wing camber, and therefore to the production of lift in unforeseen ways. To address the relative weight of each side of the stiffness vs. aerodynamics tradeoff, I tested the ability of multiple candidate models in a model selection framework to predict long bone diameter and overall wing thickness. I used an estimate of bending load derived from beam theory incorporating wing (beam) length and M_b , in addition to wing chord, wing length, the interaction of length and chord, and $M_b^{1/3}$ (correcting for the difference in dimensionality between a linear bone diameter and mass).

The model of bending load outperformed all others in its predictive power for the thickness of the handwing. I predicted that the load-bearing needs of the bones would set a minimum bound for the thickness of the wing, and the handwing results appear to bear this out. The handwing is largely composed of feathered wing surface, skin, connective tissues, and a small bony hand skeleton, which I was unable to measure due to lack of availability in the museum skeletal collection (these bones are very small and readily dissociate during

preservation). The skin and connective tissues tightly conform to the underlying skeleton in the handwing, not lending much additional thickness to the wing.

Thickness of the wing bones (humerus, radius, and ulna) and of the overall thickness of the wing diverged in the armwing (median $XST_{AW} = 1.36 \cdot$ median combined diameter of the radius and ulna), as did the models that predict those quantities. The models considering skeletal diameters as a function of bending load were, somewhat unsurprisingly, heavily favored by AICc, rather than any models including attributes of wing shape. In contrast, the overall thickness of the outer wing surface was best predicted by aspects of wing planform shape: wing length and chord. The nearest runner-up model also included length and chord along with their interaction. The bending load model received little support. These results indicate a decoupling of the wing surface from the underlying skeleton in the armwing, allowing independent evolution of each feature in response to opposing sides of the stiffness vs. aerodynamics tradeoff.

2.4.4 *Concluding remarks*

The influence of body size pervades all aspects of wing shape in its evolution. Here, I have presented a new dataset of wing morphology and provided an updated and phylogenetically-informed synthesis of how wing shape and size scale with body mass. My results confirmed prior observations that external features of wing shape do not scale with geometric similarity, but paradoxically show negative allometry. That is, they are smaller relative to body size than would be expected if birds were to maintain functional similarity across the range of their body size. In the absence of compensatory adaptations, that would

leave larger species at a comparative disadvantage in flight performance. On that account, my results show that wing camber increases with body size and can provide at least partial compensation by increasing the area-specific magnitude of lift produced by the wings.

To quantify tradeoffs and constraints on size-related diversification among wings, I collected complimentary measurements of wing skeletal morphology and primary feather dimensions to explore the relationships between these two critical units of the wing and overall wing morphology. While the wing skeleton sets the lower bound of wing thickness, as one would expect given that it must support the loads imposed by body mass and flight forces, this lower bound is not necessarily ideal aerodynamically. The armwing region shows decoupling of the outer wing surface from the underlying skeleton, with overall wing thickness there varying more predictably with other wing shape traits than with an estimate of load, presumably permitting the skeleton and wing surface to respond to different evolutionary pressures.

Despite making several advances here in the understanding of how the complex structures of the wing respond to size-related effects, much remains unknown. The contribution of neutral joint positions and resulting wing posture on outward wing morphology, in particular, is a direction that remains ripe for investigation. However, taken as a whole, my results here provide strong evidence that wings have multiple adaptive axes and that interact in an evolutionary tug of war of pressures and constraints, but that multiple configurations of morphology can potentially lead to similarly functional wings regardless of their size.

REFERENCES

- Alerstam T, Rosén M, Bäckman J, Ericson PG, Hellgren O. 2007. Flight speeds among bird species: allometric and phylogenetic effects. *PLoS Biol* 5:e197.
- Arizaga J, Campos F, Alonso D. 2006. Variations in wing morphology among subspecies might reflect different migration distances in Bluethroat. 83:8.
- Baldwin MW, Winkler H, Organ CL, Helm B. 2010. Wing pointedness associated with migratory distance in common-garden and comparative studies of stonechats (*Saxicola torquata*). *J Evol Biol* 23:1050–63.
- Baliga VB, Szabo I, Altshuler DL. 2019. Range of motion in the avian wing is strongly associated with flight behavior and body mass. *Sci Adv* 5:eaaw6670.
- Berg C, Rayner J. 1995. The moment of inertia of bird wings and the inertial power requirement for flapping flight. *J Exp Biol* 198:1655–64.
- Bergou AJ, Swartz SM, Vejdani H, Riskin DK, Reimnitz L, Taubin G, Breuer KS. 2015. Falling with Style: Bats Perform Complex Aerial Rotations by Adjusting Wing Inertia. *PLOS Biol* 13:e1002297.
- Brooke M de L, Hanley S, Laughlin SB. 1999. The scaling of eye size with body mass in birds. *Proc R Soc Lond B Biol Sci* 266:405–12.
- Brown CA. 2001. The Effect of Camber on Thin Plate Low Aspect Ratio Wings at Low Reynolds Numbers University of Notre Dame.
- Brumm H. 2009. Song amplitude and body size in birds. *Behav Ecol Sociobiol* 63:1157.
- Case TJ, Faaborg J, Sidell R. 1983. The Role of Body Size in the Assembly of West Indian Bird Communities. *Evolution* 37:1062–74.
- Chandler RM, Pyle P, Flannery ME, Long DJ, Howell SNG. 2010. Flight Feather Molt of Turkey Vultures. *Wilson J Ornithol* 122:354–60.
- Cignoni P, Callieri M, Corsini M, Dellepiane M, Ganovelli F, Ranzuglia G. 2008. MeshLab: an Open-Source Mesh Processing Tool. 8.
- Copete JL, Mariné R, Bigas D, Martínez-Vilalta A. 1999. Differences in wing shape between sedentary and migratory Reed Buntings *Emberiza schoeniclus*. *Bird Study* 46:100–103.
- Dunning Jr. J. 2007. *CRC Handbook of Avian Body Masses* CRC Press.

- Fedak MA, Heglund NC, Taylor CR. 1982. Energetics and mechanics of terrestrial locomotion. II. Kinetic energy changes of the limbs and body as a function of speed and body size in birds and mammals. *J Exp Biol* 97:23–40.
- Felsenstein J. 1985. Phylogenies and the Comparative Method. *Am Nat* 125:1–15.
- Gamble LL, Moosavian A, Inman DJ. 2017. Effects of Speed on Coupled Sweep and Camber in Morphing Wings. In: 55th AIAA Aerospace Sciences Meeting Presented at the 55th AIAA Aerospace Sciences Meeting. Grapevine, Texas: American Institute of Aeronautics and Astronautics.
- Greenewalt CH. 1975. The Flight of Birds: The Significant Dimensions, Their Departure from the Requirements for Dimensional Similarity, and the Effect on Flight Aerodynamics of That Departure. *Trans Am Philos Soc* 65:1–67.
- Grilli MG, Lambertucci SA, Therrien J-F, Bildstein KL. 2017. Wing size but not wing shape is related to migratory behavior in a soaring bird. *J Avian Biol* 48:669–78.
- Guillemette M, Pelletier D, Grandbois J-M, Butler PJ. 2007. Flightlessness and the Energetic Cost of Wing Molt in a Large Sea Duck. *Ecology* 88:2936–45.
- Habib MB, Ruff CB. 2008. The effects of locomotion on the structural characteristics of avian limb bones. *Zool J Linn Soc* 153:601–24.
- Hedrick TL, Usherwood JR, Biewener AA. 2004. Wing inertia and whole-body acceleration: an analysis of instantaneous aerodynamic force production in cockatiels (*Nymphicus hollandicus*) flying across a range of speeds. *J Exp Biol* 207:1689–1702.
- Heglund NC, Cavagna GA, Taylor CR. 1982. Energetics and mechanics of terrestrial locomotion. III. Energy changes of the centre of mass as a function of speed and body size in birds and mammals. *J Exp Biol* 97:41–56.
- Heglund NC, Fedak MA, Taylor CR, Cavagna GA. 1982. Energetics and Mechanics of Terrestrial Locomotion. IV. Total mechanical energy changes as a function of speed and body size in birds and mammals. *J Exp Biol* 97:57–66.
- Jetz W, Thomas GH, Joy JB, Hartmann K, Mooers AO. 2012. The global diversity of birds in space and time. *Nature* 491:444–48.
- Lin T, Zheng L, Hedrick T, Mittal R. 2012. The significance of moment-of-inertia variation in flight manoeuvres of butterflies. *Bioinspir Biomim* 7:044002.
- Lindstedt SL, Calder WA. 1976. Body Size and Longevity in Birds. *The Condor* 78:91–94.
- Lockwood R, Swaddle JP, Rayner JMV. 1998. Avian wingtip shape reconsidered: Wingtip shape indices and morphological adaptations to migration. *J Avian Biol* 29:273–92.

- Lovvorn J, Liggins GA, Borstad MH, Calisal SM, Mikkelsen J. 2001. Hydrodynamic drag of diving birds: effects of body size, body shape and feathers at steady speeds. *J Exp Biol* 204:1547–57.
- Lovvorn JR, Liggins GA. 2002. Interactions of body shape, body size and stroke-acceleration patterns in costs of underwater swimming by birds. *Funct Ecol* 16:106–12.
- Miller AH. 1941. The Significance of Molt Centers among the Secondary Remiges in the Falconiformes. *The Condor* 43:113–15.
- Mönkkönen M. 1995. Do migrant birds have more pointed wings?: A comparative study. *Evol Ecol* 9:520–28.
- Mulvihill RS, Chandler CR. 1990. The Relationship between Wing Shape and Differential Migration in the Dark-Eyed Junco. *The Auk* 107:490–99.
- Murphy ME. 1996. Energetics and Nutrition of Molt. In: Carey C, editor. *Avian Energetics and Nutritional Ecology* Boston, MA: Springer US. p. 158–98.
- Norberg UM. 1990. *Vertebrate Flight, Zoophysiology* Berlin, Heidelberg: Springer Berlin Heidelberg.
- Nudds RL. 2007. Wing-bone length allometry in birds. *J Avian Biol* 38:515–19.
- Nudds RL, Kaiser GW, Dyke GJ. 2011. Scaling of Avian Primary Feather Length. *PLoS ONE* 6:e15665.
- Null W, Shkarayev S. 2005. Effect of Camber on the Aerodynamics of Adaptive-Wing Micro Air Vehicles. *J Aircr* 42:1537–42.
- Olson VA, Davies RG, Orme CDL, Thomas GH, Meiri S, Blackburn TM, Gaston KJ, Owens IPF, Bennett PM. 2009. Global biogeography and ecology of body size in birds. *Ecol Lett* 12:249–59.
- Pennycuik CJ. 1967. The strength of the pigeon's wing bones in relation to their function. *J Exp Biol* 46:219–33.
- Pennycuik CJ. 1989. *Bird Flight Performance: A Practical Calculation Manual* Oxford University Press.
- Pigot AL, Sheard C, Miller ET, Bregman TP, Freeman BG, Roll U, Seddon N, Trisos CH, Weeks BC, Tobias JA. 2020. Macroevolutionary convergence connects morphological form to ecological function in birds. *Nat Ecol Evol*.
- R Development Core Team. 2013. *R: A Language and Environment for Statistical Computing* Vienna, Austria: R Foundation for Statistical Computing.

- Rader JA, Dillon ME, Chesser RT, Sabat P, Martínez Del Rio C. 2015. Morphological divergence in a continental adaptive radiation: South American ovenbirds of the genus *Cinclodes*. *The Auk* 180–90.
- Rayner JMV. 1988. Form and Function in Avian Flight. In: Johnston RF, editor. *Current Ornithology*. Current Ornithology Boston, MA: Springer US. p. 1–66.
- Revell LJ. 2012. phytools: an R package for phylogenetic comparative biology (and other things). *Methods Ecol Evol* 3:217–23.
- Rohwer S, Ricklefs RE, Rohwer VG, Copple MM. 2009. Allometry of the Duration of Flight Feather Molt in Birds. *PLOS Biol* 7:e1000132.
- Rubolini D, Liker A, Garamszegi LZ, Møller AP, Saino N. 2015. Using the BirdTree.org website to obtain robust phylogenies for avian comparative studies: A primer. *Curr Zool* 61:959–65.
- Schmitz FW. 1967. *Aerodynamics of the Model Airplane: Airfoil measurements Translation Branch, Redstone Scientific Information Center, Research and Development Directorate, U.S. Army Missile Command.*
- Shaffer SA, Weimerskirch H, Costa DP. 2001. Functional significance of sexual dimorphism in Wandering Albatrosses, *Diomedea exulans*. *Funct Ecol* 15:203–10.
- Sheard C, Neate-Clegg MHC, Alioravainen N, Jones SEI, Vincent C, MacGregor HEA, Bregman TP, Claramunt S, Tobias JA. 2019. The latitudinal gradient in hand-wing-index: global patterns and predictors of wing morphology in birds. *bioRxiv* 816603.
- Sheard C, Neate-Clegg MHC, Alioravainen N, Jones SEI, Vincent C, MacGregor HEA, Bregman TP, Claramunt S, Tobias JA. 2020. Ecological drivers of global gradients in avian dispersal inferred from wing morphology. *Nat Commun* 11:2463.
- Shyy W, Berg M, Ljungqvist D. 1999. Flapping and flexible wings for biological and micro air vehicles. *Prog Aerosp Sci* 35:455–505.
- Sibley D, Elphick C, Dunning JB. 2009. *The Sibley Guide to Bird Life & Behavior* Alfred A. Knopf.
- Speakman JR. 2005. Body size, energy metabolism and lifespan. *J Exp Biol* 208:1717–30.
- Stoddard MC, Yong EH, Akkaynak D, Sheard C, Tobias JA, Mahadevan L. 2017. Avian egg shape: Form, function, and evolution. *Science* 356:1249–54.
- Sullivan TN, Meyers MA, Arzt E. 2019. Scaling of bird wings and feathers for efficient flight. *Sci Adv* 5:eaat4269.
- Swaddle JP, Lockwood R. 1998. Morphological adaptations to predation risk in passerines. *J Avian Biol* 29:172–76.

- Taylor CR, Heglund NC, Maloiy GM. 1982. Energetics and mechanics of terrestrial locomotion. I. Metabolic energy consumption as a function of speed and body size in birds and mammals. *J Exp Biol* 97:1–21.
- Taylor G, Thomas A. 2014. *Evolutionary Biomechanics* Oxford University Press.
- Tobalske BW, Dial KP. 2000. Effects of body size on take-off flight performance in the Phasianidae (Aves). *J Exp Biol* 203:3319–32.
- Tucker VA. 1991. The Effect of Molting on the Gliding Performance of a Harris' Hawk (*Parabuteo unicinctus*). *The Auk* 108:108–13.
- Vogel S. 1981. *Life in moving fluids*. Princet Univ.
- Vogel S. 2013. *Comparative Biomechanics: Life's Physical World* Princeton University Press.
- Waldrop LD, He Y, Hedrick TL, Rader JA. 2020. Functional Morphology of Gliding Flight I: Modeling Reveals Distinct Performance Landscapes Based on Soaring Strategies. *Integr Comp Biol* 60:1283–96.
- Wang X, Nudds RL, Palmer C, Dyke GJ. 2012. Size scaling and stiffness of avian primary feathers: implications for the flight of Mesozoic birds. *J Evol Biol* 25:547–55.
- Warham J. 1977. Wing loadings, wing shapes, and flight capabilities of procellariiformes. *N Z J Zool* 4:73–83.
- Withers PC. 1981. An aerodynamic analysis of bird wings as fixed aerofoils. *J Exp Biol* 90:143–62.
- Worcester SE. 1996. The scaling of the size and stiffness of primary flight feathers. *J Zool Lond* 239:609–24.

2.5 Figures

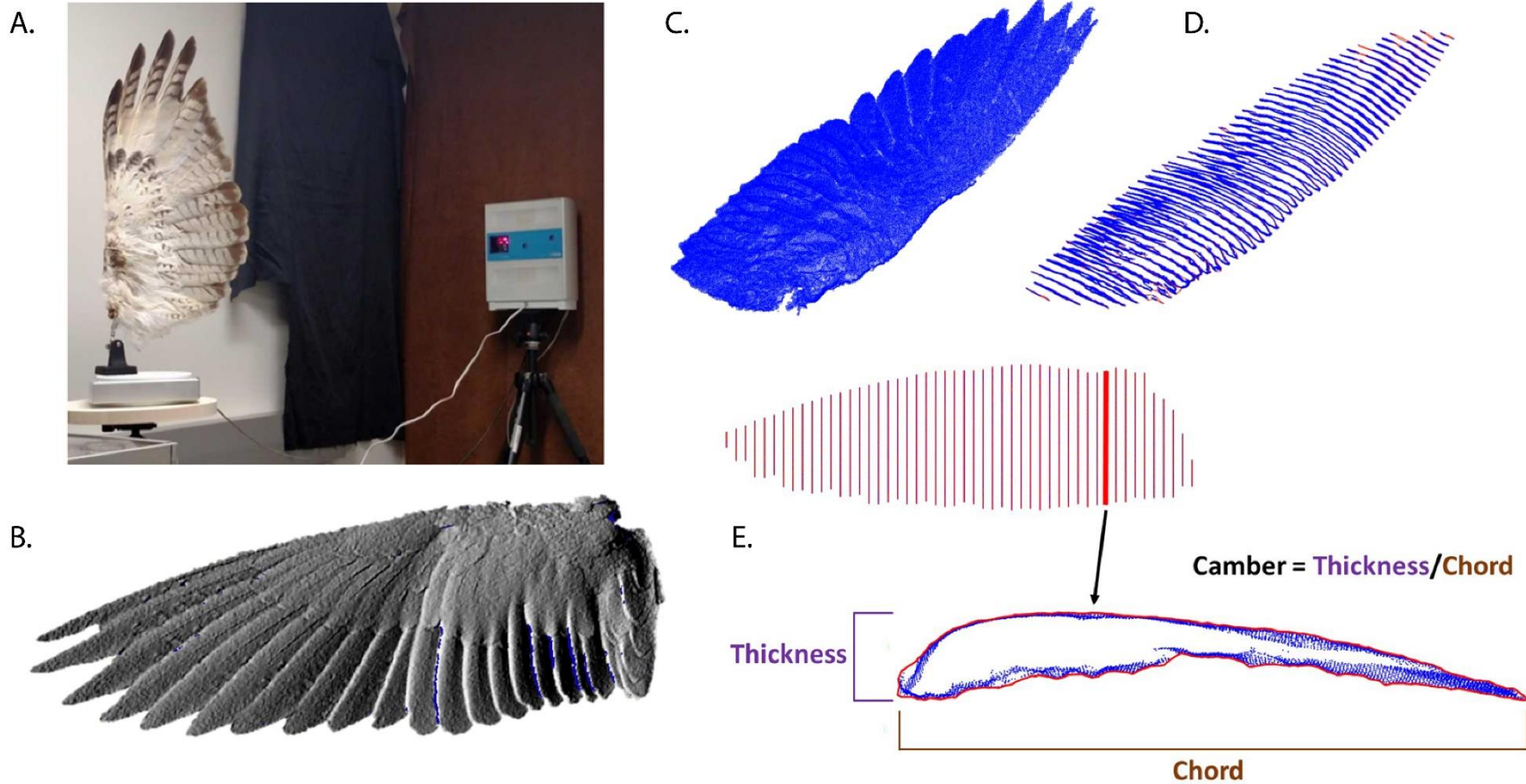


Figure 2.1 Workflow for extracting data from 3D scanned bird wings. A. Wings were scanned using a NextEngine 3D Scanner Ultra HD laser scanner (NextEngine, Inc., Santa Monica, CA). Wings were scanned at a minimum of 200 dpi to provide adequate shape information, including surface characteristics (B., in this case, a peregrine falcon, *Falco peregrinus*). The scanned wings were then stripped to their vertices (C.) and segmented into slices (D.) for further measurement, including section thickness and chords, from which my proxy of wing camber was calculated (E.)

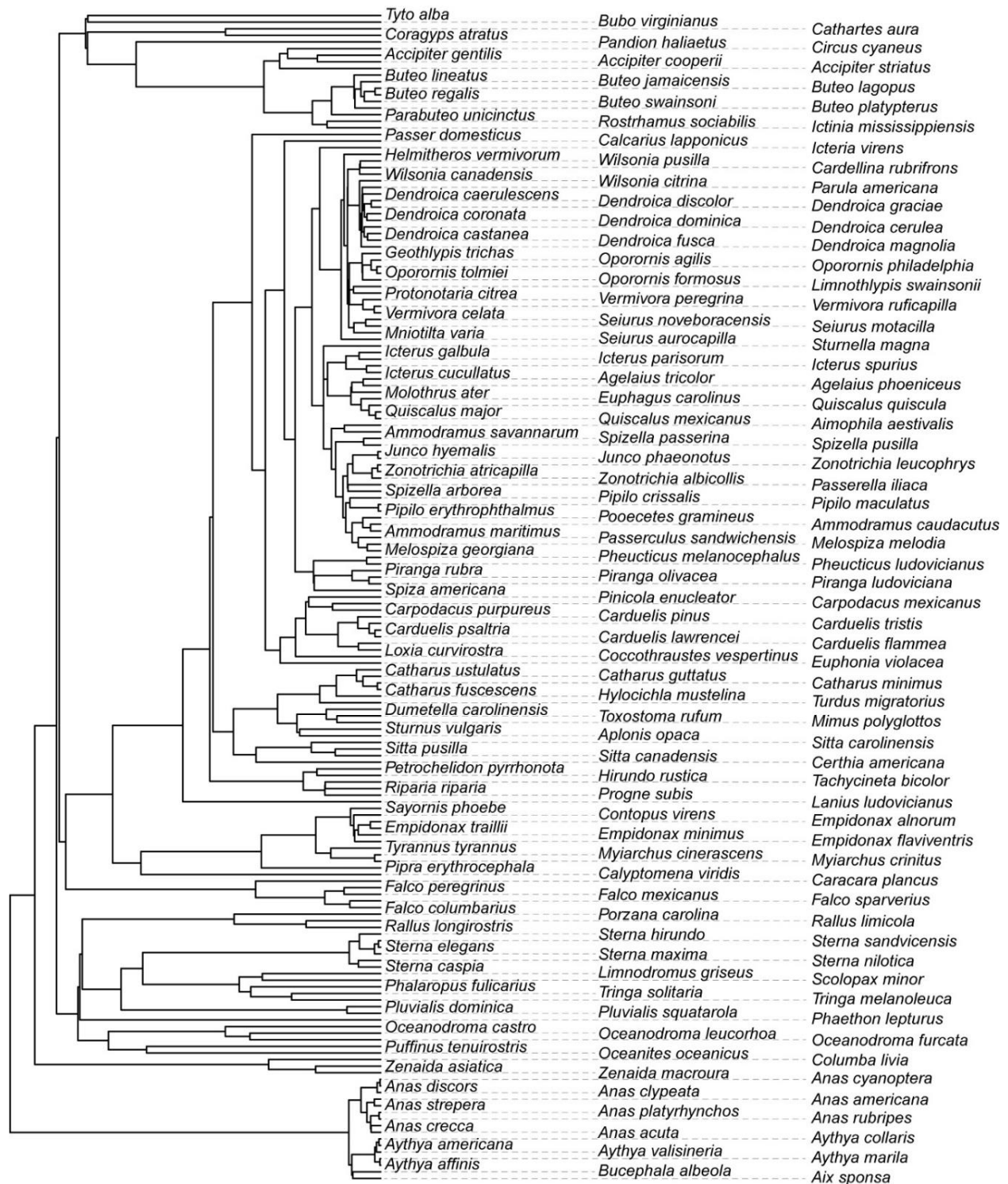


Figure 2.2 The species included in the scanned wing dataset, and their phylogenetic relationships. The tree with pruned from the Jetz et al. (2012) supertree.

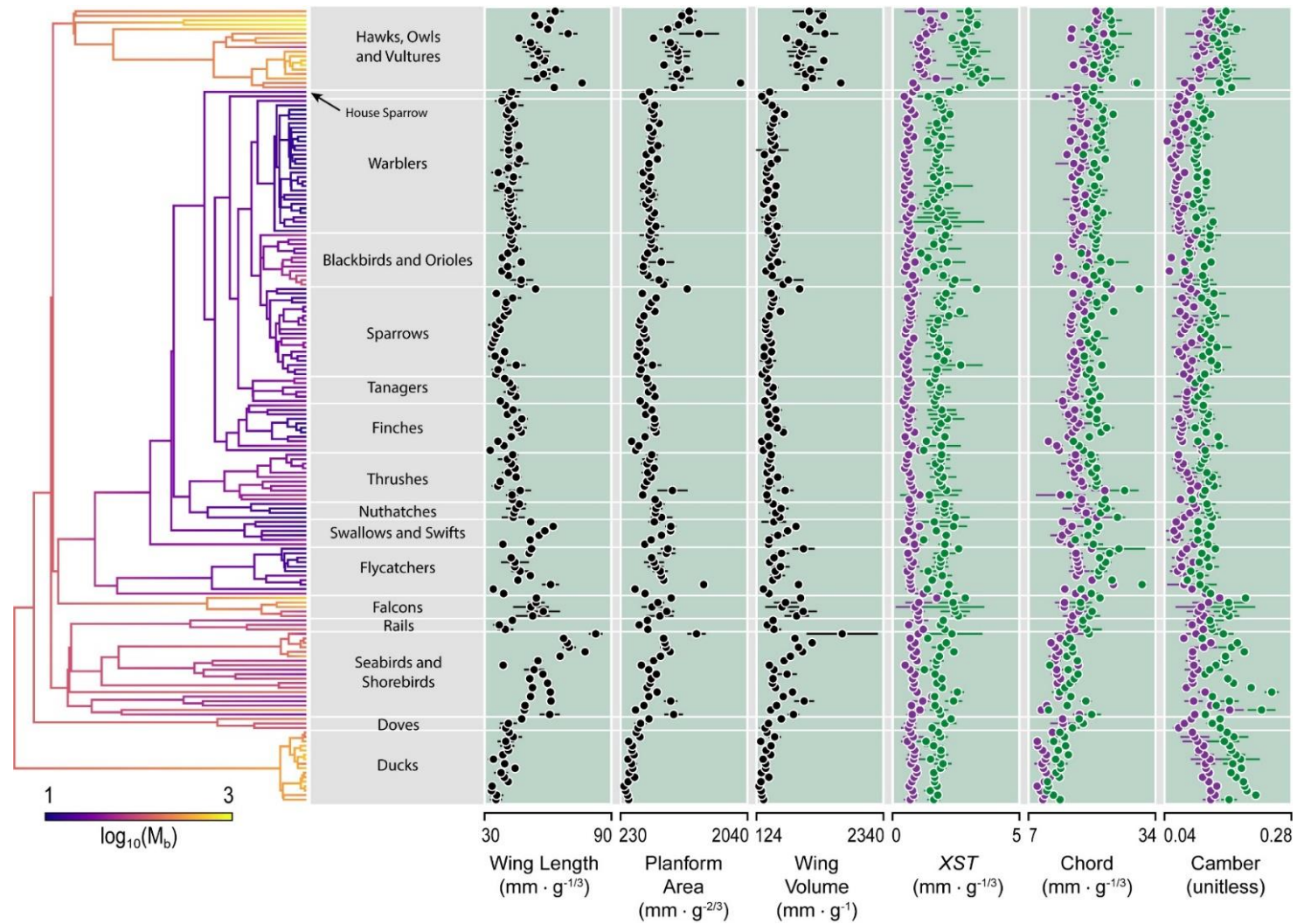
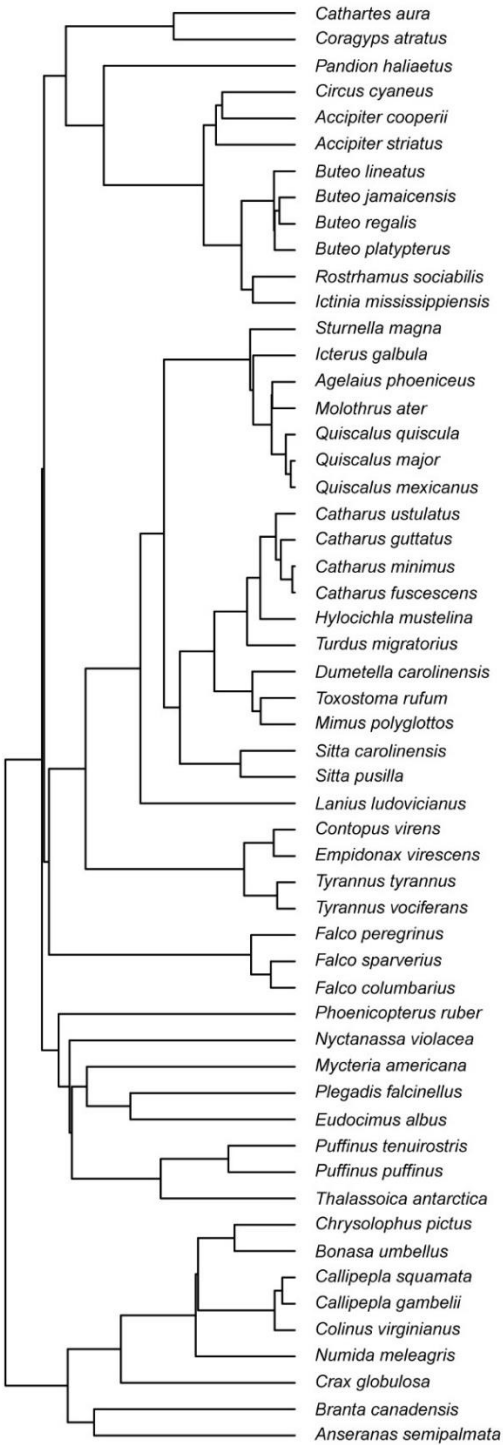


Figure 2.3 Phylogenetic distribution of shape traits. Body mass shows strong phylogenetic structure (heatmap on tree branches), and wing shape traits show similar variation. Median values of whole wing measurements are shown with black data points, and horizontal bars represent ± 1 median absolute deviation. Traits measured in the handwing are shown in purple and the armwing is shown in green. Tree topology as in Fig. 2

A.



B.

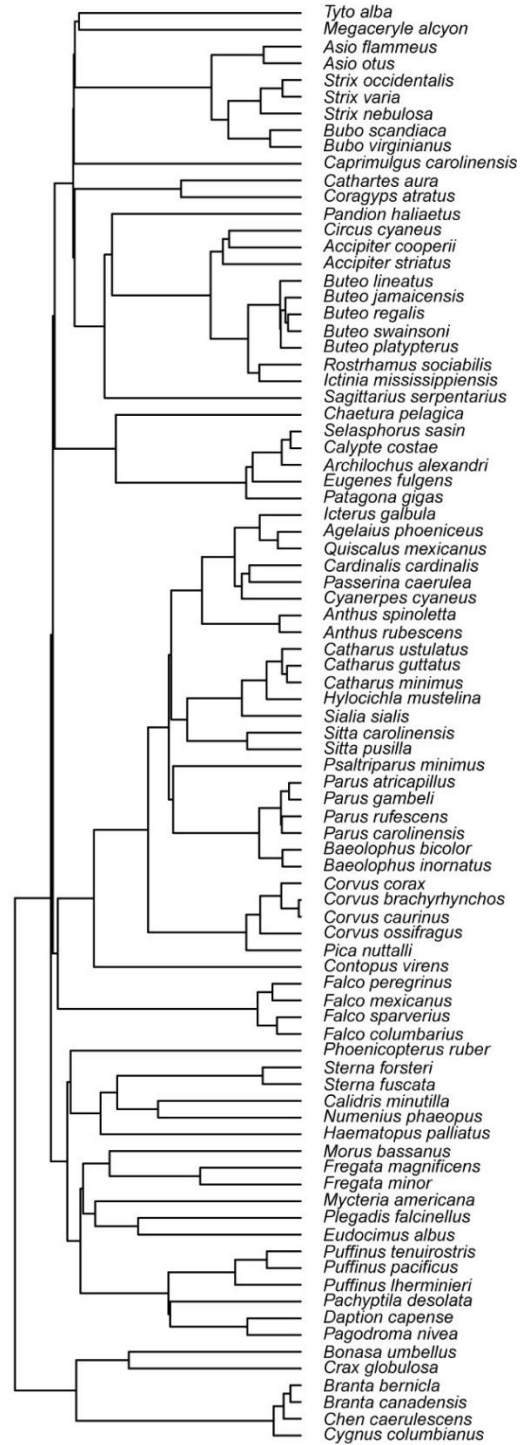


Figure 2.4 The species included in the skeleton (A.) and feather (B.) datasets. Trees were pruned from the Jetz et al. (2012) supertree.

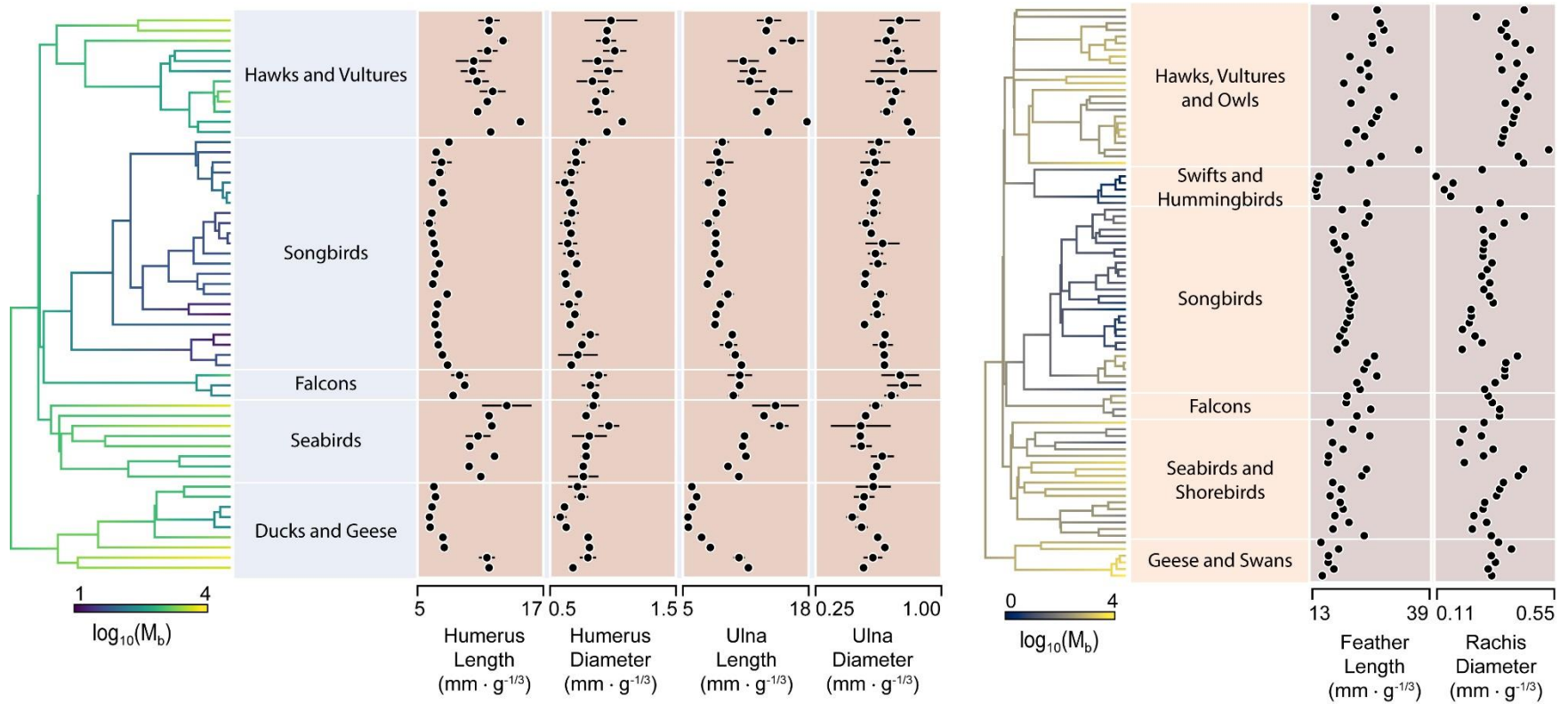


Figure 2.5 Phylogenetic distributions of the skeletal and feather datasets. Body size is shown by the heatmaps applied to the tree branches. Data points represent species medians and horizontal bars are ± 1 median absolute deviation. Tree topologies as in Fig. 4.

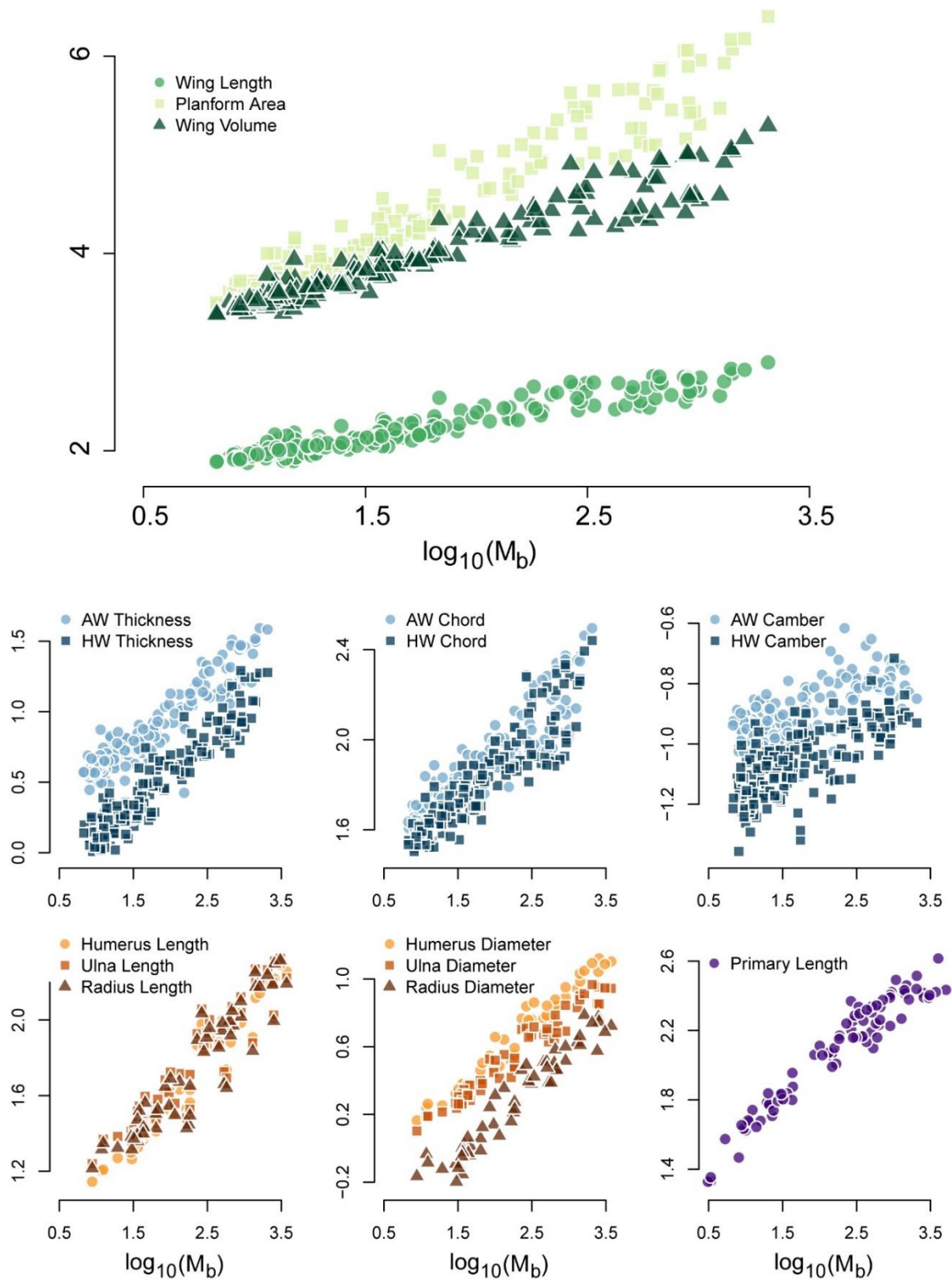


Figure 2.6 Scaling relationships of wing shape traits.

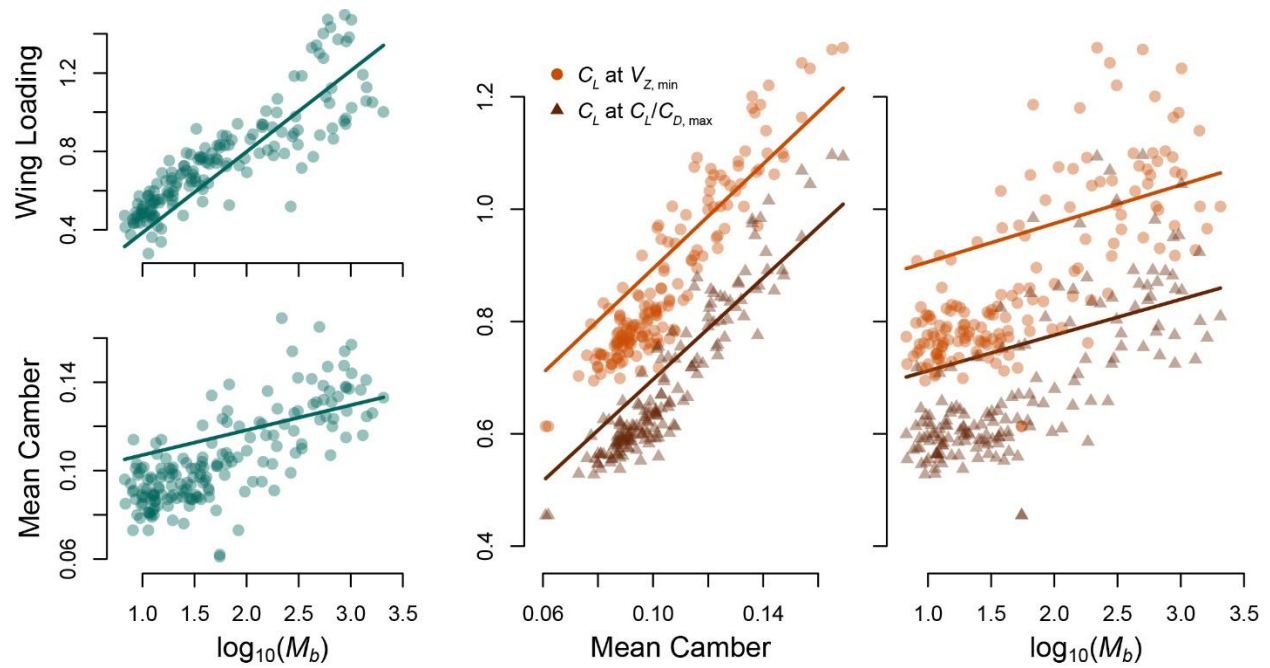


Figure 2.7 Size-related effects on wing loading, camber. Coefficient of lift (C_L), estimated using computational fluid modeling (see Waldrop et al. 2020a for detailed methods and discussion) also increased with body size, in response to increasing wing camber.

2.6 Tables

Table 2.1 Scaling relationships and phylogenetic signal of wing shape traits

Trait	Isometric Expectation	Scaling	Slope, ρ	R^2	λ
XST_{AW}	0.33	-	$0.30 \pm 0.02, <0.001$	0.52	0.85
XST_{HW}	0.33	+	$0.38 \pm 0.02, <0.001$	0.63	0.73
$Chord_{AW}$	0.33	-	$0.27 \pm 0.01, <0.001$	0.68	0.91
$Chord_{HW}$	0.33	-	$0.28 \pm 0.02, <0.001$	0.65	0.89
$Camber_{AW}$	N/A	N/A	$0.009 \pm 0.005, 0.049$	0.02	0.80
$Camber_{HW}$	N/A	N/A	$0.019 \pm 0.004, <0.001$	0.14	0.85
Length	0.33	-	$0.29 \pm 0.01, <0.001$	0.72	0.92
Area	0.67	-	$0.59 \pm 0.02, <0.001$	0.79	0.92
Volume	1.0	-	$0.91 \pm 0.04, <0.001$	0.79	0.84
Humerus len.	0.33	+	$0.40 \pm 0.02, <0.001$	0.90	0.98
Humerus dia.	0.33	+	$0.36 \pm 0.01, <0.001$	0.93	0.96
Radius len.	0.33	+	$0.39 \pm 0.02, <0.001$	0.86	0.95
Radius dia.	0.33	+	$0.36 \pm 0.02, <0.001$	0.84	0.65
Ulna len.	0.33	+	$0.39 \pm 0.02, <0.001$	0.87	0.93
Ulna dia.	0.33	=	$0.33 \pm 0.01, <0.001$	0.93	0.85
Radius + Ulna dia.	0.33	=	$0.34 \pm 0.01, <0.001$	0.91	0.81
Primary len.	0.33	=	$0.34 \pm 0.02, <0.001$	0.84	0.99
Primary rachis dia.	0.33	+	$0.41 \pm 0.02, <0.001$	0.89	0.69
Secondary len.	0.33	=	$0.35 \pm 0.02, <0.001$	0.81	0.99

Table 2.2 A comparison of the effects of phylogenetic assumptions on scaling models.

Trait	Non-phylo Slope, p	λ Slope, p , Opt	κ Slope, p , Opt	δ Slope, p , Opt
XST_{AW}	0.38, <0.001	0.31, <0.001, 0.79	0.29, <0.001, 0.33	0.39, <0.001, 35.62
XST_{HW}	0.45, <0.001	0.37, <0.001, 0.73	0.34, <0.001, 0.40	0.45, <0.001, 22.34
Chord _{AW}	0.27, <0.001	0.27, <0.001, 0.91	0.26, <0.001, 0.43	0.28, <0.001, 5.33
Chord _{HW}	0.28, <0.001	0.28, <0.001, 0.89	0.26, <0.001, 0.52	0.27, <0.001, 3.81
Camber _{AW}	0.030, <0.001	0.009, 0.048, 0.80	0.011, 0.046, 0.37	0.029, <0.001, 78.83
Camber _{HW}	0.025, <0.001	0.018, <0.001, 0.85	0.021, <0.001, 0.277	0.022, <0.001, 155.5
Length	0.37, <0.001	0.30, <0.001, 0.92	0.29, <0.001, 0.52	0.31, <0.001, 3.55
Area	0.66, <0.001	0.59, <0.001, 0.92	0.56, <0.001, 0.49	0.56, <0.001, 3.03
Volume	1.08, <0.001	0.91, <0.001, 0.84	0.87, <0.001, 0.23	1.07, <0.001, 17.24
Humerus len.	0.43, <0.001	0.38, <0.001, 0.98	0.38, <0.001, 0.62	0.38, <0.001, 0.98
Humerus dia.	0.38, <0.001	0.35, <0.001, 0.93	0.35, <0.001, 0.42	0.36, <0.001, 1.96
Radius len.	0.41, <0.001	0.39, <0.001, 0.96	0.39, <0.001, 0.65	0.38, <0.001, 0.96
Radius dia.	0.40, <0.001	0.36, <0.001, 0.63	0.35, <0.001, 0.07	0.38, <0.001, 6.89
Ulna len.	0.40, <0.001	0.39, <0.001, 0.94	0.39, <0.001, 0.55	0.38, <0.001, 1.03
Ulna dia.	0.34, <0.001	0.33, <0.001, 0.86	0.34, <0.001, 0.13	0.33, <0.001, 2.94
Radius + Ulna dia.	0.36, <0.001	0.34, <0.001, 0.83	0.34, <0.001, 0.21	0.34, <0.001, 2.88
Primary len.	0.35, <0.001	0.34, <0.001, 0.99	0.34, <0.001, 0.62	0.34, <0.001, 2.35
Primary rachis dia.	0.41, <0.001	0.41, <0.001, 0.69	0.40, <0.001, 0.33	0.40, <0.001, 4.81
Secondary len.	0.35, <0.001	0.35, <0.001, 0.99	0.36, <0.001, 0.71	0.35, <0.001, 1.11

Table 2.3 Evolutionary dynamics of wing shape traits.

Trait	Model	AICc.w	σ^2	Normalized σ^2 $\times 10^{-4}$	Phylogenetic Signal (λ K)
XST_{AW}	OU	0.60	1.22	9.17	0.96 0.97
XST_{HW}	EB	0.50	0.43	12.55	0.99 1.58
Chord _{AW}	BM	0.58	38.23	5.16	0.98 1.21
Chord _{HW}	BM	0.55	27.05	4.55	0.99 1.34
Camber _{AW}	OU	1.00	7.93×10^{-5}	29.50	0.82 0.33
Camber _{HW}	OU	1.00	5.23×10^{-5}	23.77	0.88 0.36
Length	OU	0.43	372.54	7.38	0.96 1.29
Area	EB	0.70	2.88×10^7	7.64	0.99 1.35
Volume	EB	0.97	6.16×10^9	9.66	1.00 1.14
M_b	OU	1.00	7944.51	22.08	0.89 0.37
Humerus len.	EB	0.65	70.49	21.18	1.00 2.20
Humerus dia.	BM	0.50	0.11	7.72	1.00 1.99
Radius len.	EB	0.47	71.79	19.86	1.00 1.87
Radius dia.	BM	0.54	0.02	7.65	1.00 1.95
Ulna len.	BM EB	0.48 0.37	28.45 67.72	7.53 17.93	1.00 1.79
Ulna dia.	BM	0.60	0.06	9.17	1.00 1.66
Primary len.	BM	0.58	92.6	6.07	0.96 1.09
Primary rachis dia.	BM	0.59	0.03	6.44	0.96 1.21
Secondary len.	BM	0.58	62.74	6.82	0.95 1.04

Table 2.4 Hypothesis testing results; aerodynamics predicts wing thickness while load predicts skeletal thickness.

Shape Attribute	Model	AICc	Δ AICc	AICc.w
Average Wing Thickness	$T_{ave} \sim \hat{f} + C + (\hat{f} * C)^{1/2}$	410.99		0.89
	$T_{ave} \sim \hat{f} + C$	415.21	4.22	0.11
	$T_{ave} \sim C$	443.73	32.73	0.00
	$T_{ave} \sim (M_b)^{1/3}$	461.97	50.97	0.00
	$T_{ave} \sim \text{bending load}$	468.33	57.34	0.00
	$T_{ave} \sim \hat{f}$	520.00	109.01	0.00
Handwing Thickness	$T_{hw} \sim \text{bending load}$	497.51		0.98
	$T_{hw} \sim \hat{f} + C + (\hat{f} * C)^{1/2}$	507.72	10.21	0.01
	$T_{hw} \sim \hat{f} + C$	508.01	10.50	0.01
	$T_{hw} \sim C$	515.66	18.15	0.00
	$T_{hw} \sim (M_b)^{1/3}$	540.05	42.53	0.00
	$T_{hw} \sim \hat{f}$	552.89	55.37	0.00
Armwing Thickness	$T_{aw} \sim \hat{f} + C$	598.54		0.60
	$T_{aw} \sim \hat{f} + C + (\hat{f} * C)^{1/2}$	599.32	0.78	0.40
	$T_{aw} \sim \text{bending load}$	627.18	28.64	0.00
	$T_{aw} \sim C$	627.57	29.03	0.00
	$T_{aw} \sim \hat{f}$	666.12	67.58	0.00
	$T_{aw} \sim (M_b)^{1/3}$	720.84	122.30	0.00
Humerus Diameter	$D_{hum} \sim \text{bending load}$	23.28		0.81
	$D_{hum} \sim \hat{f}$	26.97	3.69	0.13
	$D_{hum} \sim \hat{f} + C + (\hat{f} * C)^{1/2}$	28.31	5.03	0.06
	$D_{hum} \sim (M_b)^{1/3}$	42.36	19.09	0.00
	$D_{hum} \sim C$	82.09	58.82	0.00
Radius + Ulna Diameter	$D_{rad+uln} \sim \text{bending load}$	44.68		1.00
	$D_{rad+uln} \sim (M_b)^{1/3}$	58.07	13.40	0.00
	$D_{rad+uln} \sim \hat{f}$	65.00	20.33	0.00
	$D_{rad+uln} \sim \hat{f} + C + (\hat{f} * C)^{1/2}$	69.69	25.02	0.00
	$D_{rad+uln} \sim C$	105.12	60.44	0.00

CHAPTER 3: FUNCTIONAL MORPHOLOGY OF GLIDING FLIGHT. MORPHOLOGY FOLLOWS PREDICTIONS OF GLIDING PERFORMANCE

3.1 Introduction

Birds are diverse in their behavior, ecology, and morphology. Clades vary in their reliance on flight (ranging from flightless to spending most time aloft), flight style (gliding to hovering), and flight performance (burst take-off to high-efficiency soaring). Birds span four orders of magnitude in body mass, ranging from 3.5 cm (bee hummingbird, *Mellisuga helenae*) to more than 3 m in wingspan (wandering albatross, *Diomedea exulans*; Shaffer et al. 2001), and vary in habits from sedentary flightlessness to long-distance flights that nearly match the circumference of the Earth (Austin 1953).

Despite being well-studied as a group, the connections between wing morphology, the biomechanics of flight, and evolution are not well understood. Previous work has focused on studying morphology and its connection to other biological characteristics. Many studies have connected wing shape to migratory habits, with migrants having more pointed wingtips than non-migrants (Mönkkönen 1995; Lockwood et al. 1998; Bowlin and Wikelski 2008; Baldwin et al. 2010; but see Grilli et al. 2017). This pattern exists across species (Lockwood et al. 1998) and among migrant versus sedentary populations of the same species (Mönkkönen 1995). Wing shape among songbirds also correlates with the risk of predation from aerial predators; species that face more intense pressure have more pointed wings (Swaddle and Lockwood 1998).

Sheard, *et al.* (2019) described latitudinal variation the hand-wing index (the ratio of the length over the width of the wing distal to the wrist; Kipp 1959) and correlations with territoriality and habitat preference. Additionally, wing shape is linked to other attributes of avian biology, such as egg morphology (Stoddard *et al.* 2017).

While these studies are informative, observed morphological variation does not necessarily yield variation in flight performance. Recent work connecting biomechanics to morphological variation suggests that many complex systems have “many-to-one mapping” in which different morphologies result in similar performance (Wainwright 2007; Anderson and Patek 2015). Thus, the connection between variation in morphology and biomechanical consequences requires clarification.

Work in flight biomechanics has focused on flight performance of individuals within a single species (e.g.: Parrott 1970; Tucker and Heine 1990; Bowlin and Wikelski 2008; Weimerskirch *et al.* 2016) or comparative studies of a restricted number of species (e.g. Hedenström and Bone 1993; Altshuler 2003; Altshuler *et al.* 2004; but see Segre *et al.* 2015; Baliga *et al.* 2019b). Many studies were conducted using non-phylogenetically explicit analyses (Lockwood *et al.* 1998; but see Taylor and Thomas 2014; Wang and Clarke 2015; Baliga *et al.* 2019b). Direct measurement of flight performance in flying birds typically takes the form of birds flying in wind tunnels (Pennycuick 1968; Rosen and Hedenstrom 2001; Hedenstrom *et al.* 2006). While this type of work provides a mechanistic understanding of the flight of individual birds, it is too difficult and costly to implement in the broad taxonomic sampling required to understand trait evolution.

Computational modeling may provide an avenue to develop predictive relationships between morphological traits and their impact on biomechanical performance. When coupled with a survey of morphological specimens, such models could facilitate broader study of the evolution of performance traits. As an example, Tseng (2013) used numerical simulations to model the mechanical advantage of carnivorous mammal skulls across the plausible range of variation in three simple parameters of skull morphology – length, width, and depth. What resulted was a theoretical landscape linking biomechanical performance to varying morphological configurations (Tseng 2013). Similar work has also been performed by Polly et al. (2016), Keren et al. (2017), Waldrop et al. (2018), and Olsson et al. (2020) on different systems.

Here I focus on creating such performance landscapes based on flight style, a major difference in the ecology of many birds. While most birds engage in flapping flight, there are a few that mostly engage in gliding and soaring with stable, outstretched wings. Gliders trade potential energy, in the form of flight altitude, for forward motion, and the exchange rate of that transaction is largely determined by the efficiency of their wings (Vogel 1981). Soaring is a form of gliding flight wherein birds take advantage of updrafts in the air to gain altitude, and thus energy, to power their flight without flapping. Birds that soar over land typically seek out thermals (Shannon et al. 2002; Ákos et al. 2010).

While gliding and soaring birds tend to have the same flight behavior, there are subtle differences in the way these birds use gliding and soaring. Staying in updrafts requires that birds must sense rising air and maneuver to stay within it (Vogel 1981; Williams et al. 2018). This favors relatively slow flight, meaning that the wings of these birds must produce sufficient lift at low airspeeds (Vogel 1981; Taylor and Thomas 2014). By contrast, birds that glide to

travel long distances benefit from high speed and highly efficient flight – minimizing altitude lost per distance traveled (Vogel 1981; Weimerskirch et al. 1993; Taylor and Thomas 2014). Such differences in flight behavior may be associated with different selection regimes that could act to drive divergence in morphological features involved in flight. The obvious focus of these selective pressure would be the wings, but tail morphology is also known to influence aerodynamic forces (Usherwood 2005; Usherwood et al. 2020), and may also be subject to similar pressures. Furthermore, if differences in flight behavior are associated with differences in selective pressures, this may manifest in divergent trajectories toward disparate evolutionary optima, and possibly at different evolutionary rates (σ^2), for species that regularly engage in gliding flight versus those that do not.

In preceding collaborative work (Waldrop et al. 2020a), we created a computational model of fluid flow around simulated bird wings to construct aerodynamic performance landscapes of gliding flight (Waldrop et al. 2020b). We used uncertainty quantification techniques to assess the sensitivity of performance to variation in three morphological metrics among birds: wing aspect ratio, camber, and body size. We found that aspect ratio and camber both strongly influenced gliding performance in maximum C_L/C_D ratio, where C_L and C_D are the coefficients of lift and drag, as well as C_L . However, high performance in these metrics occurred at different combinations of morphology. High C_L/C_D occurred at high aspect ratio and intermediate camber, while high C_L was generated by high measures of both traits (see Waldrop et al. 2020b). Based on the sensitivity analyses and performance landscapes, we proposed two hypotheses: 1) gliding birds would exhibit higher wing aspect ratio and greater chordwise camber than their non-gliding counterparts; and 2) that two strategies for gliding

flight exist, which we labeled “aerial searching” and “aerial perching”, and which are associated with divergent morphological conformations. The first hypothesis springs from the expectation that gliding birds will have a higher maximum C_L/C_D ratio, where C_L and C_D are the coefficients of lift and drag, respectively. Within gliding taxa, the second hypothesis proposes a further split between aerial-perching birds that also exhibit high C_L and low minimum sinking speeds ($V_{z,min}$) and aerial searchers that do not. In the present work, I wielded a dataset of 3-dimensionally (3D) scanned wings to test the first hypothesis, and to provide a preliminary exploration of the second.

3.2 Methods

3.2.1 Wing scanning and 3D wing morphology

I collected morphological measurements from 3D scanned wings representing 163 species from three major ecotypes of birds, raptors (Accipitriformes and Falconiformes, also including two species of Strigiformes), seabirds, shorebirds and rails (Procellariiformes, Phaethontiformes, Charadriiformes, and Gruiformes), doves (Columbiformes), and songbirds (Passeriformes) from the collection of the North Carolina Museum of Natural Sciences (Raleigh, NC) using a NextEngine 3D Scanner Ultra HD laser scanner (NextEngine, Inc., Santa Monica, CA). Wings were scanned at resolutions of at least 200 dpi, but up to 16,000 dpi for small wings. The scanned wings were stripped down to their vertices, and 2D and 3D shape variables of the resulting point clouds were measured using a custom program in MATLAB (The MathWorks, Natick, MA, USA).

The scanned wings were aligned to X , Y , and Z axes in 3D space using a principal components (PC) analysis. The first, second and third PC axes represented the length (X), chord

(Y), and thickness (Z) of the wings, respectively. Wing length was measured as $X_{max} - X_{min}$. The wings were subdivided into chord-wise slices along their length, with the width of the slices scaled to $1/25^{\text{th}}$ of the distance between the wingtip and the wrist joint. This standardized the number of slices representing the hand portion of the wing, facilitating direct comparison across samples and taxa. The number of slices representing the arm portion of the wing varied, as wing proportions differ among species and higher order taxonomy. For each of these slices I measured wing chord as $Y_{max} - Y_{min}$ and maximum section height as $Z_{max} - Z_{min}$. The proximal portion of the wings were subject to variable preservational artifacts, owing to their removal from the birds' bodies during specimen preparation. Therefore, the proximal $1/3^{\text{rd}}$ of the arm wing slices was excluded from chordwise analyses.

3.2.2 *Measuring wing geometry*

I measured wing aspect ratio (AR), mean camber (\bar{Q}), and estimated Reynolds number (Re) as a function of wing chord. Aspect ratio (AR) was calculated as:

$$AR = \frac{4r^2}{S} \quad (\text{eq. 1})$$

where S is wing area, and r is wing length. I was unable to account for the width of the body when calculating wingspan, owing to the removal of the wings during preparation. Therefore, my measurements of aspect ratio are underestimates. Camber (Q) for each of the wing slices was measured as the ratio of wing section thickness (t) over section chord length (C) (Fig. 1). Both t and Q varied along the span of the wings, so mean camber (\bar{Q}) and mean section thickness (\bar{t}) were calculated for each wing.

Reynolds number was calculated from mean chord (\bar{C}), while air density and kinematic viscosity were held constant at $\rho = 1.225 \text{ kg m}^{-3}$ and $\nu = 1.5 \times 10^{-5} \text{ m}^2 \text{ s}^{-1}$, respectively:

$$\text{Re} = \frac{V\bar{C}}{\nu} \quad (\text{eq. 2})$$

To facilitate comparison across species, individual Re was estimated at an airspeed (V) of 8.0 ms^{-1} , the minimum airspeed reported in Alerstam et al. (2007), and may therefore be an underestimate of the actual operating Re of some taxa in my sample.

Body mass (M_b) data were collected from museum tags and used to calculate the ratio of body mass over wing planform area (wing loading) for each individual. Because M_b can fluctuate dramatically in daily and seasonal cycles, I calculated median values of mass and wing loading for each taxon. Wing length and wing chord were non-dimensionalized relative to body mass by dividing by $M_b^{0.33}$; transformed metrics are denoted by an *ND* subscript. This transformation assumes an isometric relationship between mass and length whereas birds as a whole or specific groups of birds may scale allometrically. This transformation leaves those allometries intact while controlling for the effect of body size on raw length measurements. The original measurement units are millimeters for lengths and grams for mass.

3.2.3 *Modeling effects of wing geometry on gliding flight*

In the prior work, we used the XFLR5 software (version 6.47; Deperrois 2009) to simulate airflow around wings of various morphological configurations with a simple elliptical wing planform geometry (Waldrop et al. 2020b). Detailed methods can be found in Waldrop et al. (2020b), but briefly, we tested prescribed combinations of three morphological parameters (AR , \bar{Q} and Re) of these model wings, spanning the plausible ranges for living birds, as indicated

by the scanned wing data set. I extracted estimates of several wing performance metrics from XFLR5, including: 1) minimum sinking speed (assuming a constant bird mass of 0.9 kg; $V_{z,min}$), 2) coefficient of lift at minimum sinking speed (C_L at $V_{z,min}$), and 3) maximum lift to drag ratio (C_L/C_D). I also checked that my assumption of constant bird mass didn't bias the results by iterating the analysis of $V_{z,min}$ on estimates of $V_{z,min}$ calculated assuming constant wing loading.

Surrogate functions of output performance metrics were produced using uncertainty quantification techniques. The parameter input space was sampled and output surrogates were reconstructed using generalized polynomial chaos (gPC) expansion (Wiener 1938; Xiu and Karniadakis 2002). Global sensitivity analyses were conducted by calculating Sobol indices for each input parameter and their interactions on output performance (Sobol 1993; Sudret 2008). For additional details, see Waldrop et al (2020b). In this study, gPC surrogate functions serve as performance landscapes for each output metric of flight ($V_{z,min}$, C_L at $V_{z,min}$, and max C_L/C_D).

3.2.4 Analysis and hypothesis testing

All statistical analysis was conducted in R (R Development Core Team 2013). Comparative analyses of wing geometry were conducted on median values of each shape parameter for each species, and all analyses were conducted in a phylogenetically explicit framework. Phylogenetic trees were pruned from the Jetz et al. supertree (Jetz et al. 2012), acquired from birdtree.org (Rubolini et al. 2015). Phylogenetic signal was calculated using both Pagel's λ (Pagel 1999a) and Blomberg's K (Blomberg et al. 2003) metrics using the "phylosig" command in the R package Phytools (Revell 2012).

3.2.4.1 Hypothesis 1: Wing morphology differs between gliders and non-gliders

The global sensitivity analyses suggested that the effects of Re were small and that AR and \bar{Q} had significant influences on all metrics of gliding flight performance (Waldrop et al. 2020b), so I focused my attention on AR and \bar{Q} for further analysis. Detailed discussion of the capabilities and limitations of the computational modeling is presented in the companion to this work (Waldrop et al. 2020b). I classified each of the species in my sample as a glider or a non-glider based on descriptions of flight behavior from the *Handbook of Birds of the World* (del Hoyo et al. 1992); if observations of gliding were mentioned in the text describing the species or family, the species was classified as a glider, and if the description of flight behavior did not mention gliding, species were classified as non-gliders. Further, I classified seabirds, shorebirds, and swallows as “aerial searchers” based on descriptions of their long distance flight behavior (Weimerskirch et al. 1993, 2016; Shaffer et al. 2001; Warrick et al. 2016) and hawks and new-world vultures as “aerial perchers” because of their tendency to remain aloft within relatively confined geographic areas (DeVault et al. 2004; Monsarrat et al. 2013).

Stochastic character mapping was used to map these flight behaviors onto the phylogeny (see Huelsenbeck et al. 2003; Bollback 2006) using the Phytools package in R (Revell 2012). I used the OUwie package (Beaulieu and O’Meara 2012) to fit two different models of evolution to each of the morphological traits: 1) a single-peak Ornstein-Uhlenbeck (OU) model is a Brownian motion model with a tendency toward a single trait optimum; and 2) a two-peak OU model that allows for separate evolutionary rates (σ^2) and trait optima for each behavioral group (gliders and non-gliders). I used AIC_c and a Monte Carlo-based method (package “pmc” in R, see Boettiger et al. 2012) to assess which model best fit the trait data. Support for a two-

peak model would suggest morphological divergence between flight styles, supporting my hypotheses. I checked that differences in trait means for AR and \bar{Q} were significant using phylogenetic ANOVAs, implemented in R with the “*phylANOVA*” command in the *Phytools* package (Revell 2012). I also conducted a discriminant function analysis with jackknife sampling to assess whether gliders and non-gliders could be correctly classified based on the combination of AR and \bar{Q} .

To assess whether wing morphology confers differences in glide performance among the flight styles, I used the performance landscapes (gPC surrogate functions) to estimate performance for combinations of AR and \bar{Q} representing each species. I used phylogenetically-aware ANOVAs in the R package *Phytools* (Revell 2012) to quantify divergence in $V_{z,min}$, C_L at $V_{z,min}$, and $\max C_L/C_D$.

3.2.4.2 Hypothesis 2: Two gliding strategies lead to disparate gliding morphotypes

The performance landscapes identified two regions of high gliding performance associated with different combinations of wing shape traits. The highest values of C_L/C_D were found at combinations of high AR and moderate \bar{Q} , while the highest values of C_L at $V_{z,min}$ were found at high AR and high \bar{Q} (Waldrop et al. 2020). This led to the prediction that “aerial perchers” might possess wing morphologies that confer high C_L at low sinking speeds, and “aerial searchers” may display high C_L/C_D wings that minimize glide angle but may require higher airspeeds to generate sufficient lift. To test these predictions, I restricted the dataset to just those taxa identified above as gliders, which were then subset into aerial perchers – those species that glide to survey comparatively small areas (hawks, falcons, and vultures), and aerial searchers – species that use their gliding flight while transiting long distances either in

migration or in search of foraging grounds (seabirds and shorebirds). I used a similar OUwie approach (see above) to ask whether AR and \bar{Q} showed different evolutionary patterns between these groups. I also used phylogenetically aware ANOVAs to assess differences in flight performance (estimated sinking speed, $V_{z,min}$, as well as C_L at $V_{z,min}$, C_L at max C_L/C_D and max C_L/C_D).

3.3 Results

I scanned 1094 wings from 163 species in 30 major lineages of birds (see Figure 2). Sample sizes for each species ranged from 1 to 49 with a median sample size of 5 individuals. To my knowledge, this represents the largest data set of three-dimensional wing morphology presently available.

3.3.1 Morphometric summary

Median body mass among non-gliders ranged from 6.75 g to 194.75 g and estimated Re from 16,000 to 54,500, while glider body mass ranged from 12.35 g to 2060.0 g, and Re from 17,197 to 132,577. Median within-species wing loading among non-gliders varied from 1.90 g cm⁻² to 9.97 g cm⁻² with an overall median of 4.21 g cm⁻². Wing loading in gliders ranged from 2.30 g cm⁻² to 31.40 g cm⁻² with an overall median of 8.67 g cm⁻². AR varied from 3.90 to 7.60 in non-gliders and from 5.27 to 13.26 in gliders, with medians of 5.33 and 7.58, respectively. \bar{Q} was lower in non-gliders (range 0.06 to 0.12, mean = 0.094) than in gliders (range 0.08 to 0.17, mean = 0.124). Phylogenetic signal was high in all measured traits, with $\lambda > 0.8$ and $K > 0.4$ in all cases (see Table 1).

3.3.2 Hypothesis 1:

To address the hypothesis that wing morphology differs between gliding taxa and non-gliders, I asked two questions: 1) are there different evolutionary optima for my morphological parameters, and 2) do evolutionary rates differ between flight styles? I found support for an Ornstein-Uhlenbeck (OU) model with two evolutionary optima for aspect ratio – with gliding birds being higher (7.76 ± 0.30) than non-gliding taxa (5.40 ± 0.11). This difference was supported by the results of a phylogenetic ANOVA ($p = 0.03$). I also found support for different evolutionary rates between the two groups ($\sigma^2 = 0.398$ and 0.042 , respectively, AIC_c weight = 0.99). Non-dimensional wing length (r_{ND}) was greater in gliders than non-gliders (dual-rate, two-optima OU model; estimates 55.71 ± 1.83 and 41.57 ± 1.82 , respectively), and evolutionary rate also differed between the groups ($\sigma^2 = 5.78, 2.19$, respectively, AIC_c weight = 0.99). In a dual-rate, two-optima OU model, non-dimensional wing chord (\bar{C}_{ND}) had estimated optima of 14.80 ± 0.67 for gliders and 15.90 ± 0.69 for non-gliders, and $\sigma^2 = 0.73$ and 0.28 , respectively; AIC_c weight = 0.99 . In this case the evolutionary rates differ substantially but the parameter optima for \bar{C}_{ND} are similar (7% difference). For camber (\bar{Q}), I also found support for an OU model with two optima (supported by phylogenetic ANOVA; $p = 0.03$), and again, the gliding birds had greater camber (0.12 ± 0.003 vs. 0.10 ± 0.002 , respectively). Evolutionary rate also differed between non-gliders and gliders ($\sigma^2 = 2.51 \times 10^{-5}$, 1.0×10^{-4} , respectively; AIC_c weight = 0.99). Selection of OU over simpler Brownian motion models was supported by Monte Carlo simulations, as implemented using the “pmc” command in R (Boettiger et al. 2012). Discriminant function analysis (DFA) also supported the existence of a morphological distinction between gliders and non-gliders, with an 89.6% correct classification rate. As DFA is not a

phylogenetically-aware method, I urge caution in interpretation of these results beyond the suggestion that the recovered disparity between gliders and non-gliders is robust to varying assumptions of phylogenetic relatedness.

Maximum C_L/C_D did not differ between gliders and non-gliders ($p = 0.28$), but $V_{z,min}$ was lower among gliding birds than non-gliders (1.23 ± 0.31 vs 1.89 ± 0.31 , $p = 0.03$), and C_L at $V_{z,min}$ was significantly greater (1.02 ± 0.12 vs. 0.78 ± 0.06 , $p < 0.01$). This pattern was for both the assumption of constant body mass and constant wing loading. Despite disparity in mean body mass between the different flight styles, the difference was not significant (phylogenetic ANOVA, $p = 0.09$), likely owing to the large dispersion within each group (482.25 ± 447.46 g vs. 30.82 ± 32.50 g, $p = 0.1$). Wing loading, similarly, did not differ between groups ($p = 0.16$).

3.3.3 Hypothesis 2:

I found support for dual-optima and dual-rate OU models for both AR and \bar{Q} (AIC_c weight = 0.74 and 0.90, respectively) when comparing the “aerial perch” to the “aerial search” strategies. However, dual-optima and single-rate models also performed fairly well (AIC_c weight = 0.24 and 0.09, respectively). The estimated AR optima were greater among aerial searchers than aerial perchers in both single-rate (AR = 8.96 ± 0.41 vs. 6.13 ± 0.63) and dual-rate models (AR = 8.92 ± 0.44 vs. 6.34 ± 0.35). Despite AIC_c support for the dual-optima models for \bar{Q} , the standard error bounds for the optima overlap in both the dual-rate ($\bar{Q} = 0.12 \pm 0.005$ vs. 0.12 ± 0.003) and single-rate ($\bar{Q} = 0.12 \pm 0.006$ vs. 0.12 ± 0.007) cases, lending some ambiguity to its interpretability. These results should be viewed with some caution because the sample sizes are small ($n = 21$ for aerial searchers and $n = 17$ for aerial perchers). Additionally, there were no significant differences in estimated gliding flight performance parameters between searchers

and perchers (C_L/C_D , C_L at $V_{z,min}$; both $p > 0.09$). I did, however, find that aerial searchers had significantly lower $V_{z,min}$ than non-gliders (phylogenetic ANOVA, $p = 0.02$). The aerial perchers showed no such distinction from non-gliders ($p = 0.39$).

3.4 Discussion

Waldrop et al. (2020b) proposed two hypotheses based on the analysis of a computational model of gliding flight. The first predicted that gliding birds would exhibit different combinations of wing morphology than non-gliders. The second hypothesis posits that two gliding strategies exist: one characterized by maximizing horizontal travel relative to altitude lost, and the other simply minimizing sinking speed to enhance capacity for remaining aloft or to facilitate load-carrying. Further, Waldrop et al. (2020b) suggested that these two gliding strategies may exert different selective pressures on the birds that conduct each type of flight which may result in divergence in wing morphology. As described below, I found strong support for the first hypothesis and equivocal support for the second hypothesis.

3.4.1 *Performance landscapes predict differences in gliding performance*

Consistent with the first hypothesis proposed in Waldrop et al. (2020), I found different evolutionary optima and rates (σ^2) in both wing aspect ratio (AR) and camber (\bar{Q}) for gliders and non-gliders. This result suggests that flight mode (i.e., gliding instead of flapping) exerts different selective pressures, shaping morphological evolution of bird wings. However, I caution that the present results do not show a definitive causal relationship between behavior and morphology, but rather, an evolutionary association.

Contrary to my hypothesis, I found that maximum C_L/C_D did not differ between gliders and non-gliders. Gliding birds appear to be drawn toward morphological configurations that enhance the magnitude of lift production (high C_L) rather than efficiency of lift production (high C_L/C_D ; see Fig. 3). This also translated to the hypothesized reduction in estimated $V_{z,min}$, and may therefore represent adaptation to low speed flight or load lifting. These birds, with their relatively high camber, high-aspect ratio wings did not occupy either of the regions of especially high performance in the C_L/C_D or C_L landscapes, but rather seem to be settled into a valley between the optima (Fig. 3). This may reflect conflicting selective pressures that have led to a Pareto optimization effect (Taylor and Thomas 2014), stemming from a tradeoff between the need for flight efficiency and the ability to generate sufficient lift to land, and takeoff, especially with large food loads. Furthermore, my proxy for wing camber is implicitly linked to cross-sectional thickness of the wing, as is the longitudinal stiffness of the wing structure. Wings may therefore be excluded from the region of highest C_L/C_D by a lower bound on the thickness of the wing imposed by structural demands.

Significant distinctions in gliding performance were driven by greater values of both AR and \bar{Q} in gliding taxa, relative to non-gliders, irrespective of body size and Re . Body size is tightly correlated with the phylogeny (Pagel's $\lambda = 0.90$; Pagel 1999a), so it may be difficult to explicitly disambiguate the effects of size and phylogeny in this relationship. High AR wings are a known morphological adaptation to gliding and soaring flight (for example, see Taylor and Thomas 2014), but the interaction with \bar{Q} was previously unknown. Both AR and \bar{Q} , as measured herein, are non-dimensional ratios, but the data facilitated explicit exploration of which dimensional shape attributes appeared to be under selection. Average wing chord (\bar{C}_{ND}) differed very little

among flight styles, however, body mass corrected wing length (r_{ND}) was greater in gliding birds, leading to increased AR . Similarly, because \bar{Q} is the ratio of average wing section thickness (\bar{t}) over \bar{C} , the relative lack of divergence in chord indicates that the wings of gliders have greater \bar{t} , which serves as a proxy measurement for more pronounced camber curvature.

It should be noted that few of the species in my sample are specialist gliders, as this behavior seems to be isolated to only a handful of lineages, including vultures and pelagic seabirds (Taylor and Thomas 2014), but many other lineages rely on gliding to reduce their cost of flight to varying degrees (Vogel 1981; del Hoyo et al. 1992; Taylor and Thomas 2014). I used the non-gliding songbirds and rails as a point of reference to contrast with gliders. While the performance landscapes presented here leave uncertain what adaptive value anchors the non-gliders in their region of morphospace, it is clear that gliders have diverged from them. Further exploration of how the AR and \bar{Q} relate to other flight performance metrics, particularly those associated with flapping flight, may be illuminating.

3.4.2 *Equivocal support for two gliding strategies*

Birds use gliding and soaring flight to reduce their cost of transport, with two different goals, 1) to remain aloft in a relatively discrete area (which was dubbed “aerial perching”), and 2) to transit long horizontal distances (“aerial searching”) (Ákos et al. 2008, 2010). Hawks, eagles, vultures, and other similar birds tend to forage in relatively small home ranges (Ákos et al. 2008, 2010) where they utilize discrete updrafts to remain aloft (Parrott 1970; McGahan 1973; Tucker and Heine 1990; Hedenström and Bone 1993). Pelagic seabirds such as petrels, fulmars, and albatrosses (Procellariiformes) transit long distances between island breeding sites and pelagic foraging sites (Weimerskirch et al. 1993, 2016; Ákos et al. 2008).

Based on the performance landscapes from Waldrop et al. (2020b), I predicted that aerial perchers would be adapted to maximize C_L and minimize $V_{z,min}$, and that aerial searchers would have morphological configurations that produced comparatively high C_L/C_D . My results do not support or reject this hypothesis. Despite the lack of support for the predicted differences in gliding performance between the two strategies, models do support the presence of dual evolutionary optima for AR . However, while two peak statistical models of \bar{Q} between searchers and perchers outperformed one-peak models, support was equivocal between single and dual rates, and the SE estimated confidence bounds of the two peaks overlap. However, the sample sizes of putative searchers and perchers were small, and OUwie modeling has been shown to be particularly sensitive to error at small sample sizes (Cooper et al. 2016). Additionally, most species in my sample that frequently glide are not specialist gliders like vultures (Tucker 1988) and albatrosses (Weimerskirch et al. 1993). Non-specialist species may be subject to tradeoffs imposed by flapping flight that would have less impact on gliding specialists. A more explicit test of this hypothesis should thus focus on these and similar specialist taxa.

3.4.3 *On performance landscapes*

Performance landscapes provide a useful tool to probe the relationship between form and function (Arnold 2003; Dickson and Pierce 2019). With the application of quantitative modeling of the sensitivity of performance output to changes in morphological traits, a theoretical landscape can explore configurations outside the bounds of extant organisms, and perhaps even feasibility (Koehl 2003; Waldrop et al. 2020b). When coupled with a taxonomically broad morphological survey, a performance landscape can illuminate

evolutionary exploration of topographic features (Keren et al. 2017; Olsson et al. 2020). The ability to map performance directly onto morphospaces defined by individual traits, as I have done here in the bivariate AR and \bar{Q} morphospaces (also see Tseng 2013) facilitates easier interpretability of results than morphospaces defined by composite variables, such as those produced by principal components analysis and similar dimensional reduction techniques.

In the current work, I use a performance landscapes generated by a simple model of gliding flight to estimate performance of real birds in flight. These landscapes are estimates of performance only, and come with a variety of caveats discussed in Waldrop et al. (2020). While I feel that the model matches other estimates and measurements of extant birds in gliding flight, it should be noted that neglected aspects of flight (e.g. body interactions) may affect the values and their relationships within performance landscapes.

3.4.4 Considering the third dimension

Bird wings are inherently 3-dimensional structures, but shape analysis has historically focused largely on 2d attributes (for example, Mönkkönen 1995; Lockwood et al. 1998; Taylor and Thomas 2014). Three-dimensional attributes of wing morphology, such as camber also influence the aerodynamics of the wing (Brown 2001; Null and Shkarayev 2005; Waldrop et al. 2020b). Indeed, the performance differences that I described here are a function of an interaction between aspect ratio and camber, so restricting my consideration to traditional planform metrics would have limited the ability to describe functional divergence between gliding and non-gliding birds. My results highlight the necessity of collecting and analyzing 3-dimensional wing shape metrics.

REFERENCES

- Ákos Z, Nagy M, Leven S, Vicsek T. 2010. Thermal soaring flight of birds and unmanned aerial vehicles. *Bioinspir Biomim* 5:045003.
- Ákos Z, Nagy M, Vicsek T. 2008. Comparing bird and human soaring strategies. *Proc Natl Acad Sci* 105:4139.
- Alerstam T, Rosén M, Bäckman J, Ericson PG, Hellgren O. 2007. Flight speeds among bird species: allometric and phylogenetic effects. *PLoS Biol* 5:e197.
- Altshuler DL. 2003. Kinematics of hovering hummingbird flight along simulated and natural elevational gradients. *J Exp Biol* 206:3139–47.
- Altshuler DL, Dudley R, McGuire JA. 2004. Resolution of a paradox: hummingbird flight at high elevation does not come without a cost. *Proc Natl Acad Sci U S A* 101:17731–17736.
- Anderson PSL, Patek SN. 2015. Mechanical sensitivity reveals evolutionary dynamics of mechanical systems. *Proc R Soc B Biol Sci* 282:20143088.
- Arnold SJ. 2003. Performance Surfaces and Adaptive Landscapes. *Integr Comp Biol* 43:367–75.
- Austin OL. 1953. The Migration of the Common Tern (*Sterna hirundo*) in the Western Hemisphere. *Bird-Band* 24:39–55.
- Baldwin MW, Winkler H, Organ CL, Helm B. 2010. Wing pointedness associated with migratory distance in common-garden and comparative studies of stonechats (*Saxicola torquata*). *J Evol Biol* 23:1050–63.
- Baliga VB, Szabo I, Altshuler DL. 2019. Range of motion in the avian wing is strongly associated with flight behavior and body mass. *Sci Adv* 5:eaaw6670.
- Beaulieu JM, O’Meara B. 2012. OUwie: analysis of evolutionary rates in an OU framework (R package).
- Blomberg SP, Garland T, Ives AR. 2003. Testing for Phylogenetic Signal in Comparative Data: Behavioral Traits Are More Labile. *Evolution* 57:717–745.
- Boettiger C, Coop G, Ralph P. 2012. Is your phylogeny informative? Measuring the power of comparative methods. *Evol Int J Org Evol* 66:2240–51.
- Bollback JP. 2006. SIMMAP: Stochastic character mapping of discrete traits on phylogenies. *BMC Bioinformatics* 7:88.
- Bowlin MS, Wikelski M. 2008. Pointed Wings, Low Wingloading and Calm Air Reduce Migratory Flight Costs in Songbirds. *PLoS ONE* 3:e2154.

- Brown CA. 2001. The Effect of Camber on Thin Plate Low Aspect Ratio Wings at Low Reynolds Numbers University of Notre Dame.
- Cooper N, Thomas GH, Venditti C, Meade A, Freckleton RP. 2016. A cautionary note on the use of Ornstein Uhlenbeck models in macroevolutionary studies. *Biol J Linn Soc Linn Soc Lond* 118:64–77.
- Deperrois A. 2009. XFLR5 Analysis of foils and wings operating at low Reynolds numbers. *Guidel XFLR5*.
- DeVault TL, Reinhart BD, Brisbin IL, Rhodes OE. 2004. Home ranges of sympatric black and turkey vultures in south carolina. *The Condor* 106:706–11.
- Dickson BV, Pierce SE. 2019. Functional performance of turtle humerus shape across an ecological adaptive landscape. *Evolution* 73:1265–77.
- Grilli MG, Lambertucci SA, Therrien J-F, Bildstein KL. 2017. Wing size but not wing shape is related to migratory behavior in a soaring bird. *J Avian Biol* 48:669–78.
- Hedenström A, Bone Q. 1993. Migration by soaring or flapping flight in birds: the relative importance of energy cost and speed. *Philos Trans R Soc Lond B Biol Sci* 342:353–61.
- Hedenstrom A, Van Griethuijsen L, Rosen M, Spedding GR. 2006. Vortex wakes of birds: recent developments using digital particle image velocimetry in a wind tunnel. *Anim Biol Leiden* 56:535–49.
- Hoyo J del., Elliott Andrew, Sargatal Jordi, Cabot José. 1992. *Handbook of the birds of the world* Barcelona: Lynx Edicions.
- Huelsenbeck JP, Nielsen R, Bollback JP. 2003. Stochastic Mapping of Morphological Characters. *Syst Biol* 52:131–58.
- Jackson AL, Inger R, Parnell AC, Bearhop S. 2011. Comparing isotopic niche widths among and within communities: SIBER - Stable Isotope Bayesian Ellipses in R: Bayesian isotopic niche metrics. *J Anim Ecol* 80:595–602.
- Jetz W, Thomas GH, Joy JB, Hartmann K, Mooers AO. 2012. The global diversity of birds in space and time. *Nature* 491:444–48.
- Keren T, Kiflawi M, Martin CH, China V, Mann O, Holzman R. 2017. A complex performance landscape for suction-feeding reveals constraints and adaptations in a population of reef damselfish. *bioRxiv* 239418.
- Kipp FA. 1959. Der Handflügel-Index als flugbiologisches Maß. *Vogelwarte* 20:77–86.

- Koehl M a. R. 2003. Physical modelling in biomechanics. *Philos Trans R Soc Lond B Biol Sci* 358:1589–96.
- Lockwood R, Swaddle JP, Rayner JMV. 1998. Avian wingtip shape reconsidered: Wingtip shape indices and morphological adaptations to migration. *J Avian Biol* 29:273–92.
- McGahan J. 1973. Gliding Flight of the Andean Condor in Nature. *J Exp Biol* 58:225–37.
- Mönkkönen M. 1995. Do migrant birds have more pointed wings?: A comparative study. *Evol Ecol* 9:520–28.
- Monsarrat S, Benhamou S, Sarrazin F, Bessa-Gomes C, Bouten W, Duriez O. 2013. How Predictability of Feeding Patches Affects Home Range and Foraging Habitat Selection in Avian Social Scavengers? *PLOS ONE* 8:e53077.
- Null W, Shkarayev S. 2005. Effect of Camber on the Aerodynamics of Adaptive-Wing Micro Air Vehicles. *J Aircr* 42:1537–42.
- Olsson KH, Martin CH, Holzman R. 2020. Hydrodynamic Simulations of the Performance Landscape for Suction-Feeding Fishes Reveal Multiple Peaks for Different Prey Types. *Integr Comp Biol*.
- Pagel M. 1999. Inferring the historical patterns of biological evolution. *Nature* 401:877–84.
- Parrott GC. 1970. AERODYNAMICS OF GLIDING FLIGHT OF A BLACK VULTURE *CORAGYPS-ATRATUS*. *J Exp Biol* 53:363–74.
- Pennycuik CJ. 1968. A Wind-Tunnel Study of Gliding Flight in the Pigeon *Columba Livia*. *J Exp Biol* 49:509–26.
- Polly PD, Stayton CT, Dumont ER, Pierce SE, Rayfield EJ, Angielczyk KD. 2016. Combining geometric morphometrics and finite element analysis with evolutionary modeling: towards a synthesis. *J Vertebr Paleontol* 36:e1111225.
- R Development Core Team. 2013. R: A Language and Environment for Statistical Computing Vienna, Austria: R Foundation for Statistical Computing.
- Revell LJ. 2012. phytools: an R package for phylogenetic comparative biology (and other things). *Methods Ecol Evol* 3:217–23.
- Rosen M, Hedenstrom A. 2001. Gliding flight in a jackdaw: A wind tunnel study. *J Exp Biol* 204:1153–66.
- Rubolini D, Liker A, Garamszegi LZ, Møller AP, Saino N. 2015. Using the BirdTree.org website to obtain robust phylogenies for avian comparative studies: A primer. *Curr Zool* 61:959–65.

- Segre PS, Dakin R, Zordan VB, Dickinson MH, Straw AD, Altshuler DL. 2015. Burst muscle performance predicts the speed, acceleration, and turning performance of Anna's hummingbirds. *eLife* 4:e11159.
- Shaffer SA, Weimerskirch H, Costa DP. 2001. Functional significance of sexual dimorphism in Wandering Albatrosses, *Diomedea exulans*. *Funct Ecol* 15:203–10.
- Shannon HD, Young GS, Yates MA, Fuller MR, Seegar WS. 2002. American white pelican soaring flight times and altitudes relative to changes in thermal depth and intensity. *The Condor* 104:679–83.
- Sheard C, Neate-Clegg MHC, Alioravainen N, Jones SEI, Vincent C, MacGregor HEA, Bregman TP, Claramunt S, Tobias JA. 2019. The latitudinal gradient in hand-wing-index: global patterns and predictors of wing morphology in birds. *bioRxiv* 816603.
- Sobol I. 1993. Sensitivity estimates for nonlinear mathematical models. *Math Model Comput Exp* 1:407–14.
- Stoddard MC, Yong EH, Akkaynak D, Sheard C, Tobias JA, Mahadevan L. 2017. Avian egg shape: Form, function, and evolution. *Science* 356:1249–54.
- Sudret B. 2008. Global sensitivity analysis using polynomial chaos expansions. *Reliab Eng Syst Saf, Bayesian Networks in Dependability* 93:964–79.
- Swaddle JP, Lockwood R. 1998. Morphological adaptations to predation risk in passerines. *J Avian Biol* 29:172–76.
- Taylor G, Thomas A. 2014. *Evolutionary Biomechanics* Oxford University Press.
- Tseng ZJ. 2013. Testing Adaptive Hypotheses of Convergence with Functional Landscapes: A Case Study of Bone-Cracking Hypercarnivores. *PLoS ONE* 8:e65305.
- Tucker VA. 1988. Gliding Birds: Descending Flight of the Whitebacked Vulture, *Gyps Africanus*. *J Exp Biol* 140:325–44.
- Tucker VA, Heine C. 1990. Aerodynamics of Gliding Flight in a Harris' Hawk, *Parabuteo Unicinctus*. *J Exp Biol* 149:469–89.
- Usherwood JR. 2005. Dynamic pressure maps for wings and tails of pigeons in slow, flapping flight, and their energetic implications. *J Exp Biol* 208:355–69.
- Usherwood JR, Cheney JA, Song J, Windsor SP, Stevenson JPJ, Dierksheide U, Nila A, Bomphrey RJ. 2020. High aerodynamic lift from the tail reduces drag in gliding raptors. *J Exp Biol* 223.
- Vogel S. 1981. *Life in moving fluids*. Princet Univ.

- Wainwright PC. 2007. Functional Versus Morphological Diversity in Macroevolution. *Annu Rev Ecol Evol Syst* 38:381–401.
- Waldrop LD, He Y, Hedrick TL, Rader JA. 2020. Functional morphology of gliding flight I. Modeling reveals distinct performance landscapes based on soaring strategies. *Integr Comp Biol* tbd.
- Waldrop LD, He Y, Khatri S. 2018. What Can Computational Modeling Tell Us about the Diversity of Odor-Capture Structures in the Pancrustacea? *J Chem Ecol* 44:1084–1100.
- Wang X, Clarke JA. 2015. The evolution of avian wing shape and previously unrecognized trends in covert feathering. *Proc R Soc B* 282:20151935.
- Warrick DR, Hedrick TL, Biewener AA, Crandell KE, Tobalske BW. 2016. Foraging at the edge of the world: low-altitude, high-speed manoeuvring in barn swallows. *Phil Trans R Soc B* 371:20150391.
- Weimerskirch H, Bishop C, Jeanniard-du-Dot T, Prudor A, Sachs G. 2016. Frigate birds track atmospheric conditions over months-long transoceanic flights. *Science* 353:74–78.
- Weimerskirch H, Salamolard M, Sarrazin F, Jouventin P. 1993. Foraging Strategy of Wandering Albatrosses Through The Breeding Season: A Study Using Satellite Telemetry. *The Auk* 110:325–42.
- Wiener N. 1938. The Homogeneous Chaos. *Am J Math* 60:897–936.
- Williams HJ, Duriez O, Holton MD, Dell’Omo G, Wilson RP, Shepard ELC. 2018. Vultures respond to challenges of near-ground thermal soaring by varying bank angle. *J Exp Biol* jeb.174995.
- Xiu D, Karniadakis GE. 2002. The Wiener--Askey Polynomial Chaos for Stochastic Differential Equations. *SIAM J Sci Comput* 24:619–44.

3.5 Figures

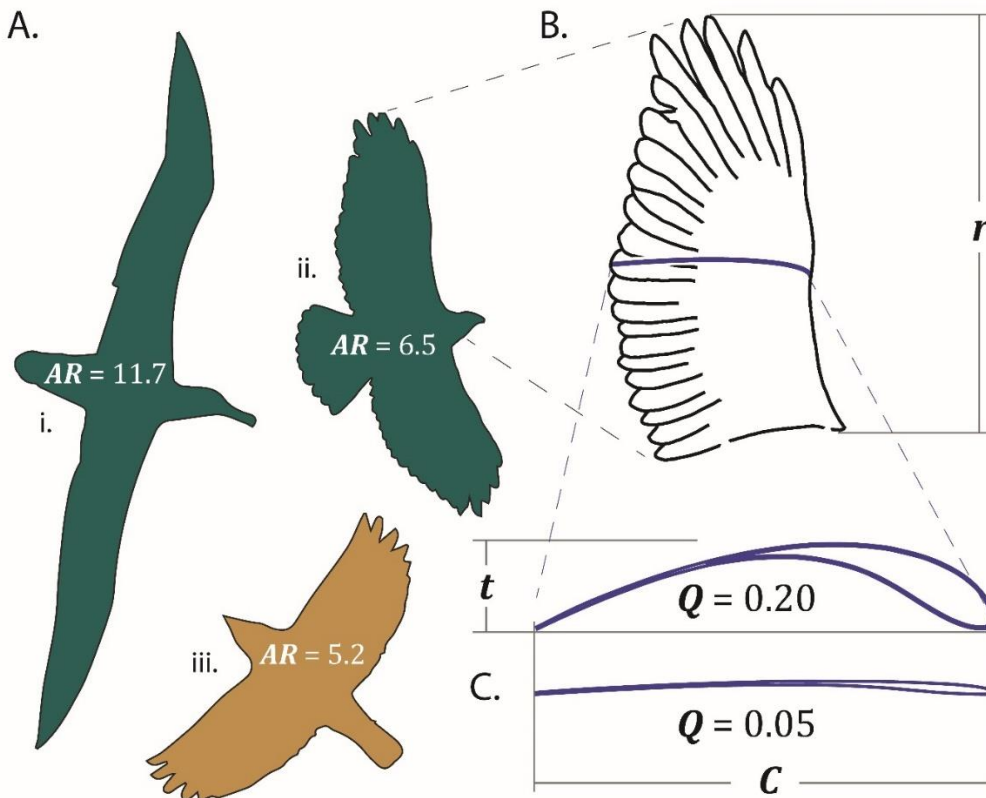


Figure 3.1 Morphological configurations and relevant metrics. Aspect ratio (AR) varied from < 5.0 to > 11.0 in my sample; examples of different AR are depicted in panel A. showing two gliders (blue-green color): *Diomedea exulans* (i.), *Buteo jamaicensis* (ii.), and a non-glider (tan color): *Junco hyemalis* (iii.). Wing length (r), chord (C) and section thickness (t) were measured as indicated (panels B. and C.) on 3-dimensionally scanned wings. Camber (Q) was calculated as the ratio of t/C and ranged in my sample from 0.07 to 0.16.

Figure 3.2 (Preceding page) Phylogenetic distribution of flight behavior and gliding strategy. The tree was pruned from the Jetz et al. (2012) supertree, and species naming follows that convention. Stochastic character mapping (Huelsenbeck et al. 2003; Bollback 2006) was used to map gliding (blue-green) vs. non-gliding (brown) flight behavior. Results of discriminant function analysis classifications of glider vs. non-glider are shown in column A., assignment of “aerial searching” and “aerial perching” gliding strategies in column B., and DFA classification of species into “aerial searcher” and “aerial percher” categories in column C.

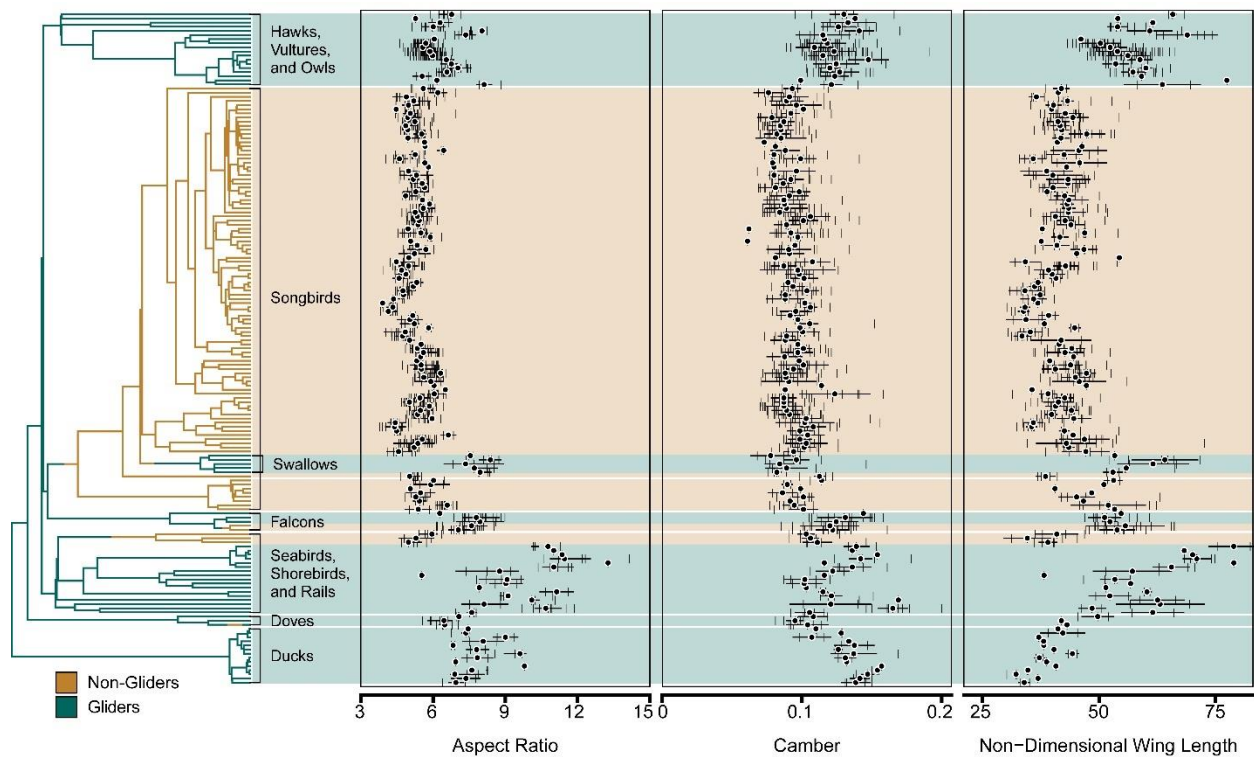


Figure 3.3 Phylogenetic distribution of shape traits: aspect ratio (AR), camber (Q) and non-dimensional wing length (r_{ND}). The tree was pruned from the Jetz et al. (2012) supertree, and stochastic character mapping (Huelsenbeck et al. 2003; Bollback 2006) was used to map gliding (blue-green) vs. non-gliding (tan) flight behavior. Vertical ticks in AR , Q and r_{ND} panes represent individual measurements, circles denote the species median, and horizontal bars reflect one median absolute deviation (MAD) on either side of the medians.

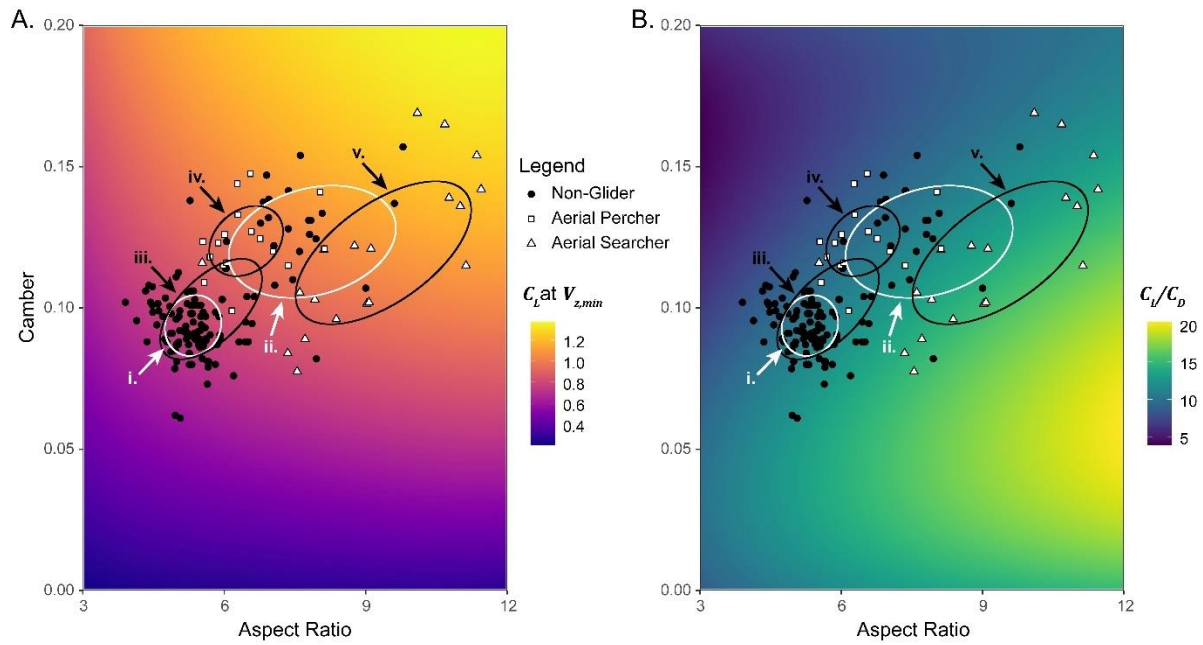


Figure 3.4 Gliding flight performance landscapes with distribution of measured bird species. Coefficient of lift measured at minimum sinking speed ($V_{z,min}$; panel A.) and maximum lift to drag ratio (C_L/C_D ; panel B.) surrogate functions are shown at Reynolds number (Re) = 105,000. Black circles in both panes represent non-gliding taxa, and light gray squares show species that glide regularly. White ellipses show 95% confidence regions (Jackson et al. 2011) for non-gliders (i.) and gliders (ii.), and black ellipses show the same for non-gliders (iii.), and two putative gliding strategies: aerial perching (iv.) and aerial searching (v.). See main text for descriptions of gliding strategies.

3.6 Tables

Table 3.1 Phylogenetic signal of body mass (M_b) camber (\bar{Q}), aspect ratio (AR), non-dimensional wing length (r_{ND}), and non-dimensional wing chord (\bar{C}_{ND}).

Shape Trait	Pagel's λ	Blomberg's K
M_b	0.90	0.37
\bar{Q}	0.83	0.41
AR	0.90	0.54
r_{ND}	0.96	0.67
\bar{C}_{ND}	0.98	1.37

Table 3.2 Model outputs from the top performing OUwie fit for camber (\bar{Q}), aspect ratio (AR), non-dimensional wing length (r_{ND}), and non-dimensional wing chord (\bar{C}_{ND}). Wing length and chord were non-dimensionalized by dividing the linear measurements by body mass^{0.33}. In all cases, dual optimum and dual rate models were preferred, as demonstrated by the high AIC_C weights. Optima are presented \pm SE.

Shape Trait	AIC _C Weight	Estimated Glider Optimum	Glider σ^2	Estimated Non- Glider Optimum	Non-Glider σ^2
\bar{Q}	0.99	0.120 \pm 0.003	1.0 x 10 ⁻⁴	0.097 \pm 0.002	2.51 x 10 ⁻⁵
AR	0.99	7.76 \pm 0.4	0.398	5.40 \pm 0.1	0.042
r_{ND}	0.99	55.71 \pm 1.83	5.78	41.58 \pm 1.82	2.19
\bar{C}_{ND}	0.99	14.80 \pm 0.67	0.73	15.90 \pm 0.7	0.28

CHAPTER 4: MORPHOLOGICAL MODULARITY AND EVOLUTION OF 3-DIMENSIONAL SHAPE IN BIRD WINGS

4.1 Introduction

Form – function relationships are one of the pillars of biodiversity. Morphological features have diverged in size and shape and impart different abilities among lineages to interact with the environment and compete for finite resources (Derryberry et al. 2011; Claramunt et al. 2012; Felice, Tobias, et al. 2019; Hedrick et al. 2020). Pleiotropy and shared function can lead to coevolution of phenotypic traits (Klingenberg 2008; Klingenberg and Marugán-Lobón 2013). The degree of integration among these coevolving traits and their organization into a mosaic of semi-independent modules is mediated by their shared development and by the magnitude of their impact on functional output (Esteve-Altava 2017; Felice, Watanabe, et al. 2019). Furthermore, individual traits within a system may vary in their influence on the functional output of the whole. In a biomechanical context, the strength of relationships between morphological traits and their mechanical function (termed mechanical sensitivity) may be an important driver of their evolutionary dynamics (tempo and mode) (Anderson and Patek 2015; Muñoz et al. 2017, 2018).

The first description of the relationship between mechanical sensitivity and evolutionary dynamics focused on four-bar linkage systems, particularly in the jaws of teleost fish (Westneat 1990; Gidmark et al. 2019) and the raptorial appendages of mantis shrimp (Patek et al. 2007).

Here, each link can be thought of as a discrete morphological module. The modules with the greatest impact on the transmission of force or motion in a four-bar linkage system also have the greatest mechanical sensitivity (Anderson and Patek 2015), which correlates with a shift in evolutionary mode (from Brownian motion toward Ornstein-Uhlenbeck) and to a higher evolutionary tempo (Muñoz et al. 2017, 2018). However, despite finding similar coupling of mechanical sensitivity and evolutionary dynamics in the four-bar linkage systems in two disparate taxa, the generalizability of these results is hampered by a lack of comparable studies of other morphological traits and biophysical systems (Muñoz et al. 2017). As such, studying morphological modularity and evolution in other systems with different biophysical interactions and tradeoffs can fill in some of the missing picture of the patterns and processes of evolution of complex biological structures. I investigated how evolutionary dynamics of wing shape in birds have responded to aerodynamic force production in flapping flight and morphological modularity within the wing.

4.1.1 Form begets function in bird wings

Birds are diverse in their ecology and behavior, which manifests in differences in their flight style, morphology, and performance. Bird wings must produce lift to support body weight during flight and asymmetrical forces for maneuvering. They must function at cruising speed, at low airspeeds during landing and maneuvering flight, and during supra-normal efforts for pursuit or escape flight. Furthermore, bird wings may experience trade-offs and constraints imposed by their structure and evolutionary development.

The geometry of a wing influences how it interacts with the air, and thus the lift and drag forces that it generates (Prandtl et al. 1957). Consequently, wing shape in birds is related

to flight and migration behavior (Mulvihill and Chandler 1990; Lockwood et al. 1998; Swaddle and Lockwood 2003; Baldwin et al. 2010; Taylor and Thomas 2014; Rader et al. 2020) and numerous other aspects of avian biology (Swaddle and Lockwood 1998; Stoddard et al. 2017; Sheard et al. 2019, 2020; Pigot et al. 2020). Much work has been done describing how planform (2-dimensional) wing shape is related to avian aerodynamics (Cone 1968; Bacon 1976; Nachtigall 1979; Tucker and Heine 1990; Hedenstrom 2002; e.g. Altshuler et al. 2015). However, wings are not two-dimensional structures. Three-dimensional (3D) shape attributes such as wing camber contribute to aerodynamic forces produced by the wing (e.g., Brown 2001; Waldrop et al. 2020a), and the distribution of mass along the wing span impacts the cost of flapping (van den Berg and Rayner 1995) and maneuverability (Lin et al. 2012; Bergou et al. 2015). Because 3D attributes of the wing are tied to its function, they are also potentially evolutionarily labile and tunable features, worthy of consideration in the story of avian wing evolution (Waldrop et al. 2020a; Rader et al. 2020).

4.1.2 *Are birds wings modular?*

Though the wing feathers create a generally contiguous wing surface, the avian wing is composed of multiple anatomical subunits (Bribiesca-Contreras et al. 2021). The most obvious of these are associated with the major skeletal regions of the forelimb (Fig. 1). The portion of the wing associated with the radius and ulna (and to a lesser degree, the humerus) is the armwing (AW), and includes the bony elements, muscles, tendons, and the secondary and tertial portions of the feathered wing surface (Bribiesca-Contreras et al. 2021). The AW also supports the propatagium on its leading edge. The handwing (HW) is comprised by the bones of the wrist and hand as well as the primary portion of the feathered wing surface, but with

minimal contribution from muscles and tendons (Bribiesca-Contreras et al. 2021). These two wing regions may be under differential selective pressures, or subject to different selective or developmental tradeoffs and constraints leading to evolutionary regionalization and modularity within the wing (Gatesy and Dial 1996; Esteve-Altava 2017; Bribiesca-Contreras et al. 2021). For these reasons, I hypothesized that morphological modularity exists in the wing, dividing it into discrete armwing and handwing modules.

4.1.3 Are evolutionary dynamics in the wing modular?

Inertial effects and aerodynamic forces from flapping flight increase as the square of the distance from the base of the wing, with the greatest effects at the tip of the wing (Weis-Fogh 1972). This gradient of aerodynamic and inertial effects may also impose a gradient of mechanical sensitivity along the length of the wing (Fig. 1c), potentially driving differences in evolutionary dynamics of shape traits along the wing (Muñoz et al. 2018). I identified three idealized patterns that might characterize evolutionary dynamics in the wing: 1) Mechanical sensitivity could be governed by steady-state (gliding) aerodynamics and be functionally unrelated to the force gradient imposed by flapping. In this case, there is no base-to-tip gradient of mechanical sensitivity, and no hypothesized differences in evolutionary tempo or mode along the wing (see Fig. 1c, pane 'i'). Alternatively, 2) mechanical sensitivity could follow the gradient, irrespective of whether the wing is organized into semi-independent morphological modules, producing a root to tip pattern of increasing evolutionary tempo (Fig. 1c, pane 'ii'). 3) If flapping flight governs mechanical sensitivity and the wing is evolutionarily modular, the HW region would display distinctly greater mechanical sensitivity than the AW region, with a faster evolutionary tempo and possibly a shift in evolutionary mode across the

wrist (Fig. 1c, pane 'iii'). Overall, the importance of flapping in avian flight led us to hypothesize that shape traits would display greater morphological disparity near the tip of the wing, and that evolutionary tempo would also increase from the base of the wing toward its tip. I investigated these hypotheses using 3D surface scans of bird wings from a wide variety of taxa, providing a basis for exploring regionalization and modularity of avian wing morphology and evolution.

4.2 Methods

4.2.1 Wing scanning and measurement

Three-dimensional wing shape data were collected from spread wings in the collection at the North Carolina Museum of Natural Sciences (NCMNS) in Raleigh, NC. Sample sizes of each taxon were limited by the availability of specimens in the NCMNS collection, but when available, I scanned 16 individuals per species and maintained a balanced sex ratio. Wings were scanned using a NextEngine 3D Scanner Ultra HD laser scanner (NextEngine, Inc., Santa Monica, CA). Scan resolution was set to optimize scanning time while preserving surface detail. Resolutions ranged from 78 dots per cm² for large wings to 6300 dots per cm² for smaller wings. The scanned wings were processed using a custom MATLAB program (MATLAB r2014b, The MathWorks, Natick, MA, USA) that extracted the vertices from the 3D object files, creating point clouds in the shape of the wings. I used a principal components analysis to align the wing point clouds by their span (PC1, X-dimension), chord, (PC2, Y-dimension), and thickness (PC3, Z-dimension). Wing length (r) was measured as $X_{\max} - X_{\min}$, and wingspan as $2r$. Because the wings were removed from the body in preservation, I was unable to account for the width of the body

in my measure of wingspan, and therefore preferred to use the simpler measure of wing length in subsequent analyses.

Three-dimensional shape traits were measured by subdividing the wings into chord-wise slices along their span. To facilitate direct comparisons between wings and among taxa, I set the width of the slices to be 1/25th of the distance from the wrist joint to the tip of the wing, ensuring that all wings would have the same number of handwing (HW) slices. The number of slices representing the armwing (AW) was allowed to vary, as the proportion of HW vs. AW differs among taxa. Substantial trauma occurs during the removal of the wing during preservation, so the proximal 1/3rd of the AW was excluded from analyses to reduce the influence of preservational artifacts.

I measured four shape traits from each wing slice. Chord was measured as $Y_{max} - Y_{min}$, and cross-sectional area (XSA) was measured as the area contained within a spline fitted to the perimeter of the wing section in the Y/Z plane. The maximum distance in the Z -dimension (i.e., the greatest distance from the upper wing surface to the lower wing surface) was recorded as the maximum cross-sectional thickness (XST). Camber was calculated as $(Z_{max} - Z_{min}) / (Y_{max} - Y_{min})$.

Body mass (M_b) was recorded from museum tag data where available. When mass was not available from specimen tags, a species mean value was filled in from the CRC Handbook of Avian Masses (Dunning Jr. 2007). Measurements of wing length, area, chord, and thickness were scaled by dividing by body mass taken to the appropriate power ($M_b^{1/3}$ for linear

measures and $M_b^{2/3}$ for areas) and summarized within each taxon. Subsequent analyses were conducted on species median values for each wing slice.

4.2.2 *Phylogenetics*

Phylogenetic analyses were based upon the Jetz. *et al.* (2012) super tree from Birdtree.org (Rubolini *et al.* 2015). The tree was pruned to include only taxa in the scanned wing dataset. Handling of the tree, data, and phylogenetic analyses was done using tools from the *Phytools* (Revell 2012) and *geiger* (Harmon *et al.* 2008) packages in the R Statistical Computing Environment version 4.1.0 (R Development Core Team 2013). Phylogenetic signal (Blomberg's K (Blomberg *et al.* 2003) and Pagel's λ (Pagel 1999b) was calculated for each wing slice using the '*phylosig*' function in the *Phytools* package.

4.2.3 *Morphological modularity analysis*

4.2.3.1 *Modularity*

To assess whether the HW and AW are morphologically distinct modules, I used the covariance ratio (CR) proposed by Adams (2016). This test compares the covariance among traits within a putative module to covariance among the modules. The test statistic (CR) ranges from 0 to infinity, with values between 0 and 1 representing greater covariance within putative modules than among them, signaling morphological modularity. CR greater than 1 indicates morphological integration, and a lack of modularity (Adams 2016). This test was implemented using code provided in the supplement of Adams' description of the method (2016). Because the mean values of the shape traits differ between wing regions, in addition to conducting the modularity test on the isometrically scaled data, I used a \log_{10} -transformation to mitigate any

biasing effect from the difference in means. Furthermore, because the wrist joint affects wing camber, thickness, and XSA, its effect on the modularity analysis was difficult to predict. To test whether inclusion of the wrist influenced my modularity interpretations, I iterated the analysis, including the wrist in each of the wing regions, while excluding it from the other. I also removed the wrist from consideration entirely, and only analyzed regions proximal and distal to it. Because inclusion of the wrist had no impact on the modularity analysis, and for the sake of simplicity, I present results excluding the wrist since this avoids arbitrarily assigning it to either the AW or HW region.

4.2.3.2 Disparity

Morphological disparity is a measure of the variation in traits among taxa. I compared morphological disparity in each of the shape traits for each wing slice using the *'disPRity'* function in the *disPRity* package (Guillerme 2018) in R. I compared disparity between the HW and the AW using regression discontinuity analysis (RDA) using the *'rdd_reg_lm'* function in the *rdd_tools* package (Stigler and Quast 2015) in R. Regression discontinuity analysis is a statistical tool to assess changes in slope or intercept in a temporal or spatial trend across an assigned X-axis cutoff point, in this case, the wrist joint. A difference in disparity in the same shape traits between different regions of the wing would indicate a difference in evolutionary lability as well.

4.2.4 Evolutionary modularity analysis

4.2.4.1 Evolutionary tempo and mode

To test whether different morphological modules expressed different evolutionary dynamics, I fit Brownian motion (BM), Ornstein-Uhlenbeck (OU), and early-burst (EB) evolutionary models to each of the shape traits at each of the wing slices using the *'fitContinuous'* function in the *geiger* package in R. I used Akaike's Information Criterion corrected for small sample size (AICc) to determine the most suitable model for each trait and estimated evolutionary rate (σ^2) for each wing slice using that model. I tested for differences in patterns of σ^2 between the wing regions using regression discontinuity analysis (RDA) as described above.

4.3 Results

4.3.1 Dataset

I scanned 1096 wings representing 178 species of birds with an average sample size of 6 individuals per species. Median wing camber across all slices, averaged within each species, ranged from 0.061 to 0.169, with an overall mean of 0.105. Armwing (AW) camber was greater than that in the handwing (HW, median \pm MAD: 0.11 ± 0.021 vs. 0.072 ± 0.017). Mean chord ranged from 30.6 mm to 249.9 mm, with an overall mean of 64.3 mm. Median chord (non-dimensionalized by dividing by $M_b^{1/3}$) was greater in the AW (20.43 ± 2.59) than in the HW (13.16 ± 2.53). Wing thickness at the most proximal measured slice of the AW varied among the study species from 2.19 mm to 41.43 mm (mean = 9.83 mm) and tapered to the wrist joint. Thickness of the wrist joint ranged from 1.03 mm to 31.69 mm with an average of 6.31 mm. Wing thickness tapered further toward the most distal measured slice of the HW (range = 0.39

– 10.31 mm, mean = 1.54 mm). Wing cross-sectional area showed a similar pattern, tapering from a mean of 556.42 mm² at the most proximal measured wing slice (range = 26.43 to 5,756.24 mm²) to a mean of 27.16 mm² at the most distal measured slice (range = 1.19 to 567.18 mm²). The profiles of camber, chord, cross-sectional thickness (*XST*) and cross-sectional area (*XSA*) across the measured portion of the wing are shown in Fig. 2.

4.3.2 *Morphological modularity*

The covariance ratio (CR) test (Adams 2016) identified significant morphological modularity ($CR < 1.0$, see Fig. 3) in the log-transformation of all shape traits (camber $CR = 0.79$, $p < 0.001$; chord $CR = 0.79$, $p < 0.001$; *XST* $CR = 0.87$, $p < 0.001$; *XSA* $CR = 0.87$, $p < 0.001$), suggesting that the AW and HW are morphologically discrete subunits of the wing. Log-transforming the data removed the biasing effect of differing means between the regions (see Adams 2013), but a similar outcome was obtained from the raw data as well. Additionally, this result was robust to inclusion of the wrist in either the hand or arm region.

4.3.3 *Morphological disparity*

Disparity of camber was greater in the HW (mean = 0.014, see Table 1) than in the AW (mean = 0.008), with maximum (0.017) near the middle of the HW and a sharp downward transition through the wrist joint (Fig. 4). Regression-discontinuity analysis (RDA) confirmed that the spanwise trend in camber is discontinuous about the wrist ($p < 0.001$). Disparity of chord exhibited no spatial trend, had comparatively low values throughout the AW (mean = 0.007), and increased distal to the wrist. Mean chord disparity in the HW was 0.012, and the distinction between the HW and the AW was supported by RDA ($p < 0.001$). Disparity of *XST* and *XSA* shared similar patterns: disparity was greatest near the tip of the wing, and decayed

toward the middle of the HW (consistent with the pattern depicted in Fig. 1C, pane “ii”). In both cases, RDA showed marginal support for the discontinuity across the wrist joint ($p_t = 0.025$, $p_A = 0.014$).

4.3.4 Evolutionary tempo and phylogenetic signal

For all shape traits, AICc supported an OU model of evolution across all wing slices (all $\Delta\text{AICc} > 4$). Evolutionary tempo (σ^2) among the shape traits (camber, chord, *XST*, and *XSA*) broadly showed similar trends, with greater rates corresponding with higher disparity (Table 1). However, the discontinuity across the wrist joint was less distinct, except in chord (RDA $p < 0.001$). Discontinuity results were marginal for *XST* ($p = 0.028$) and non-significant for *XSA* and camber. Phylogenetic signal was high throughout the wing in all shape traits (all $K < 0.35$ and all $\lambda > 0.60$, see Table 1).

4.4 Discussion

Bird wings are complex structures composed of a feathered aerodynamic surface, skeleton, muscles, and connective tissues (Fig. 1). The wing also contains two anatomical regions: the handwing (HW) distal to the wrist, and the armwing (AW) proximal to it. I hypothesized that this complexity results in morphological and evolutionary modularity, meaning that trait variation between anatomical subunits is greater than the variation within them.

I further hypothesized that mechanical sensitivity (the strength of the relationship between trait morphology and functional output; Anderson & Patek, 2015; Muñoz et al., 2017) would increase along the wing as the square of the distance from the wing base, matching the

aerodynamic force gradient and moment of inertia for flapping wings (Weis-Fogh 1972) (see Fig. 1c). High mechanical sensitivity increases the evolutionary tempo of modules in complex structures (Anderson and Patek 2015; Muñoz et al. 2017). However, in earlier studies of modularity focusing on 4-bar linkage systems, each link formed a discrete module with a similarly discrete mechanical sensitivity rather than the smooth base to tip gradient hypothesized here. I used a dataset of 1096 3D scanned wings from 178 bird species to assess the morphological modularity in bird wings and test whether higher mechanical sensitivity at the wingtip drives higher rates of evolution.

I found significant discontinuity in morphological disparity across the wrist joint in all traits, supporting discretization of the HW and AW as two morphological modules. Disparity was significantly greater in the HW for all traits, and σ^2 largely followed a similar trend. Both measures decreased away from the wingtip, following the predicted gradient of mechanical sensitivity. There was significant discontinuity for σ^2 in wing chord and marginally for *XST*. However, σ^2 for camber and cross-sectional area were not discretely separated at the wrist, despite greater values near the wingtip. These results are consistent with the hypothesis that the HW and AW are morphological modules, and that evolutionary dynamics are related to the mechanical sensitivity of the morphological traits. However, I also show that the link between mechanical sensitivity and evolutionary rate does not depend upon morphological modularity, but can also track sensitivity gradients.

4.4.1 *Bird wings are modular structures*

Gatesy and Dial (1996) proposed that locomotor modularity (the integration of anatomical subunits, such as the hindlimbs or forelimbs, into functional subunits during

locomotion) is responsible for the evolutionary diversification of avian morphology and locomotion, and potentially for the origin of flight. Here, I present a refinement to their view of modularity within the structure of the wing. My results show that bird wings are complex structures composed of at least two morphological modules, the handwing (HW) and the armwing (AW), delineated by the wrist joint. I measured morphological disparity, a quantification of the occupancy of multivariate space such as that formed by multiple morphological axes (in this case, four axes: camber, chord, *XST* and *XSA*), along the wing. I found that morphological disparity is greatest in the HW, and especially so at the wingtip. I used Regression Discontinuity Analysis (RDA) to demonstrate that the patterns of morphological disparity were different in the HW and the AW (see Fig. 4), providing evidence that the HW and AW are discrete modules. Morphological modularity in complex biological systems is the result of shared inheritance, similar developmental patterns, or shared function (Klingenberg and Marugán-Lobón 2013; Denton and Adams 2015; Esteve-Altava 2017; Jones et al. 2018). Morphological modularity has been documented in mammalian backbones, where a gradient of selective pressures along the length of the spine leads to regionalization of both form and function (Randau and Goswami 2017; Jones et al. 2018). The flight feathers of birds' wings form a set of serially-homologous elements akin to vertebrae in the mammalian backbone, and also experience a gradient of forces (Weis-Fogh 1972). My results show significant regionalization of wing morphology, however, the relationship between form and function here is only implied, and whether this regionalization of morphology also leads to regionalization of biomechanical output warrants further attention.

The finding that the HW and AW form discrete morphological modules does not imply that additional modularity cannot be found at different levels or axes of organization within the wing. The wing is composed of skeletal, muscular, and integumental components, which might experience different pressures and tradeoffs that shape their evolution across multiple levels of organization (Denton and Adams 2015; Esteve-Altava 2017). For example, the thickness of the wing skeleton is tied both to its aerodynamics – thicker wings present more frontal area to the wind and produce more drag, and to its structural rigidity – thicker wing bones are more able to resist bending (Rader and Hedrick 2019). The geometry of the wing’s feathered surface influences, in part, the magnitude and distribution of the forces the skeleton must withstand (Weis-Fogh 1972; Ellington 1984). Therefore, these features might show morphological integration, *i.e.*, that their morphologies coevolve within discrete regions of the wing, and that the strength of the integration may vary along the length of the wing. However, the flight feathers are serially homologous features arranged along the wingspan, whose relative sizes determine the dimensions and geometry of the airfoil (Kipp 1959; Lockwood et al. 1998). Each feather is potentially exposed to different evolutionary pressures based on its position on the wing, raising the possibility that each feather could be a morphological and evolutionary module. The 3D scanned wings did not permit investigation of modularity at these levels of organization, so it possible that a greater magnitude of modularity exists that could be uncovered by different measurement techniques.

4.4.2 *Trait evolution follows a gradient rather than modules*

I predicted and found that bird wings show strong morphological modularity between the HW and the AW. I also predicted that evolutionary dynamics (tempo and mode) would

differ significantly between morphological modules. While I did find that mean values of σ^2 were greater in the HW for all traits, evidence for evolutionary modularity was, at best, equivocal. Regression discontinuity analysis identified significant transitions in σ^2 for chord and marginally for *XST*, but not for camber or *XSA*. Instead, σ^2 for *XST* is consistent across much of the wing, with a notable increase near the wingtip. Camber σ^2 also shows an increase at the wingtip but is otherwise consistent within the HW and greater than in the AW. I therefore found little support for evolutionary modularity within the wing, and propose that evolutionary change of the shape traits discussed here is not beholden to morphological modules, but instead follows a smooth gradient along the span of the wing.

Aerodynamic forces in flapping flight increase as the square of the distance from the wing base (Weis-Fogh 1972), and as such, smaller morphological alterations in wing geometry near the tip of the wing will produce outsized impacts on aerodynamic performance. The result is a span-wise gradient of increasing mechanical sensitivity toward the tip of the wing. Mechanical sensitivity influences evolutionary dynamics of morphological traits, biasing toward higher rates of evolutionary diversification (Muñoz et al. 2017, 2018), as I found in the HW. Greater morphological disparity and faster evolutionary tempo in the HW (and particularly its distal tip region) relative to elsewhere along the span support my hypothesis that selective pressures driving morphological evolution in avian wings are related to the distribution of aerodynamic and inertial forces along the span of the wing. My results are also consistent with prior work demonstrating that planform wing shape has diverged primarily near the wingtips (Lockwood et al. 1998), and demonstrate that 3D shape traits (camber, *XST*, and *XSA*) behave similarly.

Prior studies linking mechanical sensitivity to evolutionary dynamics in 4-bar linkage systems have documented transitions in evolutionary mode (i.e. Ornstein-Uhlenbeck vs. Brownian motion) in addition to a shift toward higher rates (Muñoz et al. 2017, 2018). However, I found no shift in mode across the wrist joint. The OU model was best supported by AICc in all shape traits across the entirety of the wing. This is unsurprising for camber and XSA, as the RDA models for these traits did not highlight significant transitions in evolutionary rate (σ^2) across the wrist joint. However, there were significant differences in σ^2 between the wing regions for chord and, marginally, for XST, but without a shift in evolutionary mode. I posit that the lack of sharp transitions in evolutionary dynamics at the wrist joint, despite trait disparity analysis supporting discretization of the HW and AW into separate morphological modules, stems from the continuous gradient of increasing mechanical sensitivity along the span of the wing. Furthermore, this gradient is associated with flapping flight, and no such gradient of aerodynamic force output, and thus of mechanical sensitivity, exists in gliding flight. Therefore, the strength of the correlation between wingtip morphology and evolutionary dynamics might vary among lineages that differ in their reliance on flapping.

4.4.3 *Additional considerations*

Several shape indices have been developed to facilitate the broad taxonomic sampling necessary to explore how wing shape in birds relates to their behavior and ecology. The most widely adopted of these is the handwing index (HWI) (Kipp 1959; Lockwood et al. 1998), which serves as a proxy for wing aspect ratio. The present results suggest that the wingtip is evolutionarily labile and likely to be tuned to the various flight and lifestyle pressures among avian taxa, validating wingtip shape indices such as HWI. However, the utility of wingtip indices

remains limited. HWI provides an imperfect proxy for wing aspect ratio. The proportion of the AW varies among avian taxa (from approximately 30 to 60% of wing length in my sample). Birds with identical HWI can have very different AR. Camber interacts with AR and plays an important role in aerodynamic force production (Brown 2001; Waldrop et al. 2020a), but is not captured by any wingtip shape index. Wing volume (and by extension, mass) affects the inertial moment of the wing, influencing the energetic cost of flapping and the ability to use wing inertia for maneuvering.

I investigated the evolution of static wing shape, but bird wings are dynamic structures. Planform wing shape is dynamically and deliberately modified by birds in flight, termed “wing morphing” to modify aerodynamic performance (Pennycuick 1968; Lentink et al. 2007) and to react to transient perturbations (Reynolds et al. 2014; Cheney et al. 2020). Three-dimensional shape traits like camber and span-wise twist vary as the wing cycles through its flight stroke and when acted upon by aerodynamic forces in flight (Cheney et al. 2021), and the range of motion at the wing joints is a stronger predictor of flight style than 2D wing shape (Baliga et al. 2019b). A systematic understanding of how static wing shape affects the manner and to what degree birds can dynamically alter the shape of their wings in flight remains elusive and should prove to be a fruitful avenue for further investigation.

4.4.4 Concluding remarks

I assembled an unprecedented dataset of 3-dimensional wing shape in a broad taxonomic sample of birds. My analyses suggest that the wing is divided into at least two morphological modules separated by the wrist, the handwing and the armwing, and that shape divergence was greatest in the handwing. I tested competing hypotheses of how evolutionary

dynamics act upon the wing modules, and found that morphological disparity was significantly modular within the wings, but that evolutionary tempo followed a gradient of mechanical sensitivity along the span of the wing that was predicted by a simple model of aerodynamic force production and inertial moment in flapping flight (Weis-Fogh 1972). This expands our understanding of evolutionary dynamics of complex biological structures, demonstrating that morphology can be tuned along continuous gradients in addition to previously described modular processes (Muñoz et al. 2017, 2018). My results concur with prior observations that mechanical sensitivity drives evolution of biomechanical traits. Furthermore, I demonstrated that the linkage between mechanical sensitivity and evolutionary dynamics is not specific to four-bar linkages, but also exists in other biophysical systems and therefore might be fundamental to the evolution of form and function.

REFERENCES

- Adams DC. 2013. Comparing Evolutionary Rates for Different Phenotypic Traits on a Phylogeny Using Likelihood. *Syst Biol* 62:181–92.
- Adams DC. 2016. Evaluating modularity in morphometric data: challenges with the RV coefficient and a new test measure. *Methods Ecol Evol* 7:565–72.
- Altshuler DL, Bahlman J, Dakin R, Gaede AH, Goller B, Lentink D, Segre P, Skandalis D. 2015. The biophysics of bird flight: functional relationships integrate aerodynamics, morphology, kinematics, muscles and sensors. *Can J Zool*.
- Anderson PSL, Patek SN. 2015. Mechanical sensitivity reveals evolutionary dynamics of mechanical systems. *Proc R Soc B Biol Sci* 282:20143088.
- Bacon PJ. 1976. AERODYNAMIC MEASUREMENTS OF BIRDS. *Ringing Migr* 1:120.
- Baldwin MW, Winkler H, Organ CL, Helm B. 2010. Wing pointedness associated with migratory distance in common-garden and comparative studies of stonechats (*Saxicola torquata*). *J Evol Biol* 23:1050–63.
- Baliga VB, Szabo I, Altshuler DL. 2019. Range of motion in the avian wing is strongly associated with flight behavior and body mass. *Sci Adv* 5:eaaw6670.
- Berg C, Rayner J. 1995. The moment of inertia of bird wings and the inertial power requirement for flapping flight. *J Exp Biol* 198:1655–64.
- Bergou AJ, Swartz SM, Vejdani H, Riskin DK, Reimnitz L, Taubin G, Breuer KS. 2015. Falling with Style: Bats Perform Complex Aerial Rotations by Adjusting Wing Inertia. *PLOS Biol* 13:e1002297.
- Blomberg SP, Garland T, Ives AR. 2003. Testing for Phylogenetic Signal in Comparative Data: Behavioral Traits Are More Labile. *Evolution* 57:717–45.
- Bribiesca-Contreras F, Parslew B, Sellers WI. 2021. Functional morphology of the forelimb musculature reflects flight and foraging styles in aquatic birds. *J Ornithol* 162:779–93.
- Brown CA. 2001. The Effect of Camber on Thin Plate Low Aspect Ratio Wings at Low Reynolds Numbers University of Notre Dame.
- Cheney JA, Stevenson JPJ, Durston NE, Maeda M, Song J, Megson-Smith DA, Windsor SP, Usherwood JR, Bomphrey RJ. 2021. Raptor wing morphing with flight speed. *J R Soc Interface* 18:20210349.

- Cheney JA, Stevenson JPJ, Durston NE, Song J, Usherwood JR, Bomphrey RJ, Windsor SP. 2020. Bird wings act as a suspension system that rejects gusts. *Proc R Soc B Biol Sci* 287:20201748.
- Claramunt S, Derryberry EP, Brumfield RT, Renssen JV. 2012. Ecological Opportunity and Diversification in a Continental Radiation of Birds: Climbing Adaptations and Cladogenesis in the Furnariidae. *Am Nat* 179:649–66.
- Cone CDJ. 1968. THE AERODYNAMICS OF FLAPPING BIRD FLIGHT. *Va Inst Mar Sci Spec Sci Rep* 1–128.
- Denton JSS, Adams DC. 2015. A new phylogenetic test for comparing multiple high-dimensional evolutionary rates suggests interplay of evolutionary rates and modularity in lanternfishes (Myctophiformes; Myctophidae). *Evolution* 69:2425–40.
- Derryberry EP, Claramunt S, Derryberry G, Chesser RT, Cracraft J, Aleixo A, Pérez-Emán J, Renssen, Jr. JV, Brumfield RT. 2011. Lineage diversification and morphological evolution in a large-scale continental radiation: The neotropical ovenbirds and woodcreepers (aves: Furnariidae). *Evolution* 65:2973–86.
- Dunning Jr. J. 2007. *CRC Handbook of Avian Body Masses* CRC Press.
- Ellington CP. 1984. The Aerodynamics of Hovering Insect Flight. II. Morphological Parameters. *Philos Trans R Soc Lond B Biol Sci* 305:17–40.
- Esteve-Altava B. 2017. In search of morphological modules: a systematic review. *Biol Rev* 92:1332–47.
- Felice RN, Tobias JA, Pigot AL, Goswami A. 2019. Dietary niche and the evolution of cranial morphology in birds. *Proc R Soc B Biol Sci* 286:20182677.
- Felice RN, Watanabe A, Cuff AR, Noirault E, Pol D, Witmer LM, Norell MA, O’Connor PM, Goswami A. 2019. Evolutionary Integration and Modularity in the Archosaur Cranium. *Integr Comp Biol* 59:371–82.
- Gatesy SM, Dial KP. 1996. Locomotor Modules and the Evolution of Avian Flight. *Evolution* 50:331–40.
- Gidmark NJ, Pos K, Matheson B, Ponce E, Westneat MW. 2019. Functional Morphology and Biomechanics of Feeding in Fishes. In: Bels V, Whishaw IQ, editors. *Feeding in Vertebrates: Evolution, Morphology, Behavior, Biomechanics*. Fascinating Life Sciences Cham: Springer International Publishing. p. 297–332.
- Guillerme T. 2018. *dispRity*: A modular R package for measuring disparity. *Methods Ecol Evol* 9:1755–63.

- Harmon LJ, Weir JT, Brock CD, Glor RE, Challenger W. 2008. GEIGER: investigating evolutionary radiations. *Bioinformatics* 24:129–31.
- Hedenstrom A. 2002. Aerodynamics, evolution and ecology of avian flight. *Trends Ecol Evol* 17:415–22.
- Hedrick BP, Mutumi GL, Munteanu VD, Sadier A, Davies KTJ, Rossiter SJ, Sears KE, Dávalos LM, Dumont E. 2020. Morphological Diversification under High Integration in a Hyper Diverse Mammal Clade. *J Mamm Evol* 27:563–75.
- Jetz W, Thomas GH, Joy JB, Hartmann K, Mooers AO. 2012. The global diversity of birds in space and time. *Nature* 491:444–48.
- Jones KE, Benitez L, Angielczyk KD, Pierce SE. 2018. Adaptation and constraint in the evolution of the mammalian backbone. *BMC Evol Biol* 18:172.
- Kipp FA. 1959. Der Handflügel-Index als flugbiologisches Maß. *Vogelwarte* 20:77–86.
- Klingenberg CP. 2008. Morphological Integration and Developmental Modularity. *Annu Rev Ecol Evol Syst* 39:115–32.
- Klingenberg CP, Marugán-Lobón J. 2013. Evolutionary Covariation in Geometric Morphometric Data: Analyzing Integration, Modularity, and Allometry in a Phylogenetic Context. *Syst Biol* 62:591–610.
- Lentink D, Müller UK, Stamhuis EJ, de Kat R, van Gestel W, Veldhuis LLM, Henningsson P, Hedenström A, Videler JJ, van Leeuwen JL. 2007. How swifts control their glide performance with morphing wings. *Nature* 446:1082–85.
- Lin T, Zheng L, Hedrick T, Mittal R. 2012. The significance of moment-of-inertia variation in flight manoeuvres of butterflies. *Bioinspir Biomim* 7:044002.
- Lockwood R, Swaddle JP, Rayner JMV. 1998. Avian wingtip shape reconsidered: Wingtip shape indices and morphological adaptations to migration. *J Avian Biol* 29:273–92.
- Mulvihill RS, Chandler CR. 1990. The Relationship between Wing Shape and Differential Migration in the Dark-Eyed Junco. *The Auk* 107:490–99.
- Muñoz MM, Anderson PSL, Patek SN. 2017. Mechanical sensitivity and the dynamics of evolutionary rate shifts in biomechanical systems. *Proc R Soc B Biol Sci* 284:20162325.
- Muñoz MM, Hu Y, Anderson PSL, Patek S. 2018. Strong biomechanical relationships bias the tempo and mode of morphological evolution. *eLife* 7:e37621.

- Nachtigall W. 1979. THE PIGEONS WING DURING GLIDING FLIGHT GEOMETRICAL CHARACTERISTICS OF WING PROFILES AND GENERATION OF AERODYNAMIC FORCE COMPONENTS. *J Fuer Ornithol* 120:30–40.
- Pagel M. 1999. Inferring the historical patterns of biological evolution. *Nature* 401:877–84.
- Patek SN, Nowroozi BN, Baio JE, Caldwell RL, Summers AP. 2007. Linkage mechanics and power amplification of the mantis shrimp's strike. *J Exp Biol* 210:3677–88.
- Pennycuik CJ. 1968. A Wind-Tunnel Study of Gliding Flight in the Pigeon *Columba Livia*. *J Exp Biol* 49:509–26.
- Pigot AL, Sheard C, Miller ET, Bregman TP, Freeman BG, Roll U, Seddon N, Trisos CH, Weeks BC, Tobias JA. 2020. Macroevolutionary convergence connects morphological form to ecological function in birds. *Nat Ecol Evol*.
- Prandtl L, Tietjens OG, Den Hartog JP. 1957. Applied hydro-and aeromechanics Dover New York.
- R Development Core Team. 2013. R: A Language and Environment for Statistical Computing Vienna, Austria: R Foundation for Statistical Computing.
- Rader JA, Hedrick TL. 2019. Aerodynamics, not load, predicts avian wing thickness. In: INTEGRATIVE AND COMPARATIVE BIOLOGY OXFORD UNIV PRESS INC JOURNALS DEPT, 2001 EVANS RD, CARY, NC 27513 USA. p. E187–E187.
- Rader JA, Hedrick TL, He Y, Waldrop LD. 2020. Functional Morphology of Gliding Flight II. Morphology Follows Predictions of Gliding Performance. *Integr Comp Biol* 60:1297–1308.
- Randau M, Goswami A. 2017. Morphological modularity in the vertebral column of Felidae (Mammalia, Carnivora). *BMC Evol Biol* 17:133.
- Revell LJ. 2012. phytools: an R package for phylogenetic comparative biology (and other things). *Methods Ecol Evol* 3:217–23.
- Reynolds KV, Thomas ALR, Taylor GK. 2014. Wing tucks are a response to atmospheric turbulence in the soaring flight of the steppe eagle *Aquila nipalensis*. *J R Soc Interface* 11:20140645.
- Rubolini D, Liker A, Garamszegi LZ, Møller AP, Saino N. 2015. Using the BirdTree.org website to obtain robust phylogenies for avian comparative studies: A primer. *Curr Zool* 61:959–65.
- Sheard C, Neate-Clegg MHC, Alioravainen N, Jones SEI, Vincent C, MacGregor HEA, Bregman TP, Claramunt S, Tobias JA. 2019. The latitudinal gradient in hand-wing-index: global patterns and predictors of wing morphology in birds. *bioRxiv* 816603.

- Sheard C, Neate-Clegg MHC, Alioravainen N, Jones SEI, Vincent C, MacGregor HEA, Bregman TP, Claramunt S, Tobias JA. 2020. Ecological drivers of global gradients in avian dispersal inferred from wing morphology. *Nat Commun* 11:2463.
- Stigler M, Quast B. 2015. Rddtools: Toolbox for Regression Discontinuity Design ('RDD'). R package version 0.4. 0.
- Stoddard MC, Yong EH, Akkaynak D, Sheard C, Tobias JA, Mahadevan L. 2017. Avian egg shape: Form, function, and evolution. *Science* 356:1249–54.
- Swaddle JP, Lockwood R. 1998. Morphological adaptations to predation risk in passerines. *J Avian Biol* 29:172–76.
- Swaddle JP, Lockwood R. 2003. Wingtip shape and flight performance in the European Starling *Sturnus vulgaris*. *Ibis* 145:457–64.
- Taylor G, Thomas A. 2014. *Evolutionary Biomechanics* Oxford University Press.
- Tucker VA, Heine C. 1990. Aerodynamics of Gliding Flight in a Harris' Hawk, *Parabuteo unicinctus*. *J Exp Biol* 149:469–89.
- van Grouw K. 2013. *The Unfeathered Bird* Princeton University Press.
- Waldrop LD, He Y, Hedrick TL, Rader JA. 2020. Functional Morphology of Gliding Flight I: Modeling Reveals Distinct Performance Landscapes Based on Soaring Strategies. *Integr Comp Biol* 60:1283–96.
- Weis-Fogh T. 1972. Energetics of Hovering Flight in Hummingbirds and in *Drosophila*. *J Exp Biol* 56:79–104.
- Westneat MW. 1990. Feeding mechanics of teleost fishes (Labridae; Perciformes): A test of four-bar linkage models. *J Morphol* 205:269–95.

4.5 Figures

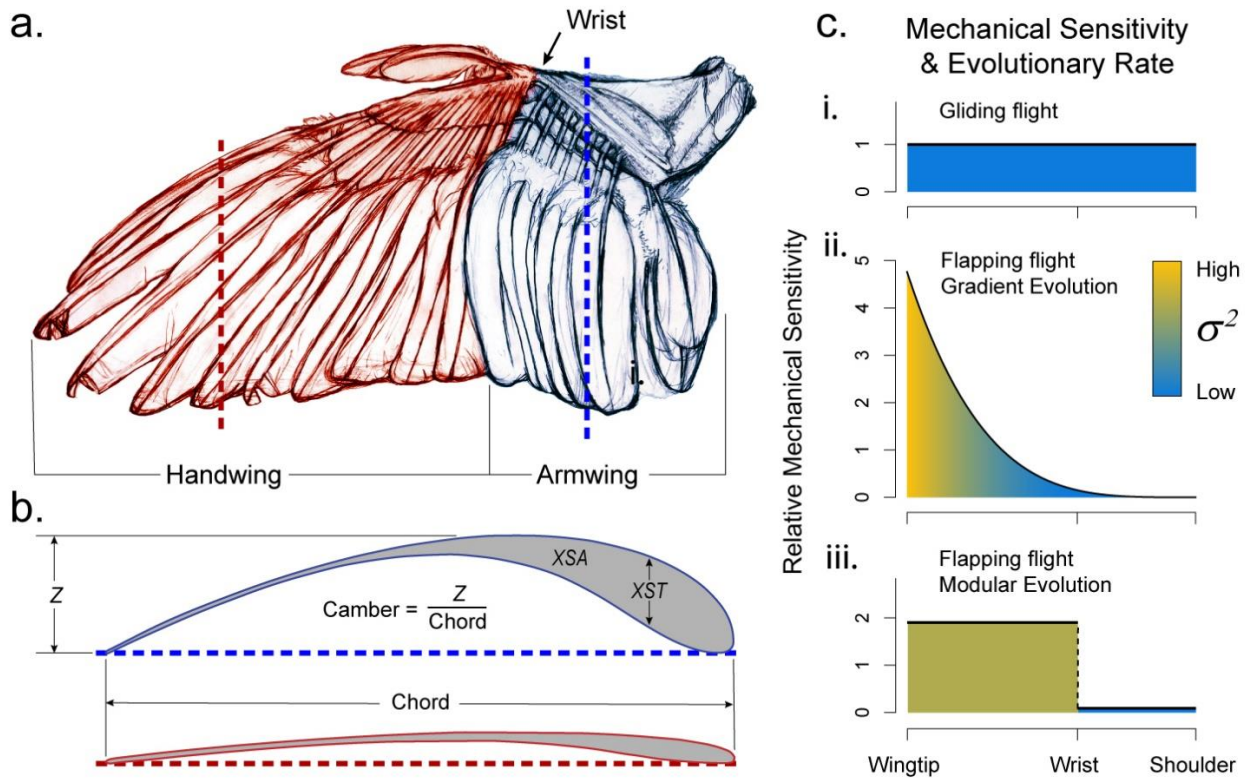


Figure 4.1 Bird wings are complex biological structures composed of musculoskeletal and integumentary elements (a; artwork by Katrina van Grouw) (van Grouw 2013). Flight feathers form the aerodynamic surface of the wing, which is divided into two regions separated by the wrist, the handwing and the armwing (a.). I divided the wing into chord-wise slices (b.) along its span, and measured chord, camber, cross-sectional thickness (XST) and cross-sectional area (XSA) from each one. Idealized hypotheses for the distribution of mechanical sensitivity along the wing were defined by flight behavior and modularity: i.) Gliding flight imposes consistent mechanical sensitivity along the wing span, ii.) Aerodynamic forces and inertial moment increase as the square of the distance from the base of the wing during flapping flight (Weis-Fogh 1972), and I hypothesized that mechanical sensitivity follows this gradient. iii.) If the handwing and armwing are discrete evolutionary modules, I expected greater mechanical sensitivity in the distal handwing relative to the armwing, owing to the gradient described in (ii.).

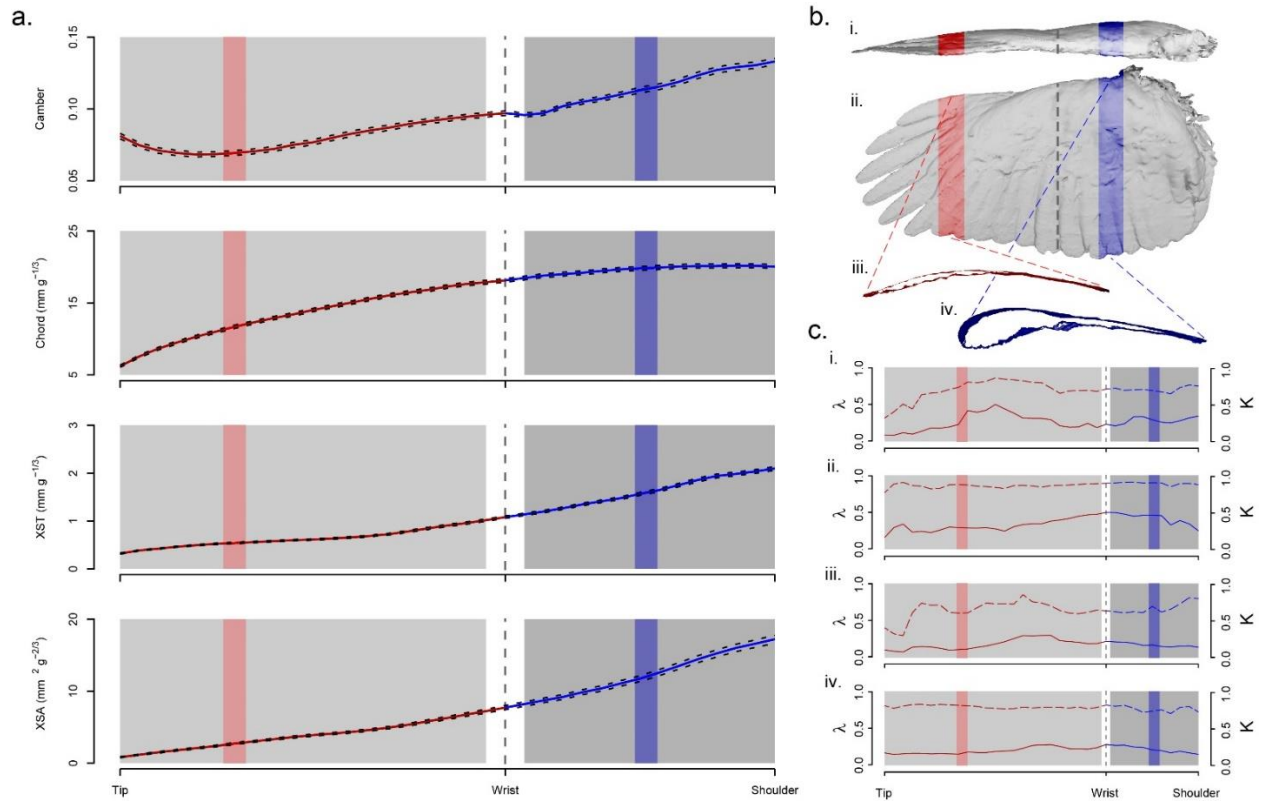


Figure 4.2 a.) Slice-wise profiles of wing shape. Mean values (solid lines) \pm SE (dashed lines), across taxa, of camber, chord, cross-sectional thickness (XST) and cross-sectional area (XSA) in the handwing (red) and armwing (blue). Gray boxes show the regions that were included in subsequent analyses of morphological and evolutionary modularity. The wrist was excluded. b.) Orthographic projection of a 3D wing scan in i.) frontal and ii.) planform views, with iii.) representative slices shown for the handwing (red) and armwing (blue). c.) Phylogenetic signal was high (Blomberg's $K < 0.35$ and Pagel's $\lambda > 0.6$) in all shape traits in both wing regions.

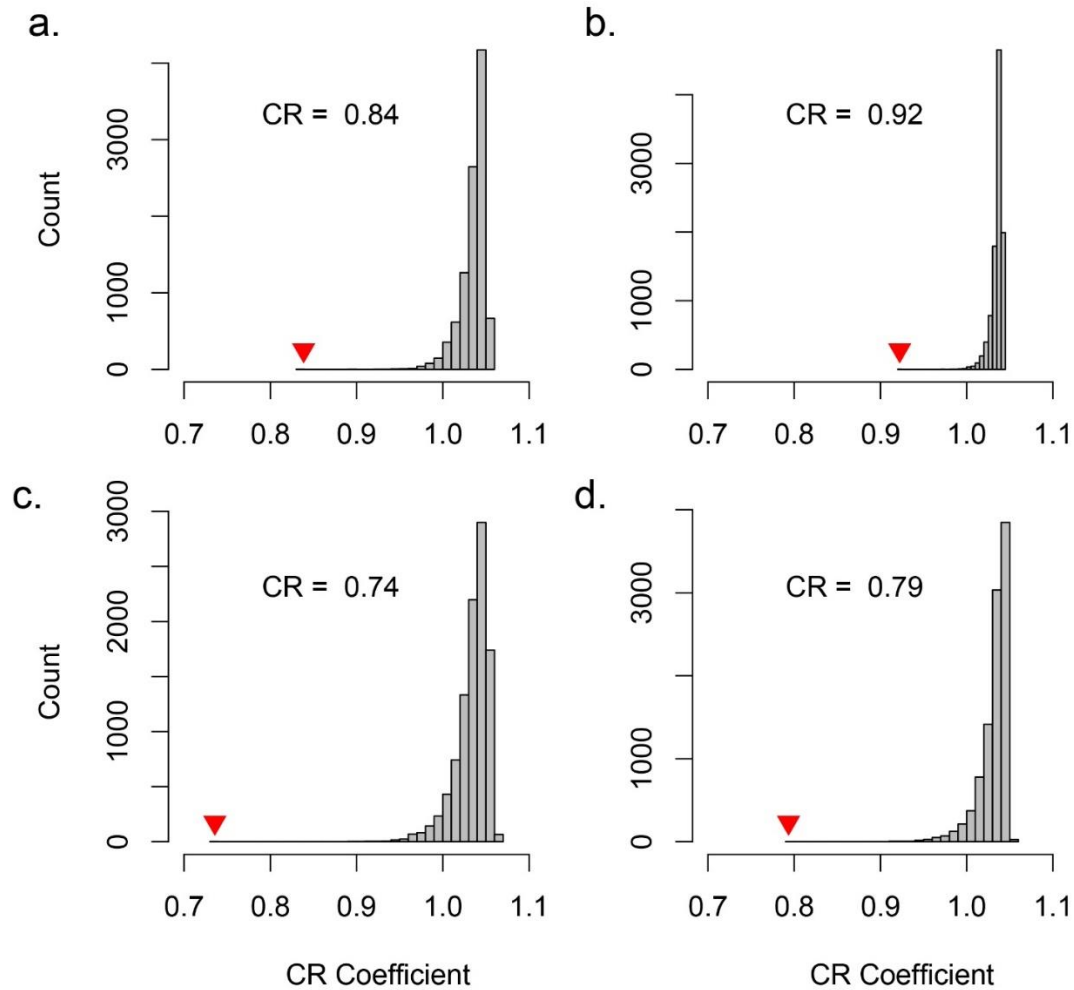


Figure 4.3 The covariance ratio test (CR) (Adams 2016) identified significant modularity between the handwing and the armwing for a.) camber, b.) chord, c.) cross-sectional thickness, and d.) cross-sectional area. A measured CR (inverted red triangle) that is less than 1.0 indicates morphological modularity between the two wing regions. In all cases, the measured CR value was significantly less than the mean recovered from 10,000 bootstrap replicates wherein I randomly assigned slices to each of the wing regions (Adams 2016).

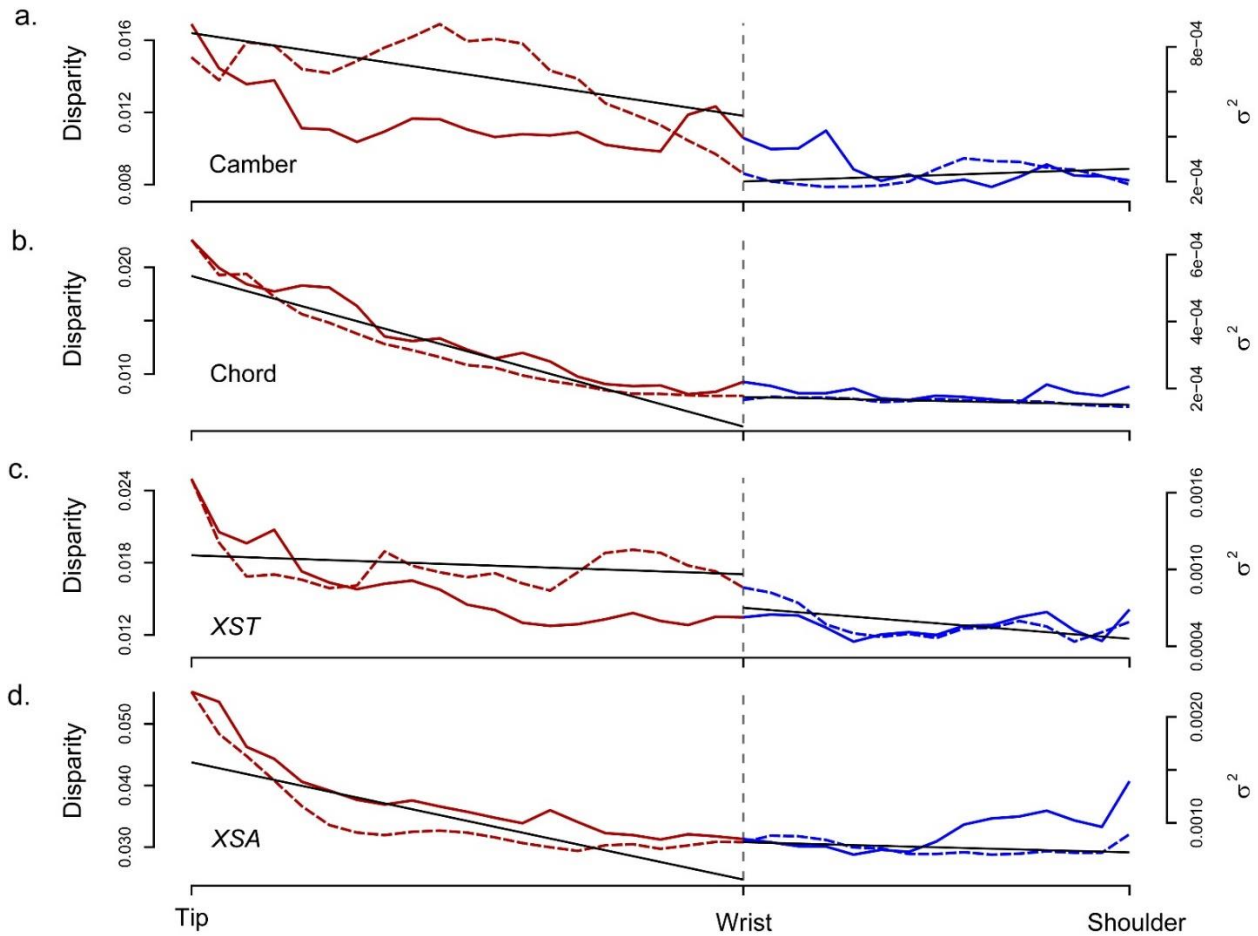


Figure 4.4 Morphological disparity (dashed line) and evolutionary rate (σ^2 , solid line) for a.) camber, b.) chord, c.) cross-sectional thickness (XST), and d.) cross-sectional area (XSA) were all greater in the handwing (red) than in the armwing (blue), and especially so near the wingtip. Regression discontinuity analyses (RDA) of morphological disparity (solid black lines) showed significant discontinuity across the wrist joint (see Table 1). The distinction across the wrist was less clear for σ^2 , except in wing chord and marginally in XST.

4.6 Tables

Table 4.1 Evolutionary dynamics. Phylogenetic signal, morphological disparity, evolutionary tempo (σ^2) and regression discontinuity analyses for four wing shape traits: wing camber, chord, cross-sectional thickness (*XST*), and cross-sectional area (*XSA*).

Shape Trait	Mean Phylogenetic Signal (HW λ, K AW λ, K)	Mean Disparity (HW AW)	Mean σ^2 (HW AW)	Disparity RDA effect p	σ^2 RDA effect p
Camber	0.69, 0.25 0.71, 0.28	0.014 0.008	0.0005 0.0003	0.000156*	0.721920
Chord	0.86, 0.32 0.90, 0.41	0.012 0.008	0.0004 0.0002	0.000114*	0.000351*
<i>XST</i>	0.64, 0.17 0.67, 0.16	0.018 0.013	0.0009 0.0006	0.0257*	0.0282*
<i>XSA</i>	0.79, 0.19 0.76, 0.21	0.035 0.030	0.0012 0.0009	0.0141*	0.487

* $P < 0.05$

CHAPTER 5: BEHAVIORAL COMPENSATION FOR LOW AIR DENSITY IN TURKEY VULTURES (CATHARTES AURA)

4.7 Introduction

The breadth of environmental conditions that species tolerate and exploit may, in large part, determine their geographic extent. Intuitively, species that can tolerate only a narrow set of environmental variables may be expected to have smaller geographic distributions than species that thrive in more diverse conditions (Slatyer et al. 2013). Thus, exploring how species whose ranges span broad environmental gradients or inhabit variable environments compensate for environmental challenges may shed light on how geographic range is constrained.

Life at high elevation, and the correspondingly reduced air density, presents a two-fold challenge to locomotor performance in flying animals (Altshuler and Dudley 2006). First, a physiological challenge of low air density stems from the reduction of available oxygen for respiration (Altshuler and Dudley 2006; Storz 2007), which can lead to hypoxia and decreased metabolic power output. Additionally, reduced air density poses a physical challenge to fliers, as it decreases the effectiveness of lift generation (Altshuler and Dudley 2006; Dillon and Dudley 2014). However, birds can be found at the highest elevations (Hiebl and Braunitzer 1988; McCracken, Barger, Bulgarella, Johnson, Sonsthagen, et al. 2009), suggesting that some species are able to compensate for these hardships. A variety of cardiopulmonary adaptations

allow high flying birds, such as bar-headed geese (Hiebl and Braunitzer 1988; Liu et al. 2001) and several lineages of Andean waterfowl (McCracken, Barger, Bulgarella, Johnson, Kuhner, et al. 2009; McCracken, Barger, Bulgarella, Johnson, Sonsthagen, et al. 2009), to obtain the oxygen that they need for aerobic respiration. There are a variety of mechanisms that fliers can use to compensate for the aerodynamic consequences of flight in low air density. High elevation species tend to have larger wings, relative to their body mass, than their low-elevation counterparts. This has been documented in tropical hummingbirds by Feinsinger et al. (1979). Additionally, birds can adapt to flight in low air density by increasing power output (Feinsinger et al. 1979), flapping more than they would in higher density air (Schmaljohann and Liechti 2009), or by using higher amplitude wingstrokes (Chai and Dudley 1996). One question that has received less attention, though, is whether birds are capable of compensating for reduced air density at high elevation behaviorally, such as through modulation of airspeed. Modern techniques that facilitate high-resolution tracking of birds in the field, either via GPS technology (e.g.: Weimerskirch et al. 2016), or by high-definition videography (Shelton et al. 2014; Theriault et al. 2014), can be used to explore differences in flight speed among bird populations living at different elevations.

Bird species with broad geographic ranges may be exposed to large elevation gradients, and this provides an opportunity to study how they tune their locomotor performance to different environmental conditions. Turkey vultures (*Cathartes aura*) are common throughout North America, and inhabit an elevation range of >3000 m (del Hoyo et al. 1992), and have been reported flying at much higher altitude (Estrella 1994; Devault et al. 2005; Avery et al. 2011). No evidence is available to suggest that any flight-related morphological differences exist

among *C. aura* throughout their range, though this has not been addressed explicitly. It seems unlikely that vulture populations differ systematically in the power output of their flight muscles, however they could alter their power output via increased flapping frequency or higher amplitude wing strokes. Vultures are primarily gliding fliers (Tucker 1988, 1991b, 1993; Arrington 2003), and could also adopt a strategy where they maintain the same true airspeed (which is the same as ground speed in still air) by increasing their glide angle, effectively increasing their power output by cashing in potential energy at a greater rate. Furthermore, *C. aura* consume almost exclusively carrion, which is a food resource that is sparsely distributed and highly ephemeral (DeVault et al. 2003; Kelly et al. 2007). Thus, it would seem advantageous for *C. aura* to minimize their energetic expenditure while foraging, and suggests that increased flight power output is an unlikely adaptation to high elevation life. Thus, I hypothesized that vultures accommodate flight at varying air densities by changing their true (i.e. observed) airspeed, increasing it as air density decreases. Mathematically, this is identical to the vultures maintaining the same equivalent airspeed (i.e. airspeed corrected for air density) at all air density conditions they experience. I further predicted that vultures would avoid activities that increase their cost of flight: that they would not increase flapping in low air density, and that they would maintain similar glide angles throughout the elevation range.

I addressed this hypothesis by recording vultures flying at three sites along a ~2000 m elevation gradient to examine how they tune their flight performance to compensate for the air density gradient. As expected, and regardless of the recorded vulture flight behavior, there was a negative relationship between observed airspeed and air density. Vultures did not flap more frequently in lower density air, and the observed change in speed was a near perfect match to

that theoretically required to maintain lift, suggesting that other factors such as wing morphing are also unimportant in this case. This study demonstrates how field studies can illuminate the relationship between biomechanical performance and ecology.

4.8 Methods

4.8.1 Vulture recordings

I recorded vultures returning to roost sites on 22 separate afternoons in May, June, and July 2015, and September 2016 at three locations: the Orange County Landfill, Chapel Hill, NC, USA (35°58'9.23"N, 79° 4'54.71"W), the University of Wyoming campus, Laramie, WY, USA (41°18'44.15"N, 105°35'1.04"W, see Fig. 1) and the Alcova Lakeside Marina, Alcova, WY, USA (42°31'45.99"N, 106°46'44.21"W). Each roost colony was comprised by >50 individuals. I was unable to identify and track identities of individual bird and birds readily transited into and out of the camera field of view multiple times during recording bouts, so to avoid the problem of pseudoreplication of these individuals, I collapsed each recording session to the median airspeed of all birds in that recording. Subsequent analyses of airspeed were conducted on those medians. There were multiple recordings per day, however I treated each of these separately because ambient temperature and humidity change throughout the day, so air density also varied among recordings.

Video data were collected with three digital SLR cameras (Canon OES 6d, Canon inc., Ōta, Tokyo, Japan) at 29.97 Hz and images had dimensions of 1920 by 1080 pixels. The cameras were arranged in a staggered setup, with intersecting views of the tops of roost trees and airspace above and around them (Fig. 1). Due to the altitude at which the vultures approached the roost trees, and the requisite upward angle of the cameras, I was unable to use a standard

wand calibration (e.g.: Shelton et al. 2014; Theriault et al. 2014). Instead, I obtained a preliminary calibration using shared views of the flying vultures, digitized using the MATLAB (The MathWorks, Natick, MA, USA) package DLTdv5 (Hedrick 2008). After the initial calibration was complete, I automated tracking of the vultures using an automatic tracking workflow adapted from that used in Evangelista et al. (2017). In brief, birds were detected in each video file by using a 30-frame moving average background subtraction routine plus a fixed background mask for the trees. The resulting background-subtracted images were cleaned with an erosion-dilation operation. The $[u,v]$ pixel coordinate of each remaining foreground object was recorded as a possible vulture detection. These 2D detections from the three cameras were combined to compute a 3D point by searching the possible 2D point combinations for ones that produced a 3D reconstruction residual of less than 3 pixels. Points generated from either two or three cameras were accepted. Once the sets of 3D points for all video frames were generated, I joined the resulting 2D+3D datasets across time using a set of Kalman filters to predict the expected position of the birds from frame n in frame $n+1$ and then a Hungarian assignment operation to match the observations in frame $n+1$ to these predicted positions. Unmatched observations started new tracks, and tracks with more than 20 missed detections in sequence were discontinued. Tracks with fewer than 300 data points were dropped from the dataset. The calibration was refined using the complete set of digitized points from the vulture tracks for each recording session, and I used the distances between the cameras to scale the scene. The cameras were aligned to gravity using their onboard roll-leveling feature, and I measured their pitch inclination using a digital inclinometer affixed to the hot-shoe mount on the top of the

base camera body. Finally, the scene was oriented to a geographic frame of reference by aligning to the compass vector between the base camera and the roost tree.

Individual bird 3D tracks in the scaled and aligned dataset were smoothed using a zero-lag digital Butterworth low-pass filter with an 8 Hz cutoff frequency. Velocity vectors were calculated from this position time-series by fitting a quintic spline polynomial and differentiating it. I added the wind speed vector (see below) to this ground reference frame velocity vector to get each bird's observed airspeed.

4.8.2 *Air density and airspeed*

Wind and weather conditions during the recording sessions were recorded from the closest NOAA weather station for all locations, and from a rooftop-mounted weather station atop the University of Wyoming Biological Sciences building, adjacent to the roost. Because of the distance between the recording sites and the weather stations, and because ground-level wind conditions may not reflect the conditions experienced by the birds, I estimated the magnitude and direction of wind conditions during each recording session from the ground speeds of the birds as they flew in different directions, following the methods of Sherub et al. (2016). Absent any wind or other directional factors, bird ground speeds are not expected to vary with flight direction such that a plot of the two components of their horizontal velocity vector form a circle centered on $[0,0]$. A wind alters the center of the circle. For example, a 5 ms^{-1} wind in the +X direction moves the center to $[5,0]$. Thus, I estimated the wind speed and direction experienced by the vultures as the center point of a circle fit to the X and Y components of their measured groundspeeds over a recording session. This method depends on having a sample of flights headed in all compass directions. Consequently, I omitted trials

with vulture tracks comprising less than 90% of the full circle. Ground speed was calculated as the first derivative of vulture position with respect to time (see above). Vulture airspeed was then obtained by subtracting the X and Y components of the estimated wind speed from their respective ground speed components of the vulture tracks. No thermal soaring behavior was observed during the recording periods, and I was unable to assess vertical movement of the air, so I assumed that non-flapping tracks represented gliding flight.

Air density (ρ) was calculated from mean barometric pressure, ambient air temperature, and dew point readings from the NOAA weather stations during the recording periods using the formula for density of moist air from (Brutsaert 2013, pg. 37):

$$\rho = \left(\frac{Pressure}{Gas\ constant_{dry\ air} * T} \right) * \left(1 - \frac{0.378 * Pressure_{vapor}}{Pressure} \right) \quad (1)$$

I calculated median airspeeds for each track. Because I was unable to assign individual ID's to birds and track them beyond the camera field of view, it is highly probably that individual vultures contributed multiple tracks to the dataset.

I predicted that vulture airspeed would decrease as a function of air density (ρ) in my sample (predicted slope = -5.22) based on a linear approximation of the theoretical relationship between airspeed and ρ and the median airspeed of vultures at the maximum ρ in my sample ($\rho = 1.227$):

$$m_{pred} = \frac{V_1 - V_1 \sqrt{\frac{1}{\rho_1}}}{\rho_1 - \rho_2} \quad (2)$$

where m_{pred} is the predicted linear approximation slope, ρ_1 is the highest air density in my sample, ρ_2 is the lowest air density in my sample, and V_1 is the median airspeed of vultures flying in the highest ρ conditions in my sample. The estimate of airspeed at ρ_2 is based on equation 5 in Pennycuick (2001). Although the theoretical relationship between V and ρ is non-linear, because the range of ρ is small, a linear approximation provides a convenient and testable hypothesis.

I tested a set of multiple linear regression models to evaluate the relationship between median airspeed and ρ as well as the impact of wind speed on the relationship. I used AICc to select the best fit among these candidate models. Additionally, to assess whether flight behavior (i.e. climbing, descending, or level flight) might influence the relationship between air density and airspeed, I parsed the data into climbing, descending, and level flight tracks using vertical speed thresholds of ($V_{z,med} > 0.25$ m/s), ($V_{z,med} < -0.25$ m/s), and (0.5 m/s $> V_{z,med} > -0.5$ m/s) respectively, and used ordinary least-squares (OLS) regression to evaluate the relationship between V and ρ in each set. I used a Wald χ^2 test to assess whether the model slopes differed from m_{pred} .

4.8.3 Air density and flapping behavior

The automatic tracking algorithm detects and tracks the visual centroid of the vultures in each video frame (as opposed to a fixed point on the body, such as the head). Because of this, and due to the large size of the birds' wings, their tracks appear as a sinusoidal wave pattern when the birds flap, contrasting with comparatively smooth gliding tracks. I exploited this to assess whether the vultures flapped more in lower air density, a sign that they might be compensating for decreased lift by modulating power output. I used a custom MATLAB

program to detect that characteristic sinusoidal track pattern and coded each video frame of each track with a binary (0) gliding, or (1) flapping. I then used the mean to quantify the proportion of the track the bird spent flapping vs. gliding. Further analyses of flapping behavior were restricted to tracks closer than 350 m from the cameras, as this appeared to be the maximum distance at which flapping is detectable (see Fig. 3). I also excluded tracks within 50 meters of the roost to avoid tracks in which the birds were making their final landing approach, which was characterized by a large amount of flapping not necessarily related to the density of the air. Data were again collapsed to medians for each recording bout. I used OLS regression to look for a relationship between incidence of flapping and ρ . Finally, I assessed whether the proportion of flapping in tracks using OLS regression on the mean or the probability of detecting flapping (binary logistic regression) varied with wind speed.

4.9 Results

4.9.1 Vulture tracks, air density, and flight speeds

I collected 3027 vulture tracks representing 18 hours of vulture flight time. Median vulture airspeeds, summarized by recording bout, ranged from 7.5 to 12.58 ms^{-1} with an overall median airspeed of $10.12 \pm 0.87 \text{ ms}^{-1}$. There was a large amount of variation in airspeed among vulture flight tracks in each recording session, median absolute deviations (MAD) ranged from 16% to 68% of the median (Fig. 2). After correcting for ambient temperature and relative humidity, ρ ranged from 0.890 to 1.227 kgm^{-3} (see Fig. 2).

The best performing model, via AICc, included effects of ρ and wind speed (AICc weight = 0.66). Median vulture airspeed (V_{med}) decreased with ρ (estimated slope $m_{\rho} = -3.73$, $F_{3,27} = 7.82$, slope $p = 0.003$; see Fig. 2) and increased with wind speed ($m_{wind} = 0.24$, slope $p = 0.004$).

Full model results are presented in Table 1. Similar relationships existed when the data were subset into vultures that were climbing (slope = -4.63, $F_{1,29} = 7.57$, $p = 0.01$, adj. $r^2 = 0.18$) and flying approximately level (slope = -4.52, $F_{1,29} = 7.51$, $p = 0.01$, adj. $r^2 = 0.18$), however the relationship between V_{med} and ρ was not significant when the birds were descending (slope = -2.72, $F_{1,29} = 2.81$, $p = 0.10$, adj. $r^2 = 0.06$). A model of airspeed as a function of wind speed alone had roughly as much predictive ability as ρ alone ($F_{1,29} = 9.64$, $p = 0.004$, adj. $r^2 = 0.22$; see Table 1).

The estimated slope of the relationship between V_{med} and ρ was not statistically distinguishable from the predicted slope (m_{pred}) in the best performing model, which included both ρ and wind speed (Wald χ^2 test, $F_{2,28} = 2.04$, $p = 0.16$), the runner-up model with the wind speed-by- ρ interaction ($F_{3,27} = 0.15$, $p = 0.70$), or the model which included only ρ ($F_{1,30} = 0.67$, $p = 0.42$). Similarly, the slopes of the test of climbing, level flight were indistinguishable from m_{pred} (Wald χ^2 test, all $p > 0.65$).

4.9.2 Flapping analysis

I was only able to detect flapping in tracks that were in close proximity to the cameras, so I restricted analysis of flapping behavior to tracks that were within 350 m of the roost, and at least 50 m away from it to avoid analyzing landing tracks. Fortunately, 84% of the tracks in my overall dataset fit this criterion (see Fig. 3). There was no relationship between the proportion of flapping in the tracks and ρ (OLS regression, $F_{1,29} = 1.91$, $p = 0.18$), however, the proportion of flapping in tracks decreased steeply away from the roost (Fig. 3). There was also no relationship between wind speed and the proportion of tracks where flapping was detected (p

= 0.59), but the probability of detecting flapping did increase ($p < 0.01$) with wind speed (see Fig. 4).

4.10 Discussion

4.10.1 Summary of results

I predicted that median airspeed in vultures flying across a range of elevations and ambient conditions would increase in response to decreasing air density (ρ). Based on a simple linear approximation of the relationship between airspeed and ρ , I predicted a slope of -5.22 across the sampled range of ρ . I found that median vulture airspeed (V_{med}) largely conformed with this prediction, despite a large amount of variation among individual tracks. This relationship was also largely invariant with flight behavior; climbing and level tracks also followed the predicted relationship. These results agree with prior observations of Himalayan vultures (*Gyps himalayensis*) tracked via GPS (Sherub et al. 2016).

The relationship between airspeed and wind speed was surprising, as the nature of calculating airspeed should remove such an effect. Several possible explanations exist. First, it is possible that the circle wind method that I used to estimate wind speed produced imperfect results. The positive relationship between airspeed and wind speed means that the circle-wind method would have to systematically underestimate the magnitude of the wind, with the amount of the underestimate increasing with wind speed. Such an effect might occur if the vultures do not fly at the same airspeed regardless of direction with respect to the wind. For example, if vultures flying into a headwind use a higher airspeed and vultures in a tailwind a lower airspeed, this would cause the circle method to systematically underestimate the wind

strength. However, if the vultures did consistently alter speed in this manner, the behavior that causes the circle method to underestimate should also hide the underestimate from a ground reference frame observer, so this possibility cannot explain the observations. Second, the motivation of the birds may also play a role here. It is possible that the birds were taking advantage of unsteady winds to extract energy from the environment. The windiest recording bouts among my recording sessions preceded the arrival of afternoon storms, and the birds may have been seeking refuge. Anecdotally, I observed vultures making more expedient approaches and landings in windier conditions. As partial support for this, I conducted a linear regression between median track altitude above the roost and wind speed and found that birds maintained lower flight levels relative to the roost trees on windy days. This result should be viewed with caution, however, as it was non-significant when I collapsed the tracks to medians for each recording bout.

4.10.2 Increased airspeed compensates for decreased air density

Drag forces also decrease with air density (Vogel 1981), and is a likely mechanism for the observed increase in airspeed. However, this assumes that birds among the different populations are geometrically similar, having roughly the same wing loading and wing shape, and the morphological disparity (the variation in body shape and size) is roughly equivalent across populations. Local adaptation of wing morphology to high elevation in my sample would likely have manifested in less change in V_{med} relative to ρ , or a difference in the ratio of sinking speed (V_z) relative to horizontal speed (V_{xy}). There was no difference in the relative contribution of horizontal vs. sinking speed in my sample ($p = 0.99$). This, plus the agreement

between the predicted and estimated slopes of the V_{med} vs. ρ relationship suggest no localized adaptation in wing morphology or loading. Further, if the increase in airspeed is simply a passive effect related to the reduction of drag, it implies that birds do not alter their flapping behavior (Schmaljohann and Liechti 2009) or increase their glide angle in low density air. Vultures in my recordings flapped more as they neared their roost trees, perhaps as part of their approach and landing maneuvers. Flapping also increased in response to greater wind speed, but did not vary with ρ . Taken together, my results do not indicate any localized behavioral or morphological adaptations to maintain similar airspeed among populations of turkey vultures residing at different elevations.

Though I was able to sample a 27% reduction in air density among my sample sites, this is small compared to the range of conditions that vultures are exposed to during flight. Air density decreases exponentially as altitude increases, necessitating proportionally greater airspeed increases to maintain lift as birds climb higher. It is possible that the relationship between V_{med} and ρ might change for vultures flying at especially high altitudes, necessitating that they modify their flapping behavior or glide angle. Vultures have been seen at altitudes exceeding 1000 m (Avery et al. 2011), however their typical flight altitudes are much lower, around 150 m (Devault et al. 2005; Avery et al. 2011). Therefore, it is likely that my results are largely representative of turkey vulture flight throughout their range.

4.10.3 Concluding remarks

Animals interact with their physical environment to move, forage, migrate, and a host of other functions, and their ability to do so effectively can be limited by physical constraints

imposed by their environment. I examined how turkey vultures respond to a fundamental environmental gradient that could alter their flight performance, the decrease of air density at high elevation. The tool that I used was developed for field studies of biomechanics (Hedrick 2008; Shelton et al. 2014; Theriault et al. 2014; Hedrick et al. 2018), but this study also demonstrates that tools from the biomechanics toolchest can be successfully applied to ecological questions.

REFERENCES

- Altshuler DL, Dudley R. 2006. The physiology and biomechanics of avian flight at high altitude. *Integr Comp Biol* 46:62–71.
- Arrington DP. 2003. Flight characteristics of non-migrating and migrating populations of turkey vultures. Theses Diss Available ProQuest 1–73.
- Avery ML, Humphrey JS, Daughtery TS, Fischer JW, Milleson MP, Tillman EA, Bruce WE, Walter WD. 2011. Vulture flight behavior and implications for aircraft safety. *J Wildl Manag* 75:1581–87.
- Brutsaert W. 2013. *Evaporation into the Atmosphere: Theory, History and Applications* Springer Science & Business Media.
- Chai P, Dudley R. 1996. Limits to flight energetics of hummingbirds hovering in hypodense and hypoxic gas mixtures. *J Exp Biol* 199:2285–95.
- del Hoyo J, Elliott Andrew, Sargatal Jordi, Cabot José. 1992. *Handbook of the birds of the world* Barcelona: Lynx Edicions.
- Devault TL, Reinhart BD, Brisbin IL, Rhodes OE, Bechard. 2005. Flight behavior of black and turkey vultures: implications for reducing bird–aircraft collisions. *J Wildl Manag* 69:601–8.
- DeVault TL, Rhodes Jr Olin E, Shivik JA. 2003. Scavenging by vertebrates: behavioral, ecological, and evolutionary perspectives on an important energy transfer pathway in terrestrial ecosystems. *Oikos* 102:225–34.
- Dillon ME, Dudley R. 2014. Surpassing Mt. Everest: extreme flight performance of alpine bumble-bees. *Biol Lett* 10:20130922.
- Estrella RR. 1994. Group Size and Flight Altitude of Turkey Vultures in Two Habitats in Mexico. *Wilson Bull* 106:749–52.
- Evangelista DJ, Ray DD, Raja SK, Hedrick TL. 2017. Three-dimensional trajectories and network analyses of group behaviour within chimney swift flocks during approaches to the roost. *Proc R Soc B Biol Sci* 284:20162602.
- Feinsinger P, Colwell RK, Terborgh J, Chaplin SB. 1979. Elevation and the Morphology, Flight Energetics, and Foraging Ecology of Tropical Hummingbirds. *Am Nat* 113:481–97.
- Hedrick TL. 2008. Software techniques for two- and three-dimensional kinematic measurements of biological and biomimetic systems. *Bioinspir Biomim* 3:034001.

- Hedrick TL, Pichot C, Margerie E de. 2018. Gliding for a free lunch: biomechanics of foraging flight in common swifts (*Apus apus*). *J Exp Biol* 221:jeb186270.
- Hiebl I, Braunitzer G. 1988. ADAPTATION OF THE HEMOGLOBINS OF BARHEADED GOOSE ANSER-INDICUS ANDEAN GOOSE CHLOEPHAGA-MELANOPTERA AND RUPPELL'S GRIFFON GYPS-RUEPPELII TO LIFE UNDER HYPOXIC CONDITIONS. *J Fuer Ornithol* 129:217–26.
- Kelly NE, Sparks DW, DeVault TL, Rhodes OE. 2007. Diet of Black and Turkey Vultures in a Forested Landscape. *Wilson J Ornithol* 119:267–70.
- Liu X-Z, Li S-L, Jing H, Liang Y-H, Hua Z-Q, Lu G-Y. 2001. Avian haemoglobins and structural basis of high affinity for oxygen: Structure of bar-headed goose aquomet haemoglobin. *Acta Crystallogr D Biol Crystallogr* 57:775–83.
- McCracken KG, Barger CP, Bulgarella M, Johnson KP, Kuhner MK, Moore AV, Peters JL, Trucco J, Valqui TH, Winker K, Wilson RE. 2009. Signatures of High-Altitude Adaptation in the Major Hemoglobin of Five Species of Andean Dabbling Ducks. *Am Nat* 174:631–50.
- McCracken KG, Barger CP, Bulgarella M, Johnson KP, Sonsthagen SA, Trucco J, Valqui TH, Wilson RE, Winker K, Sorenson MD. 2009. Parallel evolution in the major haemoglobin genes of eight species of Andean waterfowl. *Mol Ecol* 18:3992–4005.
- Pennycuik CJ. 2001. Speeds and wingbeat frequencies of migrating birds compared with calculated benchmarks. *J Exp Biol* 204:3283–94.
- Schmaljohann H, Liechti F. 2009. Adjustments of wingbeat frequency and air speed to air density in free-flying migratory birds. *J Exp Biol* 212:3633–42.
- Shelton RM, Jackson BE, Hedrick TL. 2014. The mechanics and behavior of cliff swallows during tandem flights. *J Exp Biol* 217:2717–25.
- Sherub S, Bohrer G, Wikelski M, Weinzierl R. 2016. Behavioural adaptations to flight into thin air. *Biol Lett* 12:20160432.
- Slatyer RA, Hirst M, Sexton JP. 2013. Niche breadth predicts geographical range size: a general ecological pattern. *Ecol Lett* 16:1104–14.
- Storz JF. 2007. Hemoglobin function and physiological adaptation to hypoxia in high-altitude mammals. *J Mammal* 88:24–31.
- Theriault DH, Fuller NW, Jackson BE, Bluhm E, Evangelista D, Wu Z, Betke M, Hedrick TL. 2014. A protocol and calibration method for accurate multi-camera field videography. *J Exp Biol* 217:1843–48.

- Tucker VA. 1988. Gliding Birds: Descending Flight of the Whitebacked Vulture, *Gyps Africanus*. *J Exp Biol* 140:325–44.
- Tucker VA. 1991. Stereoscopic Views of Three-Dimensional, Rectangular Flight Paths in Descending African White-Backed Vultures (*Gyps africanus*). *The Auk* 108:1–7.
- Tucker VA. 1993. Gliding birds: Reduction of induced drag by wing tip slots between the primary feathers. *J Exp Biol* 180:285–310.
- Vogel S. 1981. *Life in moving fluids*. Princet Univ.
- Weimerskirch H, Bishop C, Jeanniard-du-Dot T, Prudor A, Sachs G. 2016. Frigate birds track atmospheric conditions over months-long transoceanic flights. *Science* 353:74–78.

4.11 Figures

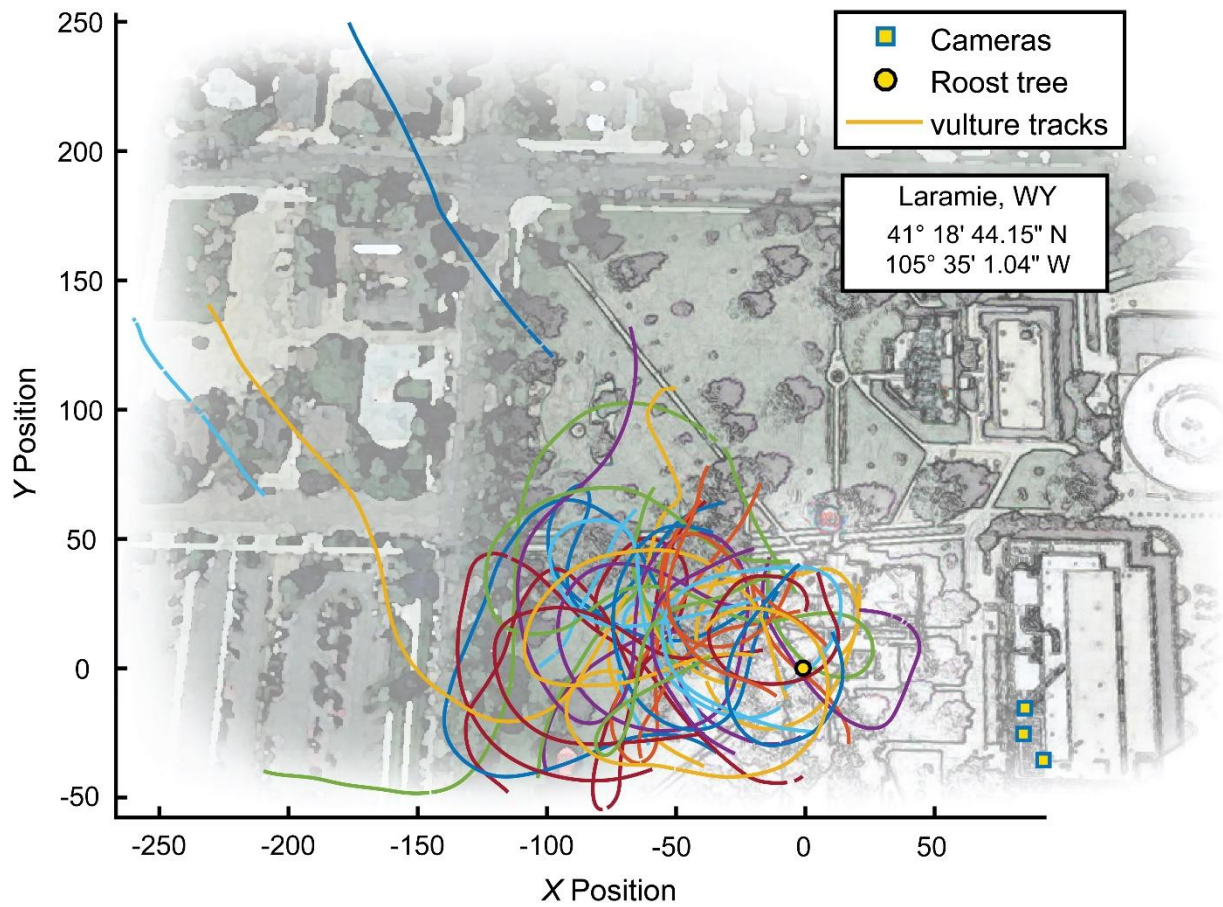


Figure 0.1 Overhead view of the Laramie, WY recording site. Blue squares denote camera locations atop the Biological Sciences building at the University of Wyoming, and the black circle shows the center of the roost trees. The multicolored tracks depict a sampling of the vulture tracks recorded from one recording bout.

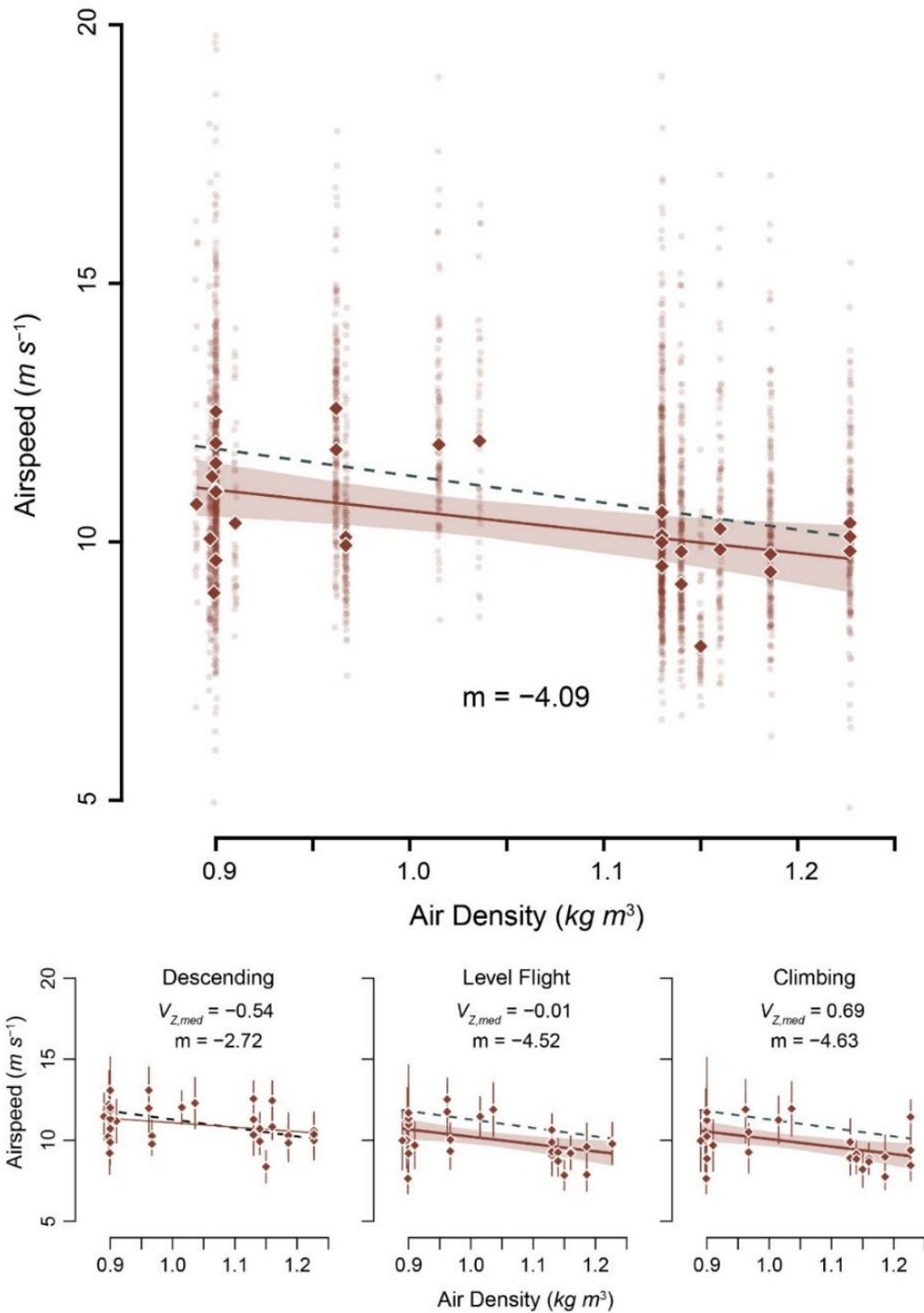


Figure 0.2 Median airspeed decreased with increasing air density. Transparent data points show median values for each track, highlighting the large variation in the sample. Analyses were conducted on median values for each recording session, depicted by solid diamonds. The dashed green line shows the predicted slope (-5.22), while the solid brown line shows the modeled slope with its 95% confidence interval (shaded region)

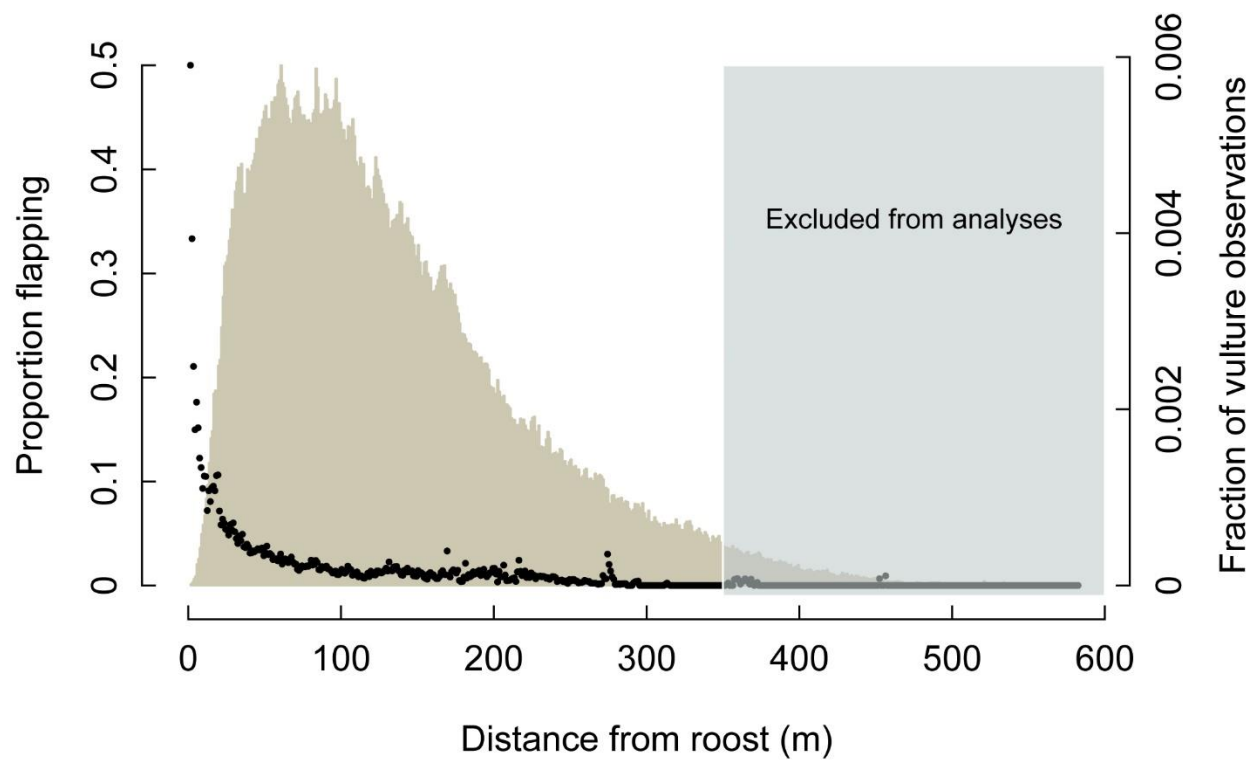


Figure 0.3 Proportion of detected flapping events, indicated by black points, decreased with distance from the roost trees. The histogram depicts distribution of tracked birds, relative to the roost position. The ability to detect flapping diminished with distance from the cameras, so tracks greater than 350 m from the roost were excluded from further analyses.

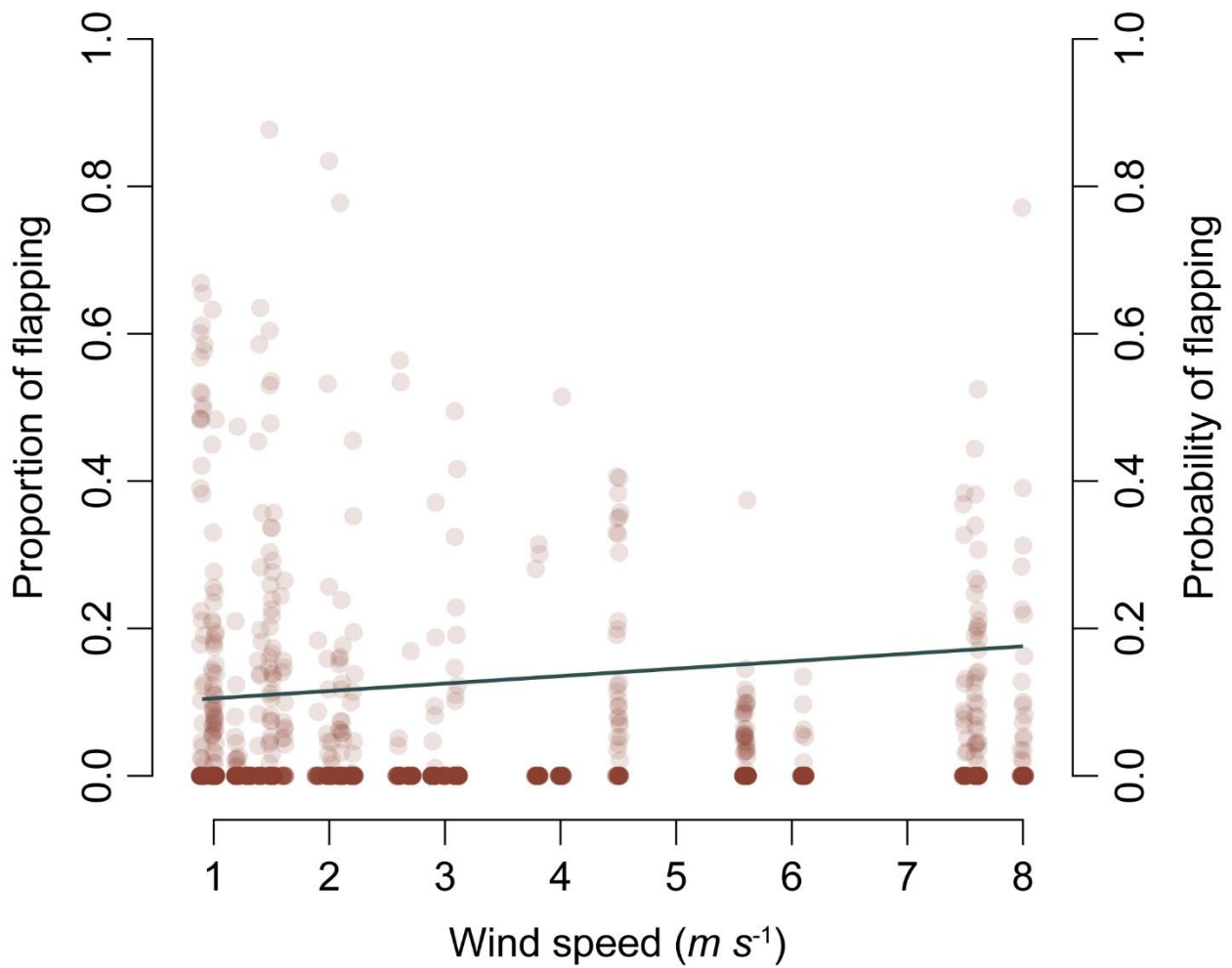


Figure 0.4 Flapping behavior as a function of wind speed. The proportion of time that birds spent flapping was low across all wind conditions but increased slightly (though not significantly) with wind speed. Points show individual track values to depict the dispersion of the data, but analyses were conducted on median values for each recording session. The line shows the mean probability of observing flapping in a track, which increased with wind speed.

4.12 Tables

Table 0.1 Model selection results.

Model	Model Statistics	AICc	AICc.w	m_ρ m_{wind} m_{int}
$V \sim \rho + Wind$	$F_{2,28} = 11.09, p = 0.003, \text{adj. } r^2 = 0.40$	82.77	0.658	-3.73** 0.24**
$V \sim \rho + Wind + (\rho \cdot Wind)$	$F_{3,27} = 7.82, p < 0.001, \text{adj. } r^2 = 0.41$	84.34	0.300	-6.64* -0.81 1.07
$V \sim Wind$	$F_{1,29} = 9.64, p = 0.004, \text{adj. } r^2 = 0.22$	89.31	0.025	0.26**
$V \sim \rho$	$F_{1,29} = 8.80, p = 0.006, \text{adj. } r^2 = 0.21$	89.99	0.017	-4.09**

Significance codes for estimated slope coefficients: * $p < 0.05$, ** $p < 0.01$

CHAPTER 6: CONCLUSIONS

In this dissertation, I have used modern methodologies and an unprecedented new dataset to describe the evolution of 3-dimensional (3D) wing shape in birds. Although many studies have looked at wing shape in a variety of different contexts, wing shape was treated as a two-dimensional (2D) problem, despite the inherently 3D nature of wings. Furthermore, many were hampered by composite datasets and analysis methods that failed to properly account for statistical non-independence resulting from phylogenetic relatedness, yielding contradictory results among different studies. Many of these studies were also correlational in nature, and thus could not explore the mechanisms driving trait evolution.

To address these shortcomings, I collected a new dataset using modern techniques to acquire and analyze 3D shape from preserved bird wings. I used a first-principles approach to predict how morphology should respond to evolutionary pressures imposed by the physics of flight which allowed me to generate testable hypotheses. To test those hypotheses, I used phylogenetically-informed analyses, accounting for the relatedness among species. My work revealed a complex mosaic of evolutionary patterns among wing shape traits that is influenced both by body size and the anatomy of the wing, explored a paradox in the scaling of wings with body size, and demonstrated that specialization to gliding flight is associated with long, more heavily-cambered wings. Finally, and perhaps above all, my work emphasized that bird wings

are 3D structures, and that variation in 3D shape has implications not only for the function of the wings, but also for their evolution, and warrants continued attention. In this chapter, I will summarize the main findings of the preceding chapters, and provide discussion of how the combined results advance the overall understanding of avian wing shape and the pressures that have shaped and constrained its evolution. Finally, I will comment on what I see as fruitful directions for future investigations.

5.1 Body size and evolving wings

5.1.1 Resolving a paradox

In Chapter 2, I investigated how wing shape and size scale across the range of body size in my sample of 1096 individuals from 178 species of birds (roughly six grams to two kilograms). What I found confirmed prior observations that large birds have disproportionately small wings relative to their body size in a paradox that, on its face, could lead to functional limitations on their flight performance. All else being equal, larger species would produce relatively less lift as a result of decreased wing area when compared to smaller species. However, I also showed that all else is not equal, and that wing camber increases with body size. Combined with work from Chapter 3, I propose that increased camber is a compensatory adaptation, allowing larger species to maintain, at least in part, functional similarity to their smaller counterparts by increasing the area-specific magnitude of lift produced by the wings, even in the face of negative wing allometry.

5.1.2 *Constraints and tradeoffs affect wing size*

To quantify tradeoffs and constraints on size-related diversification among wings, I collected complimentary measurements of wing skeletal morphology and primary feather dimensions to explore the relationships between these two critical components of the wing and overall wing morphology. The wing skeleton imposes a lower limit on wing thickness, as one would expect given that it must support the birds' weight and forces generated during flight, but this lower bound is not necessarily ideal aerodynamically. As a result, unless the underlying skeleton completely constrains wing shape, the outer surface of the wing is expected to vary in aerodynamically-relevant ways. Indeed, my results show that the region of the wing associated with the long bones of the arm (the armwing) was evolutionarily decoupled from the skeleton, and overall wing thickness there varied more predictably with other wing shape traits – with known aerodynamic effects – than with a model of load. This suggests that the skeleton and wing surface are independently evolvable units, capable of responding to different evolutionary pressures. However, the feathered surface of the handwing – the region of the wing associated with the hand bones, and largely composed of the primary flight feathers, was more associated with the loading model of the wing, and therefore to evolution of the wing skeleton. That the handwing and armwing appear to be differentially constrained in their shape evolution portends to the work that I present in Chapter 5, that the wing is divided into discrete morphological modules delineated by the wrist joint. Overall, I provided strong evidence that wings have multiple adaptive axes that interact in complex and sometimes contrary ways to shape their evolution. My results also suggest that multiple configurations of morphology can potentially lead to similarly functional wings, regardless of their size.

5.1.3 *Important questions remain*

Although the results that I discussed in Chapter 2 made significant refinements to our understanding of wing allometry, there is still much that remains unknown. Of particular interest is the contribution of wing posture to the outward shape of the wing. Future studies should combine measurement of the surface of the wing, the wing skeleton, and individual feathers, all within the same individual, perhaps using micro-CT scanning to collect data. Doing so will permit explicit investigation of how each of the constituent components of the wing interact with joint posture and contribute to the outward shape of the wing. Furthermore, understanding how shape and posture are related in a static sense may inform hypotheses about how birds can modify wing shape through postural changes that can be tested in the field and lab. Finally, this dissertation has largely considered how wing morphology is shaped by the evolutionary pressures of steady-state aerodynamics. However, flapping flight is also characterized by numerous unsteady aerodynamic effects (Kawachi, 2006). While it is known that shape traits, particularly camber, interact with unsteady aerodynamic effects (Gardiner et al., 2013), it remains difficult to formulate discrete predictions about how the relationship between morphology and the aerodynamic forces produced by unsteady effects might impact evolutionary dynamics, presenting an exciting frontier for future research.

5.2 **Gliding specialists have diverged in wing shape**

Chapter 3 used two hypothetical performance landscapes developed from simulations of gliding flight (Waldrop et al. 2020a) based on two aspects of wing shape, wing aspect ratio (AR , the ratio of length over width of the wing) and mean wing camber (\bar{Q} , the upward

curvature of the wing surface) coupled with the scanned wing data to explore how gliding-specialist birds have evolved on those landscapes (Rader et al. 2020). The landscapes predicted that two important aerodynamic quantities that are relevant to gliding flight, coefficient of lift (C_L , measured at minimum sinking speed: $V_{z,min}$) and lift to drag ratio (C_L/C_D) were maximized at different combinations of wing morphology: high \bar{Q} and high AR , and at high AR but moderate \bar{Q} , respectively. I mapped birds in my sample onto these landscapes and tested two hypotheses: 1) Gliding-specialist birds should have distinctly different combinations of AR and \bar{Q} relative to non-gliders, leading to higher C_L/C_D than in non-gliders, and 2) that there are two different strategies of gliding flight: 1) “aerial perching”, wherein birds have adapted to minimize their loss of altitude relative to forward travel, allowing them to remain aloft with minimal energy expenditure, and 2) “aerial searching”, with birds adapted to efficiently traverse large distances. More specifically, I hypothesized that each of these strategies corresponds with a discrete combination of AR and \bar{Q} , drawing aerial perchers across the hypothetical performance landscapes toward high C_L at $V_{z,min}$ and the searchers toward high C_L/C_D . I will discuss the conclusions of my tests for each of these hypotheses in turn.

5.2.1 *Gliding versus non-gliding morphology*

I found strong support for the first hypothesis, that gliding specialist birds had divergent wing morphologies from non-gliding taxa. Both AR and \bar{Q} were greater in gliding birds than in non-gliders. My results showed that gliders and non-gliders were being pulled toward different evolutionary optima for AR (as well as its constituent dimensions of wing length and chord) and \bar{Q} , and that wing morphology in gliders has evolved at a faster rate than in non-gliders. Further,

I showed that flight behavior (gliding vs. non-gliding) can be predicted with high accuracy (~87% for my sample) from the combination of AR and \bar{Q} . Despite finding clear differences in wing shape between the flight styles, my hypothesis that gliders would be adapted to maximize C_L/C_D was not supported. Rather, gliding birds have diverged from non-gliders on a path across the landscape taking them toward maximizing C_L at $V_{z,min}$. Gliding birds had greater C_L at $V_{z,min}$ than non-gliders, which is advantageous for them, as it reduces the effort required for them to maintain altitude and enhances their ability to extract energy from air currents and updrafts.

5.2.2 *Two strategies for gliding*

Among the birds in my sample that rely heavily on gliding flight, I hypothesized that two different gliding flight strategies exist, 1) “aerial perching”, where birds minimize their energy expenditure to remain aloft, but only travel within a relatively small geographic area, and 2) “aerial searching” where birds minimize their cost of transport and fly at high speeds, allowing them to efficiently traverse great distances. Hawks and vultures exemplify the first strategy, while seabirds specialize on the second. I predicted that each of these strategies would lead to a split within gliding birds toward two different performance optima, maximum C_L at $V_{z,min}$ for aerial perchers and maximum C_L/C_D for the aerial searchers. However, support for this prediction was equivocal. I did find support for distinct morphological optima between the strategies, however they did not appear to diverge toward different performance optima. Instead, the aerial searchers were simply further than the perchers along the same trajectory toward maximum C_L at $V_{z,min}$.

5.2.3 *Beyond the hypotheses: Performance landscapes and 3D wings*

This chapter provided a vignette of how performance landscapes can be used to make predictions about evolutionary dynamics in morphology which can then be tested using empirical data. With my collaborator, I showed that gliding performance is sensitive not only to changes in AR and \bar{Q} , but also to their interaction (Waldrop et al. 2020a). The resulting performance landscape allowed me to make explicit predictions about how gliding birds should have diverged across the landscape from birds that rely more heavily on flapping flight. I was then able to use an empirical dataset of 1094 wings from 163 bird species to test whether my predictions held. This is a particularly robust approach, as the predictions and landscapes are created from first-principles, rather than being inferred *post-hoc* from the morphological data. Finally, this chapter highlighted the importance considering three-dimensional shape in bird wings. Both of the performance optima that I tested between occurred at high AR , but at different values of \bar{Q} . Past attempts to link wing morphology considered only AR and would therefore have been unable to differentiate between evolution toward either of the two putative performance optima.

5.3 **Wing anatomy and modular evolution**

In Chapter 4, I noted that the wing is subdivided into two anatomical regions, separated by the wrist joint. I hypothesized that these two regions of the wing might be distinct morphological modules, as each has its own developmental tradeoffs (some of which were highlighted in Chapter 2). Also, noting that there is a non-linear gradient of aerodynamic forces that increases from the base of the wing toward its tip (as a function of the square of distance

from the wing base), I hypothesized that the strength of the relationship between trait morphology and functional output (mechanical sensitivity), would increase along the wing, matching the aerodynamic force gradient for flapping wings. High mechanical sensitivity corresponds with increased evolutionary tempo (σ^2) within morphological modules in complex structures (Anderson and Patek 2015; Muñoz et al. 2017).

I tested three competing predictions about how evolutionary dynamics of shape traits in the wing would respond to the gradient of mechanical sensitivity. 1) If the mechanical sensitivity gradient is important to trait evolution in wings, I predicted that evolutionary tempo would increase along the wing following the gradient. 2) If the sensitivity gradient is important, but wing morphology can only respond in a modular fashion, the handwing module should show greater evolutionary tempo, with a step down across the wrist to a lower rate in the armwing. 3) If the hypothesized gradient of mechanical sensitivity does not exist or is unimportant to wing shape evolution, I expected no particular base-to-tip pattern of evolutionary dynamics in the wing.

5.3.1 Looking for modules in the wing

In addition to the whole-wing measurements that I analyzed and discussed in the preceding two chapters, I sliced the 3D wing scans up into chord-wise segments along their span and measured chord, camber, cross-sectional thickness, and cross-sectional area from each of the slices. I calculated morphological disparity – essentially a measure of evolutionary diversity in shape across the phylogeny, and evolutionary tempo for each shape trait in each slice. I compared the amount of variance within each of the hypothetical wing regions, the

handwing and armwing, to the variance between them. This analysis demonstrated that the wing is divided into at least two morphological modules separated by the wrist. Analysis of morphological disparity showed that shape divergence was greatest in the handwing.

5.3.2 *Testing evolutionary dynamics of the wing modules*

Despite strong evidence for morphological modularity in the wing, evolutionary tempo followed the gradient of mechanical sensitivity along the span of the wing that was predicted based on aerodynamic force production and inertial moment in flapping flight. Evolutionary rate in all of the shape traits was greatest near the tip of the wing, decreased through the wrist, and was lowest in the armwing. This means that even in the face of morphological modules that have disparate tradeoffs, morphology can be tuned along continuous gradients. These results concur with prior observations that mechanical sensitivity drives evolution of biomechanical traits. Finally, and perhaps most significantly, I demonstrated that the linkage between mechanical sensitivity and evolutionary dynamics is not system-specific and may therefore be fundamental to the evolution of form-function relationships.

5.4 **Flying in thin air**

Animals face a variety of environmental challenges to their movement. The decrease in air density with increasing altitude is a fundamental environmental gradient that can affect flight performance in birds, especially for species that fly at high altitudes, migrate across elevations, or whose geographic range spans a large range of elevation. Birds can compensate

for changes in air density by modifying their wing morphology – having larger wings relative to body mass, increasing power output – flapping more frequently or at higher amplitude, or by modifying their airspeed. My 5th chapter investigated how turkey vultures (*Cathartes aura*), which is a bird species that is ubiquitous throughout much of the New World and is exposed to a large elevation gradient throughout its range, copes with reduced air density.

There is no evidence of morphological variation among populations of vultures that would hint at local adaptation to high elevation (though this lack of evidence does not provide *prima facie* evidence of a lack of local adaptation). I used 3D field tracking techniques to record vultures flying at three sites across a ~2,000 m elevation gradient. I measured airspeed and recorded flapping behavior of the birds as they approached their roost sites at the end of the day. By selecting roost sites, I was able to position myself where the birds would repeatedly arrive, but more importantly, I was able to record gliding flight without the confounding influence of the thermal soaring behavior for which vultures are famous.

5.4.1 *Vultures flew faster at high elevation*

I recorded roughly 18 hours of vulture flight and found that vultures displayed a large amount of variation in their flight speeds as they approached the roost. Despite the large amount of variation in airspeed among the vulture tracks, I found that median airspeed for each recording bout varied as a function of air density, and that the slope of the relationship was statistically indistinguishable from that which I predicted from the physical relationship between air density and equivalent airspeed. Additionally, the birds did not appear to alter their glide ratio, either. Birds did lose altitude more quickly in less dense air, but only at a rate

commensurate with their increased airspeed. What's more, the vultures did not alter their flapping behavior in response to air density. They were more likely to be observed flapping on windy days, and as they approached the roost trees. Otherwise, vultures seemed equally lazy (or clever) across all of my study sites.

5.5 What does it all mean?

5.5.1 The challenge of deep time

Morphological variation has long been a subject of keen interest among bird biologists, with fascinating and sometimes conflicting results. My dissertation work also encountered many of the same pitfalls that have plagued prior researchers, stemming mostly from the depth of the evolutionary history of birds. The majority of the major bird clades emerged in the Paleocene epoch, between 66 and 56 million years ago (Prum et al. 2015). This mega-radiation of taxonomic diversity among birds was also associated with rapid ecological and morphological diversification among the emerging clades (Cooney et al. 2017). The rapid expansion into novel niches and morphospace was followed by a deceleration in the accumulation of morphological disparity (Cooney et al. 2017; Phillips et al. 2020). Further morphological evolution followed a pattern of niche packing, with small-scale divergence among taxa within the larger lineages (Phillips et al. 2020).

Among other aspects of avian morphology, wing shape diverged early in the avian mega-radiation (Phillips et al. 2020), which is why birds within the modern clades tend to have relatively conserved wing shape (Rayner 1988; Taylor and Thomas 2014). An unfortunate consequence of this deep evolutionary history is that it effectively reduces the number of

independent emergences of each observed morphotype because there are simply fewer branches at the base of the tree (Felsenstein 1985). This makes it difficult to disentangle the effects of phylogeny from ecological or other aspects of bird biology (such as body size) – because those, too, diverged early in their evolution and often in parallel with one another.

5.5.2 *A new dataset and analytical techniques*

Prior attempts at a taxonomically-broad analysis of wing shape in birds have, to a large extent, relied upon a composite dataset compiled and presented by Greenewalt (1975), which was expanded upon and reanalyzed by Rayner (1988). Taylor and Thomas (2014), in a recent and phylogenetically aware approach, noted that the data were collected with varying methods, assumptions, and levels of precision, and restricted their analyses to only the subset of the data that met the definition of wing area given by Pennycuik (2008). Still, while restricting the dataset permitted comparison of the same metric (specifically, wing area), it did little to solve the problem of varying levels of precision among the measurements.

Phylogenetically-informed regression models are known to be sensitive to measurement error (Silvestro et al. 2015), so the effects of composite data might be hard to predict and correct for. This may be especially true given the depth of the phylogeny connecting bird species.

Recent technological advances in 3D scanning, enhanced computing abilities, and established approaches to handling large datasets made it possible to collect an entirely new dataset on wing shape. The 3D scanned data that I present here have a high degree of fidelity to the preserved wings, exceeding even the most careful of researchers and precise of digital calipers. Also, by taking measurements from the scan files programmatically, I avoided arbitrary

decisions of what and where to measure that can arise when surface landmarks on the object being measured are ambiguous. Additionally, I was able to collect a greater density of data than would be possible by hand. For example, I was able to collect 38 different measurements from each wing, several of which were iterated over ~40 slices along the wing's length. Though I have only presented and discussed results from a selection of those metrics in this dissertation, what I have presented can be revisited and replicated, and new measurements and analyses taken from the original wing scans much more readily than by traditional morphological techniques.

Despite the fundamental limitations of working with deep phylogenetic covariance, the dataset that I have collected for my dissertation, in concert with substantial methodological improvement and theoretical advances provided new insight into the patterns and processes of evolution in one of the fundamental form-function relationships of avian biology.

5.5.3 Evolution in three dimensions

I have shown that bird wings are complex structures, not only anatomically, but also evolutionarily. Rather than being flat, planar structures as they have frequently been treated, bird wings have complex three-dimensional shapes (Chapter 2) that contribute to their function in multiple ways (Chapter 3). Nor are wings integrated morphological units; they are regionalized into at least two morphological modules, the handwing and the armwing (Chapter 4). The work presented here has barely scratched the surface of the interplay of modularity and three-dimensionality within wing function and evolution, but I have discovered a tradeoff between weight bearing and aerodynamic function that differentially shapes the handwing and the armwing (Chapter 2), and that specializing on gliding flight selects for high aspect-ratio

wings and increased wing camber. Furthermore, the interaction of camber and aspect ratio is key to enhancing the coefficient of lift in bird wings (Chapter 4). Even though wings are morphologically modular, the evolution of shape within wings tracks a smooth gradient predicted by the forces produced by flapping wings (Chapter 5), an insight that might hint that the strength of the relationship between a shape trait and its functional output (mechanical sensitivity; Anderson and Patek 2015; Muñoz et al. 2017) is a fundamental driver of evolutionary dynamics across multiple varieties of form-function systems.

Wing shape varies with body size in complex and surprising ways. Large birds appear to be constrained in several ways to have disproportionately small wings, which on its face would put them at a disadvantage for producing enough lift to support themselves in the air (Chapter 2). However, wing camber also increases with body size (Chapter 2), and camber enhances lift production by increasing the coefficient of lift (Chapter 3). This example demonstrates that shape traits within wings can evolve somewhat independently of one another, in response to specific physical demands and tradeoffs of their function, leading to multiple configurations that confer similar performance in an intricate many-to-one mapping (Wainwright 2005) of wing morphology. Finally, birds can address challenges to their flight behaviorally, without specific morphological adaptation (Chapter 5), perhaps reducing the selective pressure that would otherwise drive local adaptation (Muñoz and Losos 2018; Muñoz 2021).

5.5.4 Looking forward

Overall, while the work that I have presented here has answered some questions concerning avian wing shape and its evolution, it has raised many more. For example, though I

was able to explore how the components of the wing (feathers and skeleton) scale relative to each other, my results here are still correlational because my measurements of the outer wing surface, its underlying skeleton, and the flight feathers were taken from different individuals, and in some cases, different species. Methods that permit measurement of all these features from the same wing will provide more robust insights. Further, the role of posture in shaping the outward geometry of the wing remains a tantalizing future avenue. Much of the success of my work came from the formulation of well-defined hypotheses that could be tested using empirical measurements of wings. I believe strongly that a hypothesis-first approach yields clearer results, and I hope that the framework I have presented herein will prove valuable to others as they continue to explore relationships of animal form and function.

REFERENCES

- Anderson PSL, Patek SN. 2015. Mechanical sensitivity reveals evolutionary dynamics of mechanical systems. *Proc R Soc B Biol Sci* 282:20143088.
- Cooney CR, Bright JA, Capp EJR, Chira AM, Hughes EC, Moody CJA, Nouri LO, Varley ZK, Thomas GH. 2017. Mega-evolutionary dynamics of the adaptive radiation of birds. *Nature* 542:344–47.
- Felsenstein J. 1985. Phylogenies and the Comparative Method. *Am Nat* 125:1–15.
- Gardiner, J., Norizham, A. R., Dimitriadis, G., Tickle, P., Codd, J., & Nudds, R. (2013). Simulation of bird wing flapping using the unsteady vortex lattice method. *Proceedings of the International Forum on Aeroelasticity and Structural Dynamics, IFASD 2013*.
- Greenewalt CH. 1975. The Flight of Birds: The Significant Dimensions, Their Departure from the Requirements for Dimensional Similarity, and the Effect on Flight Aerodynamics of That Departure. *Trans Am Philos Soc* 65:1–67.
- Kawachi, K. 2006. Unsteady wing characteristics at low Reynolds number. In R. Liebe (Ed.), *WIT Transactions on State of the Art in Science and Engineering* (1st ed., Vol. 2, pp. 420–434). WIT Press. <https://doi.org/10.2495/1-84564-095-0/5d>
- Muñoz MM. 2021. The Bogert effect, a factor in evolution. *Evolution evo*.14388.
- Muñoz MM, Anderson PSL, Patek SN. 2017. Mechanical sensitivity and the dynamics of evolutionary rate shifts in biomechanical systems. *Proc R Soc B Biol Sci* 284:20162325.
- Muñoz MM, Losos JB. 2018. Thermoregulatory Behavior Simultaneously Promotes and Forestalls Evolution in a Tropical Lizard. *Am Nat* 191:E15–26.
- Pennycuik CJ. 2008. *Modelling the Flying Bird*. Burlington: Elsevier.
- Phillips AG, Töpfer T, Böhning-Gaese K, Fritz SA. 2020. Rates of ecomorphological trait evolution in passerine bird clades are independent of age. *Biol J Linn Soc* 129:543–57.
- Prum RO, Berv JS, Dornburg A, Field DJ, Townsend JP, Lemmon EM, Lemmon AR. 2015. A comprehensive phylogeny of birds (Aves) using targeted next-generation DNA sequencing. *Nature* 526:569–73.
- Rader JA, Hedrick TL, He Y, Waldrop LD. 2020. Functional Morphology of Gliding Flight II. Morphology Follows Predictions of Gliding Performance. *Integr Comp Biol* 60:1297–1308.
- Rayner JMV. 1988. Form and Function in Avian Flight. In: Johnston RF, editor. *Current Ornithology*. Current Ornithology Boston, MA: Springer US. p. 1–66.

Silvestro D, Kostikova A, Litsios G, Pearman PB, Salamin N. 2015. Measurement errors should always be incorporated in phylogenetic comparative analysis. *Methods Ecol Evol*.

Taylor G, Thomas A. 2014. *Evolutionary Biomechanics* Oxford University Press.

Wainwright PC. 2005. Many-to-One Mapping of Form to Function: A General Principle in Organismal Design? *Integr Comp Biol* 45:256–62.

Waldrop LD, He Y, Hedrick TL, Rader JA. 2020. Functional Morphology of Gliding Flight I: Modeling Reveals Distinct Performance Landscapes Based on Soaring Strategies. *Integr Comp Biol* 60:1283–96.